MSC-06085

GRUMMAN

MSC-06085

GRUMMAN AEROSPACE CORPORATION

AERODYNAMICS SECTION

AN ANALYTICAL PROCEDURE FOR EVALUATING SHUTTLE ABORT STAGING AERODYNAMIC CHARACTERISTICS

May 31, 1973

FINAL REPORT
SUBMITTED IN PARTIAL FULFILLMENT
ON NASA CONTRACT NAS 9-12581

Prepared by:

R. C. Meyer

R. Meyer; Project Engineer

Checked & Approved by:

G. DaForno

G. DaForno; Shuttle R & T Aerothermodynamics, Mgr.

Approved by:

Charles J. Dragowitz

C. Dragowitz; Head, Configuration Group

Approved by:

W. R. Murphy

W. R. Murphy; Head, Aerodynamics Section

SUMMARY

An engineering analysis and computer code (AERSEP) for predicting NASA Shuttle Orbiter - HO Tank longitudinal aerodynamic characteristics during abort separation has been developed. Computed results are applicable at Mach numbers above 2 for angle-of-attack between $\pm$ 10 degrees. No practical restrictions on orbiter-tank relative positioning are indicated for tank-under-orbiter configurations. Input data requirements and computer running times are minimal facilitating program use for parametric studies, test planning, and trajectory analysis. In a majority of cases AERSEP Orbiter-Tank interference predictions are as accurate as state-of-the-art estimates for interference-free or isolated-vehicle configurations. AERSEP isolated-orbiter predictions also show excellent correlation with data.

TABLE OF CONTENTS

INTRODUCTION

Wind tunnel tests to define Shuttle Orbiter-Tank abort staging characteristics are particularly time consuming and expensive. In addition to the many test variables the problem is compounded by the extensive data required to define the aerodynamic characteristics during the early most critical phase of tank separation. Given these circumstances it is imperative to maximize the information obtained during test by early identification of major problem areas. Recognizing the need NASA MSC awarded Grumman the present contract to develop an engineering capability for predicting Shuttle Orbiter-Tank longitudinal characteristics during abort separation. The primary flight envelope was to cover Mach No. > 2 and angle-of-attack between $\pm$ 10 degrees. Secondary objectives were to develop a corresponding capability for large angle-of-attack, $\alpha > 25^{\circ}$, and to assess the feasibility of a mid angle-of-attack analysis, $10^{\circ} < \alpha < 25^{\circ}$.

Both primary and secondary contract objectives have been successfully accomplished. This report documents the engineering analysis for the Aerodynamics of Separation, AERSEP, computer code satisfying the primary contract objective. The code prepared by Mr. A. Vachris of the Grumman Aerodynamics Department is functionally structured to permit program generalization as future needs may dictate. AERSEP is compatible with the NASA JSC UNIVAC 1108 Executive 8 System. Input data requirements and running time are minimal facilitating its use for parametric studies, test planning, and trajectory analysis.

Technical requirements dictated a non-linear analysis which would reproduce the predominant orbiter-tank aerodynamic interference phenomenon during staging. The selected approach combines principal elements of slender body theory, linear theory, and accepted hypersonic approximations.

The data comparisons in Section 10 of this report indicate AERSEP Orbiter-Tank interference predictions are consistent in accuracy with state-of-the-art computer predictions limited to interference-free or isolated vehicle situations. AERSEP isolated orbiter predictions also show excellent correlation with data.

Results to date indicate that the present AERSEP code can be generalized to cover the mid and high angle-of-attack range. Accomplishing this would require added program logic to phase in the appropriate engineering analysis best suited to each angle-of-attack range. This phasing can become complicated since different criteria would apply to forebodies, afterbodies, and wings. Developing a satisfactory mid α interference analysis may have to be predicated on the availability of isolated orbiter wing-body and body-alone test data. The high α case could be patterned after the analysis of Mr. R. Hendrikson of Grumman already incorporated into a computer code delivered to NASA MSC under the present contract. For the near term it is recommended that AERSEP be modified to accept the glove geometry characteristizing the current Shuttle Orbiter double-delta design. Until such time the present code can be employed in a manner that will approximate the net glove effect.

LIST OF FIGURES

Section 1: General Discussion

Sections 2 through 8 of the present report document the engineering analysis for the AERSEP code. Section 9 summarizes input data requirements and offers practical recommendations on configuration modeling. This section provides a brief overview emphasizing the key assumptions, approximations, and practical expediencies adopted to realize a working code within contract resource limitations.

The major objective is to develop an engineering capability to predict Shuttle Orbiter/HO Tank longitudinal aerodynamic characteristics during staging/abort-separation. The primary flight envelope covers $M \geq 2$ and α between $\pm$ 10 degrees. The crux of the problem is to evaluate the orbiter-tank mutual interference since isolated configuration data are generally available. It is apparent that aerodynamic estimates for the mated vehicle will inherently be less accurate than isolated vehicle predictions since both the flow field and the vehicle loading must now be calculated. Experience suggests that NASA MSC 040-A mated vehicle interference estimates within $\Delta C_m, \Delta C_N \leq .010$ to .015 (based on reference wing area and MAC) are consistent with the accuracy level of such programs as the GAC-HAPP or MacDonnell-Douglas HARB for isolated vehicles. Larger discrepancies would indicate the potential improvement available through further refinement of either the analysis or computer code. A review of AERSEP correlation with NASA test data indicate that the majority of AERSEP estimates satisfy the stated criteria.

The analysis divides into two essential steps; determining the combined flow field of the orbiter-tank combination and evaluating the surface pressure loading on both vehicles. A rigorous solution for either is beyond the state-of-the-art. To break the deadlock AERSEP employs an iterative

approach. The first approxmation assumes that the incident flow on the orbiter is the same as the isolated tank flow field.

The analytic basis for constructing the isolated tank and orbiter flow fields is covered in Sections 2, 3, and 4. Perhaps the most notable feature here is the selection of a Mach dependent non-linear body flow field analysis which accounts for fuselage fineness ratio , camber, and cross-sectional shape effects. The predicted flow fields approach the correct slender body limit for high fineness ratio configurations at low M, low α, ($M \sim 2, \alpha < 10^{\circ}$) and the appropriate hypersonic limit when non-linear effects predominate.

The next step is to evaluate the "Primary Loading" on the orbiter as situated in the isolated tank flow field. Section 5 describing the fuselage primary load evaluation may appear simple, however, success depends critically on the technique employed. The analysis in AERSEP will approximate linear theory results at low Mach number (for slender configurations) and approaches the appropriate hypersonic limit at high Mach number ($M > 5$). Both linear and non-linear contributions are accounted for at intermediate Mach No., α, and fineness ratio.

Primary loads on the orbiter wing are obtained by determining the trace of the tank shock/wing intersection and integrating the non-uniform upwash loading over the affected wing area. Orbiter fuselage-on-wing upwash is allowed for by including a $K_{W(B)}$ interference factor (Section 6). Primary loads for the HO Tank are calculated in the same manner as for the orbiter.

The last phase of the aerodynamic analysis, "reflected waves," is covered in Sections 7 and 8. It was noted earlier that the isolated tank flow field serves as the first approximation to the combined flow field as seen by the orbiter. As a result the primary loads on the orbiter do not include the

effect of orbiter disturbances reflecting off the tank and back onto the orbiter. AERSEP accounts for this by constructing an improved approximation. For the orbiter the incident flow is now taken to be the sum of the isolated tank flow field (first approximation) and a perturbation flow due to the primary loads on the tank. The strength of the outgoing distrubances, i.e., tank reflections, is determined from slender body theory and their outward propagation calculated along the characteristic structure of the isolated tank flow field. The subsequent (improved) loads on the orbiter are then calculated in much the same manner as the primary loads.

At this point the aerodynamic loading on the tank and orbiter in proximity have been evaluated. To obtain the corresponding interference characteristics the isolated orbiter and tank loading must also be calculated. Isolated orbiter force and moment characteristics are handled as a special case by the AERSEP primary loading subroutines.

Comparison of AERSEP estimates and wind tunnel data for the isolated tank shows a consistent tendency to underestimate normal force and pitching moment. This is attributed to tank forebody-on-afterbody lift carryover not accounted for in the current AERSEP code. Although the net effect of this carryover on orbiter-tank interference estimates should be less (compensating effects) their inclusion in AERSEP is one potential area for refinement. Wing twist and camber are also not accounted for in AERSEP since their net effect on orbiter-tank interference is small compared to root incidence and angle-of-attack. The only consequence is that C_{m_0} estimates for the isolated orbiter are invalid. AERSEP isolated longitudinal stability estimates, however, show excellent agreement with NASA MSC 040-A data at M = 1.96 and 4.0 using $K_{W(B)} = 1.0$ (see Figure 10.3).

AERSEP aerodynamic and geometric input data requirements are treated in Section 9. It may be noted that only a minimum of "set up time" is required. Computer running time is low, approximately 9 CPU seconds for 6 vertical separations at a given M, α, and incidence on the IBM 370/165.

Section 2: Isolated Flowfield - HO Tank

The Shuttle Orbiter wing-body flowfield in AERSEP is represented by an overlay of the isolated fuselage and exposed wing flows. Since the general approach is simply an extension of that for the HO Tank it is expedient to begin with the isolated tank analysis.

The tank consists of a blunted nose cone, Sketch 2-A, followed by a constant diameter cylindrical section with a short boat-tail.

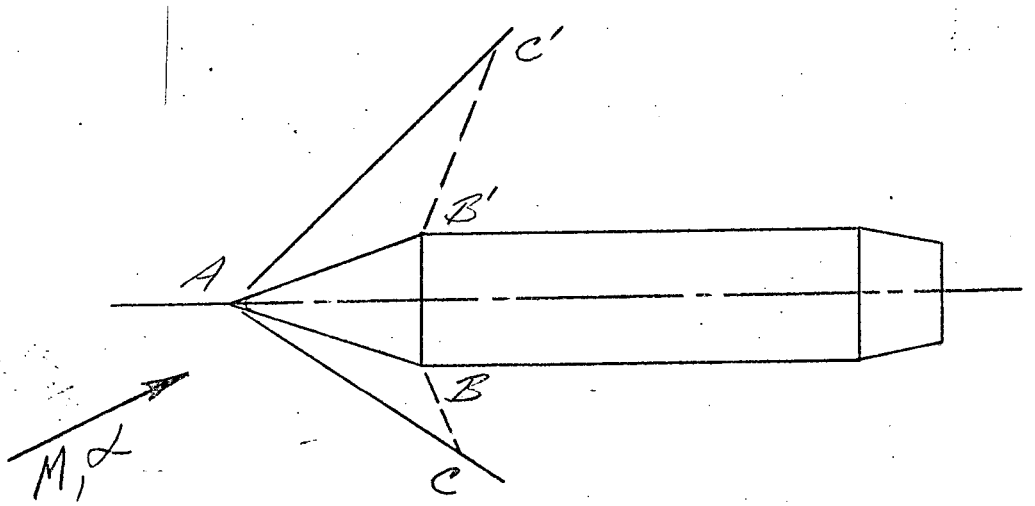

SKETCH 2-A: NOSE CONE FLOWFIELD

Ignoring tip blunting the nose flow is conical throughout the region ABC, AB'C' determined by the closing characteristics (Mach waves BC and B'C') defining the upstream influence of the shoulder. All flow variables in this region can be obtained from the exact inviscid flow tabulations in Reference 1 and 2 for unyawed/yawed pointed cones. For obvious reasons these numerical data had to be condensed before inclusion into the AERSEP code, specifically into four correlation plots.

The windward centerline surface pressure is given by the expression

$$C_{p_S} = C_{p_{OS}} + \Delta C_{p_{\alpha^*_S}} \qquad \text{Eq. 2:1}$$

where

$C_{p_{OS}}$ = cone surface pressure coefficient at $\alpha = 0$

$\Delta C_{p_{\alpha^*_S}}$ = increment in surface pressure due to angle of attack, α^*

The zero angle-of-attack term is obtained from Figure 2-1 where $C_{p_{OS}} / TAN^2 \theta_c$ (θ_c = cone half angle) is correlated with the supersonic-hypersonic simularity parameter $\beta\, TAN\, \theta_c = \sqrt{M_\infty^2 - 1}\; TAN\, \theta_c$.

The numerical data in this figure are from Ref. 1. Note that for large β Tan θ_C the exact cone solutions approach the Newtonian result $C_p / TAN^2 \theta_c = 2 Cos^2 \theta_c$. For moderate or low βTan θ_C, however, the C_p at $\alpha = 0$ is substantially greater than given by Newtonian. AERSEP calculations are based on the faired curve shown.

The second term in Eq. 2:1 accounts for angle-of-attack effects on the nose cone surface pressure. Despite the fact that Newtonian theory does not consistently give good results for the surface pressure at $\alpha = 0$ it adequately predicts the change in surface pressure with angle-of-attack. This is amply demonstrated in Figure 2-1. Accordingly,

$$\Delta C_{p_{\alpha^*_S}} = 2\{SIN^2(\theta_c + \alpha) - SIN^2 \theta_c\} \qquad \text{Eq. 2:2}$$

WINDWARD

Similarly, for the leeward centerline

$$\Delta C_{p_{\alpha^*_S}} = 2\{SIN(\theta_c - \alpha) SIN(\theta_c - \alpha) - SIN^2 \theta_c\} \qquad \text{Eq. 2:3}$$

These equations, Eq. 2:1, and Figure 2-1 determine the cone centerline surface pressures for $\beta TAN\,\theta_c \geq .0.15$.

The corresponding nose cone shock wave strength is determined from the equation

$$C_{p_W} = \left[\frac{C_{p_{oW}}}{C_{p_{oS}}}\right] C_{p_{oS}} + \left[\frac{dC_{p_W}/d\alpha}{dC_{p_S}/d\alpha}\right] \Delta C_{p_{\alpha^* S}} \qquad \text{Eq. 2:4}$$

where

$C_{p_{oW}}$ = static pressure coefficient immediately behind wave at $\alpha = 0$

The wave to surface pressure ratio at $\alpha = 0$ appearing in the first term is given by the correlation in Figure 2-3. This plot also demonstrates that most of the cone surface pressure rise at low $\beta TAN\,\theta_c$ is the result of isentropic compression through the cone shock layer. Conversely, shock compression is the dominant mechanism at large $\beta TAN\,\theta_c$. Angle-of-attack effects on C_{p_W} are given by the second term in Eq. 2:4 where the ratio $(dC_{p_W}/d\alpha)/(dC_{p_S}/d\alpha)$ is given in Figure 2-4. The selected AERSEP fairing favors are the most significant Shuttle cases, i.e., $\theta_c \leq 25^\circ$, $\alpha \leq 10^\circ$.

Once C_{p_W} is known the shock wave angle, θ_W, (relative to the freestream) can be calculated from the equations:

$$\left.\begin{array}{l} \text{IF } C_{p_W} \leq 0 : \text{ SET } \quad C_{p_W} = 0 \\ M_W = M_\infty \\ \delta_W = 0 \end{array}\right\} \qquad \text{Eq. 2:5}$$

IF $C_{P_W} \geq 0$: (SEE REF 3)

$$M_{I_N} = \left\{ 1 + \frac{3\gamma}{7} M_\infty^2 C_{P_W} \right\}^{1/2} \qquad \text{Eq. 2:6}$$

$$\sin \theta_W = M_{I_N} / M_\infty \qquad \text{Eq. 2:7}$$

$$\tan S_W = \frac{5 \cot \theta_W (M_{I_N}^2 - 1)}{5 + M_\infty^2 (6 - 5 \sin^2 \theta_W)} \qquad \text{Eq. 2:8}$$

$$M_W^2 = \frac{36 M_\infty^2 M_{I_N}^2 - 5(M_{I_N}^2 - 1)(7 M_{I_N}^2 + 5)}{(7 M_{I_N}^2 - 1)(M_{I_N}^2 + 5)} \qquad \text{Eq. 2:9}$$

where

M_{I_N} = component of freestream Mach No. normal to shock wave

S_W = flow deflection through shock

M_W = Mach No. immediately behind shock wave

At this point all essential flow properties at the shock and surface are known with the exception of the surface Mach No., M_S . The latter is related to M_W by the isentropic relation

$$M_S^2 = 5\left\{\left(1 + \frac{M_W^2}{5}\right)\left(\frac{P_S}{P_W}\right)^{-2/7} - 1\right\} \qquad \text{Eq. 2:10}$$

Flow properties within the shock layer are evaluated assuming a linear variation with distance between the cone surface and shock.

A special provision is included in AERSEP to preclude the predicted pressure from falling below the base pressure level $c_{p_b} \simeq -1/M_\infty^2$. In the event lower pressures are predicted the code over-rides the prediction with a $c_p = -1/M_\infty^2$ statement. This requirement is justified by available high speed orbiter pressure data.

The HO tank flow development downstream of the nose cone is characterized by an expansion fan emanating from the shoulder as shown in Sketch 2-B. In AERSEP the overall fan is subdivided into small expansion fan increments which describe the progressive surface flow turning from θ_c (relative to the tank FRL) on the nose to 0° on the cylindrical tank section. In two dimensional flow the required Mach No. variation with expansive flow turning angle can be determined from the well known Prandtl-Meyer relation. This equation, however, is not generally applicable in three dimensional flow and gives completely erroneous results near the shock wave at low supersonic Mach Nos. In AERSEP the problem is resolved by visualizing the expansion fan as a succession of conical flows generated by a stacked set of cone frustrums as in Sketch 2-C below.

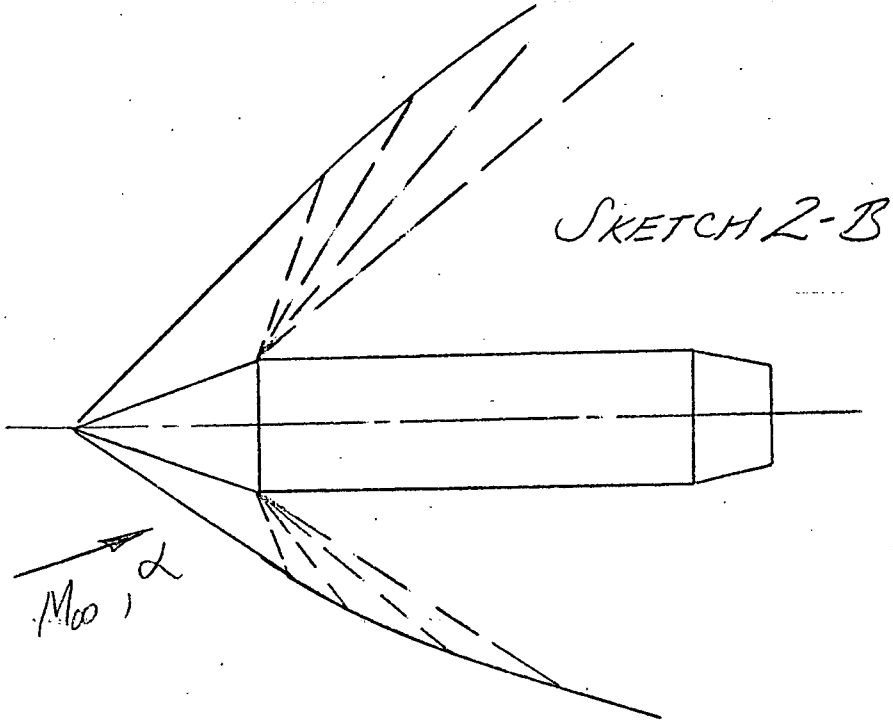

SKETCH 2-B: EXPANSION FAN FLOWFIELD

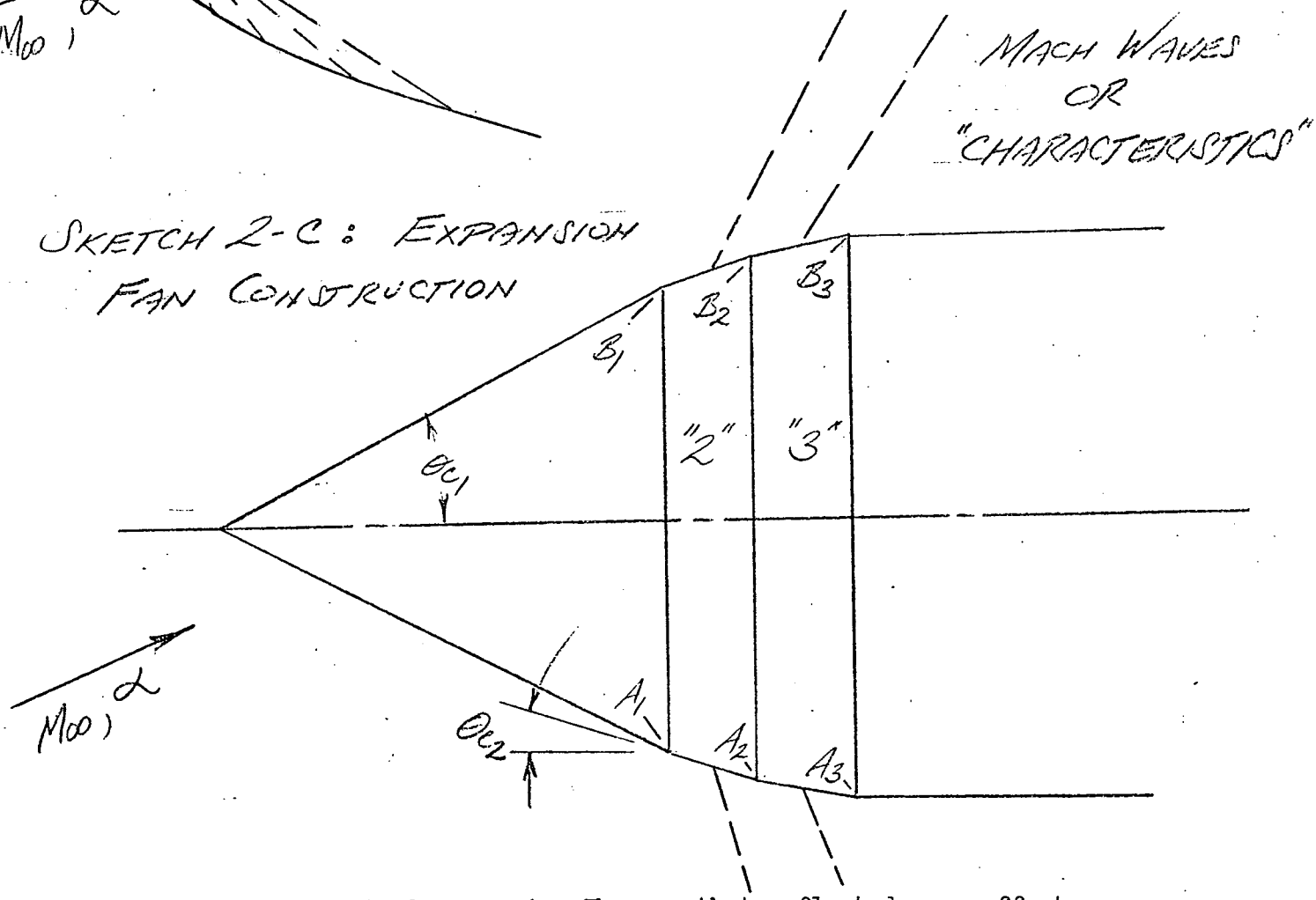

SKETCH 2-C: EXPANSION FAN CONSTRUCTION

Assuming, as in Shock-Expansion Theory, that reflected wave effects are negligible it follows that the flow properties along the outgoing characteristic from "Frustrum 2" are identical to those for the conical flow field generated by a pointed cone of half angle θ_{c_2}. This means that the surface and shock wave properties for each frustrum can be determined in exactly the same manner as for the nose cone. For the HO tank in Sketch 2-B

the cone-cylinder shoulder is treated as a limiting case of the geometry in Sketch 2-C, i.e., B_1, B_2, B_3 coalesce at the corner.

A substantially different analysis must be employed to determine the flow field generated by the cylindrical section of the tank where $\beta \tan \theta_c = 0$. AERSEP's description in this region is based on yawed cylinder reasoning. The prescribed centerline surface c_p variation with α is given by the following equations.

Lower Surface

IF: $\alpha \leq -M_\infty$ Eq. 2:11

$$c_{p_s} = -2\left(\frac{c_D}{2}\right) \sin^2(-M_\infty)$$

IF: $-M_\infty \leq \alpha \leq 0$ Eq. 2:12

$$c_{p_s} = -2\left(\frac{c_D}{2}\right) \sin^2(-\alpha)$$

IF: $0 \leq \alpha \leq M_\infty$ Eq. 2:13

$$c_{p_s} = 0$$

IF: $M_\infty \leq \alpha$ Eq. 2:14

$$c_{p_s} = 2\left(\frac{c_D}{2}\right)\left\{\sin^2(\alpha) - \sin^2(M_\infty)\right\}$$

Upper Surface

IF: $\alpha \geq \mu_\infty$ Eq. 2:15

$$C_{p_S} = -2\left(\frac{C_D}{2}\right) SIN^2(-\mu_\infty)$$

IF: $0 \leq \alpha \leq \mu_\infty$ Eq. 2:16

$$C_{p_S} = -2\left(\frac{C_D}{2}\right) SIN^2(-\alpha)$$

IF: $-\mu_\infty \leq \alpha \leq 0$ Eq. 2:17

$$C_{p_S} = 0$$

IF: $\alpha \leq -\mu_\infty$ Eq. 2:18

$$C_{p_S} = 2\left(\frac{C_D}{2}\right)\left\{SIN^2(\alpha) - SIN^2(\mu_\infty)\right\}$$

A little patience will verify that the foregoing equations give the C_p variation shown in Sketch 2-D(a) and 2-D(b) for the upper and lower centerlines respectively. The resulting $C_{p_\ell} - C_{p_u}$ varies as shown in Sketch 2-D(c). Interpreting C_{p_ℓ} and C_{p_u} as average pressures acting over the full width of the tank cylinder, it follows that the normal force per unit length of tank cylinder is

$$\frac{N}{qD\Delta X} = 2\left(\frac{C_D}{2}\right) SIN^2\alpha \qquad \text{Eq. 2:19}$$

For $\alpha > \mu_\infty$, i.e., for supersonic crossflow, Newtonian theory and test data predict $\frac{C_D}{2} = 0.67$ for a circular cross-section. For $\alpha \leq \mu_\infty$,

i.e., subsonic crossflow, the data of Ref. 4 indicates $\frac{C_D}{2} \simeq .5$ to .65. For practical purposes one can assume the crossflow C_D is constant for all M and α. The only significant flowfield distinction between the subsonic and supersonic crossflow case is that leeward base drag is predominant in the former while windward pressure drag (shock wave drag) dominates in latter. This distinction is recognized in AERSEP by the surface C_p formulation given in Eqs. 11 through 18.

The corresponding shockwave properties for the tank-cylinder are given by Eqs. 2:20 to 2:28 below.

Lower Surface

IF $\alpha \leq -\mu_\infty$ Eq. 2:20

$C_{p_W} = 0, \quad M_W = M_\infty$

θ_W (REL TO FRL) $= \alpha - \mu_\infty$

θ_{fW} (REL TO FRL) $= \alpha$

θ_{fW} = FLOW DIRECTION IMMEDIATELY BEHIND SHOCKWAVE

IF $-\mu_\infty \leq \alpha \leq 10$ Eq. 2:21

$C_{p_W} = 0, \quad M_W = M_\infty$

θ_W (REL TO FRL) $= \alpha - \mu_\infty$

θ_{fW} (REL TO FRL) $= \alpha$

IF: $0 \leq \alpha \leq M_\infty$ Eq. 2:22

$C_{P_W} = 0$, $M_W = M_\infty$

θ_W (REL TO FRL) $= \alpha - M_\infty$

θ_{f_W} (REL TO FRL) $= \alpha$

IF: $M_\infty \leq \alpha$ Eq. 2:23

θ_W (REL TO FRL) $= 0$

θ_{f_W} (REL TO FRL) $= 0$

$$C_{P_W} = 2\left(\frac{C_D}{2}\right)\left\{\sin^2\alpha - \sin^2 M_\infty\right\}$$

i.e., $C_{P_W} = C_{P_S}$

$$M_{IN}^2 = \frac{36 M_\infty^2 M_{IN}^2 - 5(M_{IN}^2 - 1)(7M_{IN}^2 + 5)}{(7M_{IN}^2 - 1)(M_{IN}^2 + 5)}$$

WHERE

$$M_{IN} = \left\{1 + \frac{35}{7} M_\infty^2 C_{P_W}\right\}^{1/2}$$

Surface Mach No., M_S , for each of the above can be determined from the isentropic relation

$$M_S^2 = 5\left\{\left(1+\frac{M_W^2}{5}\right)\left(\frac{P_S}{P_W}\right)^{-2/7}-1\right\} \qquad \text{Eq. 2:24}$$

Upper Surface

IF: $\alpha \geq M_\infty$ Eq. 2:25

$C_{P_W} = 0$, $M_W = M_\infty$

θ_W (REL TO FRL) $= \alpha + M_\infty$

θ_{W_f} (REL TO FRL) $= \alpha$

IF: $0 \leq \alpha \leq M_\infty$ Eq. 2:26

$C_{P_W} = 0$, $M_W = M_\infty$

θ_W (REL TO FRL) $= \alpha + M_\infty$

θ_{W_f} (REL TO FRL) $= \alpha$

IF: $-M_\infty \leq \alpha \leq 0$ Eq. 2:27

$C_{P_W} = 0$, $M_W = M_\infty$

θ_W (REL TO FRL) $= \alpha + M_\infty$

θ_{W_f} (REL TO FRL) $= \alpha$

IF: $\alpha \leq -M_\infty$ Eq. 2:28

θ_W (REL TO FRL) $= 0$

θ_{W_f} (REL TO FRL) $= 0$

$C_{P_W} = 2\left(\frac{C_D}{2}\right)\left\{\sin^2\alpha - \sin^2 M_\infty\right\}$

M_W FROM Eq. 2:23

Upper surface Mach No., M_S , is again calculated from M_W and Eq. 2:24

Discussion of the tank boat-tail and base expansion flowfields will be deferred to the next section where arbitrary bodies (non-axisymmetric and cambered) are considered.

SKETCH 2-D

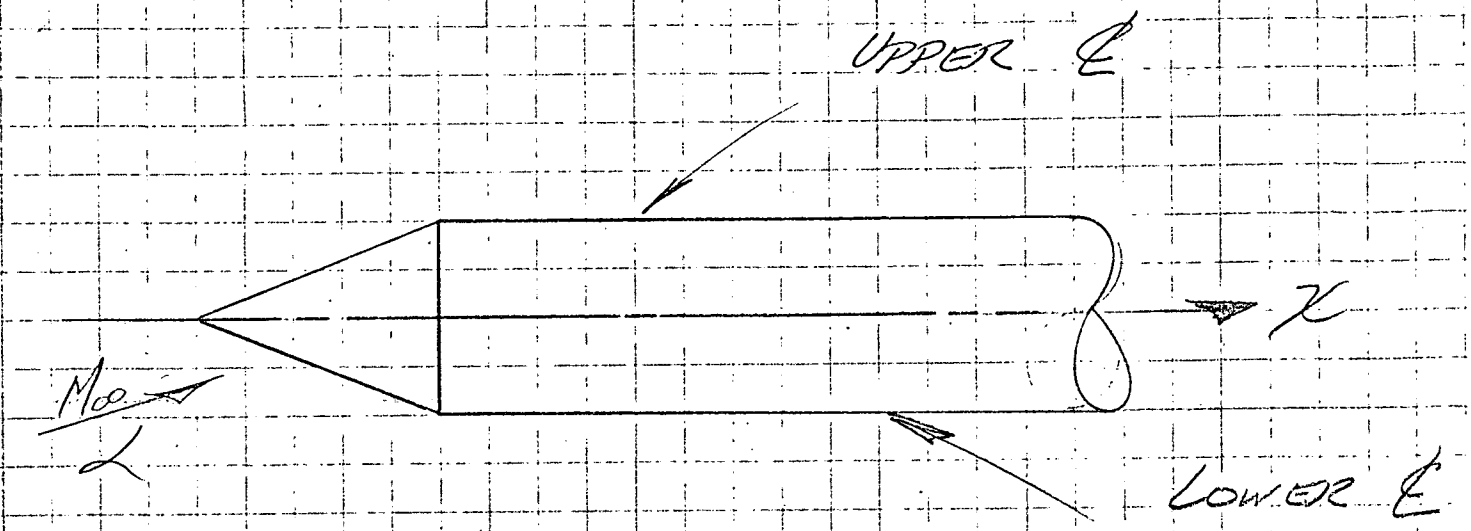
UPPER ℄
X
M_∞
α
LOWER ℄

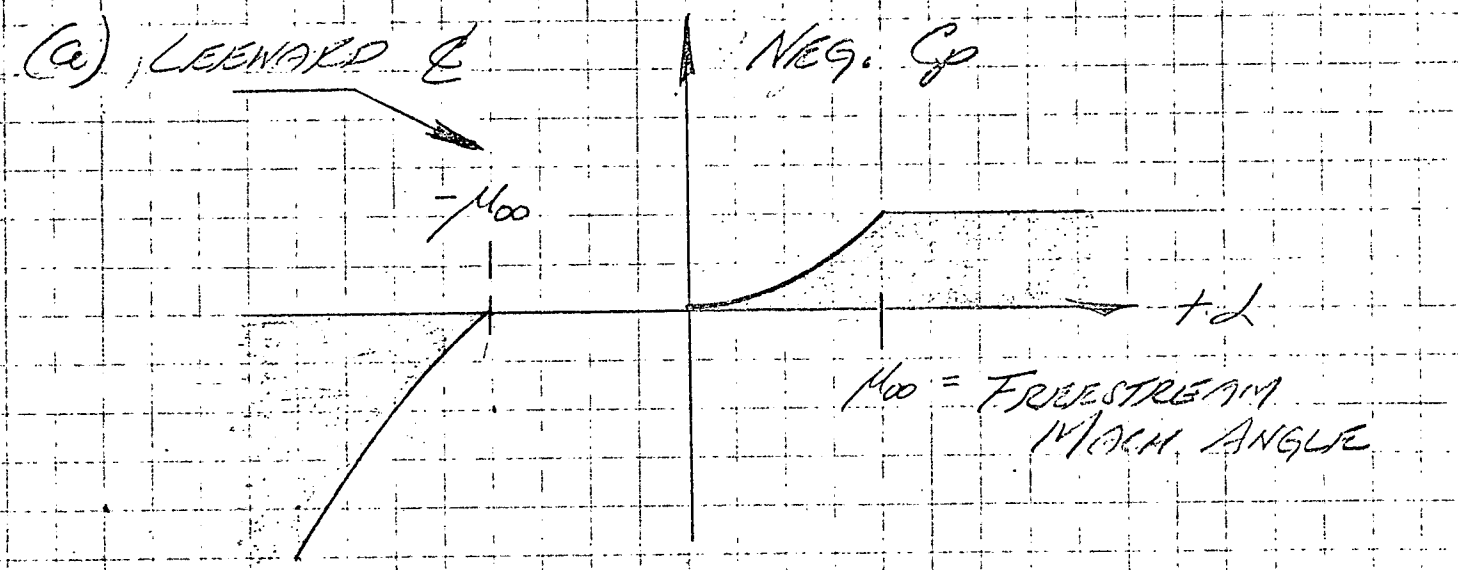
(a) LEEWARD ℄
NEG. C_p
$-\mu_\infty$
$+\alpha$
M_∞ = FREESTREAM MACH ANGLE

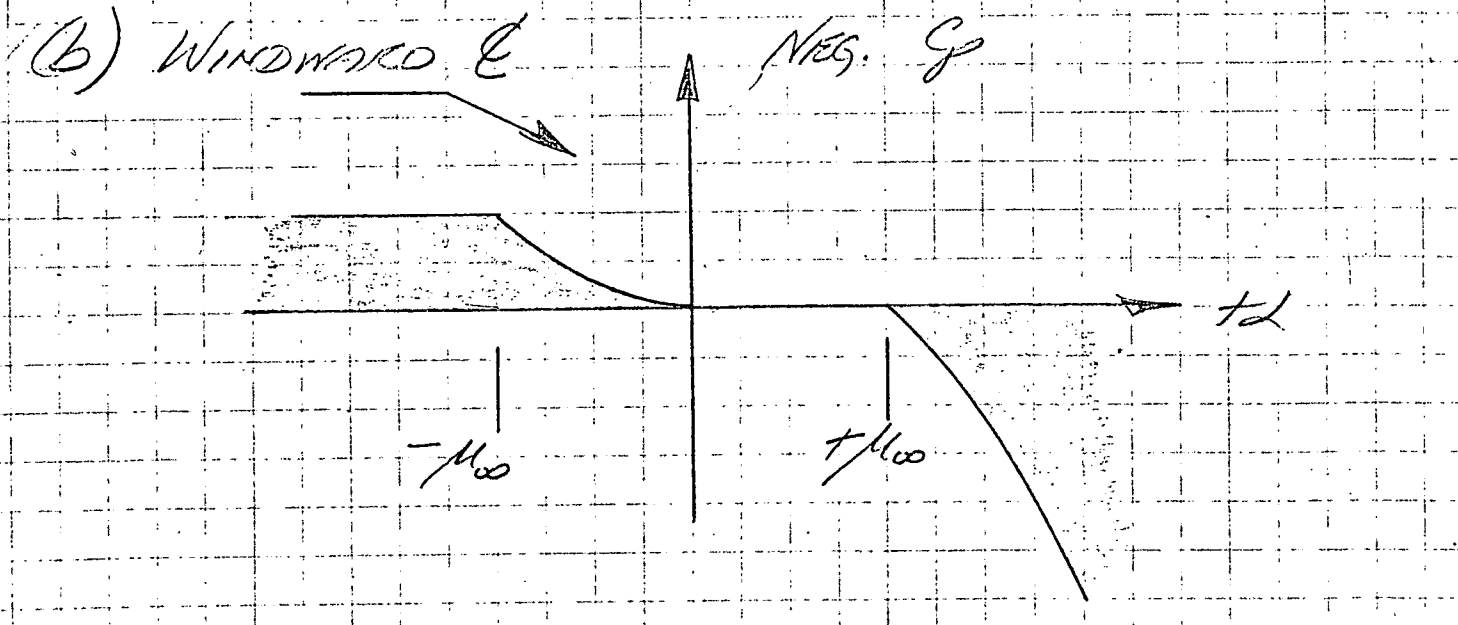
(b) WINDWARD ℄
NEG. C_p
$+\alpha$
$-\mu_\infty$
$+\mu_\infty$

SKETCH 2-D (C) $C_{p_l} - C_{p_u}$

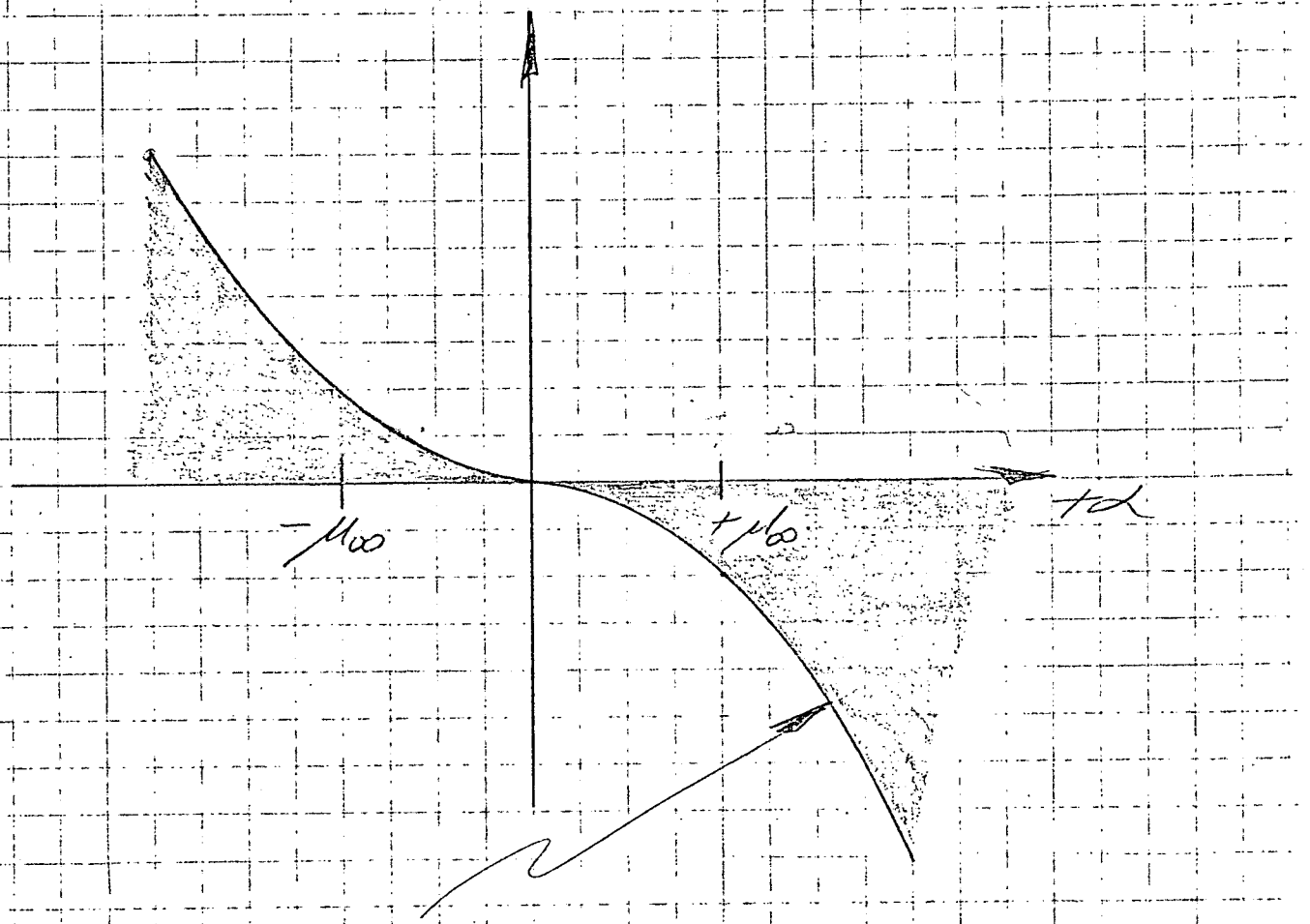

$$C_{p_l} - C_{p_u} = 2\left(\frac{C_D}{2}\right) \sin^2 \alpha$$

NO. 340-L220 DIETZGEN GRAPH PAPER
SEMI-LOGARITHMIC
2 CYCLES X 20 DIVISIONS PER INCH

EUGENE DIETZGEN CO.
MADE IN U. S. A.

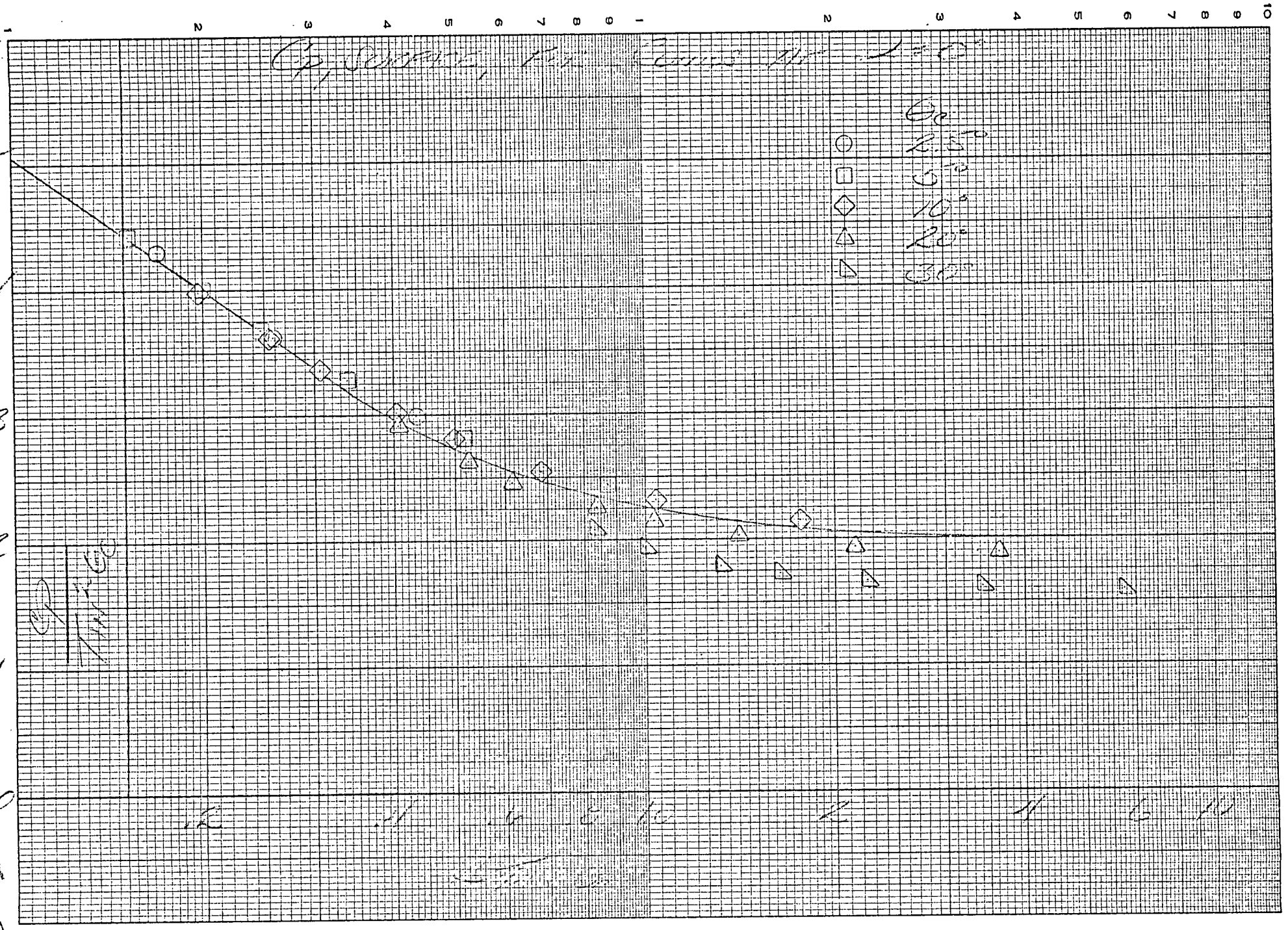

NO. 340-L220 DIETZGEN GRAPH PAPER
SEMI-LOGARITHMIC
2 CYCLES X 20 DIVISIONS PER INCH

EUGENE DIETZGEN CO.
MADE IN U. S. A.

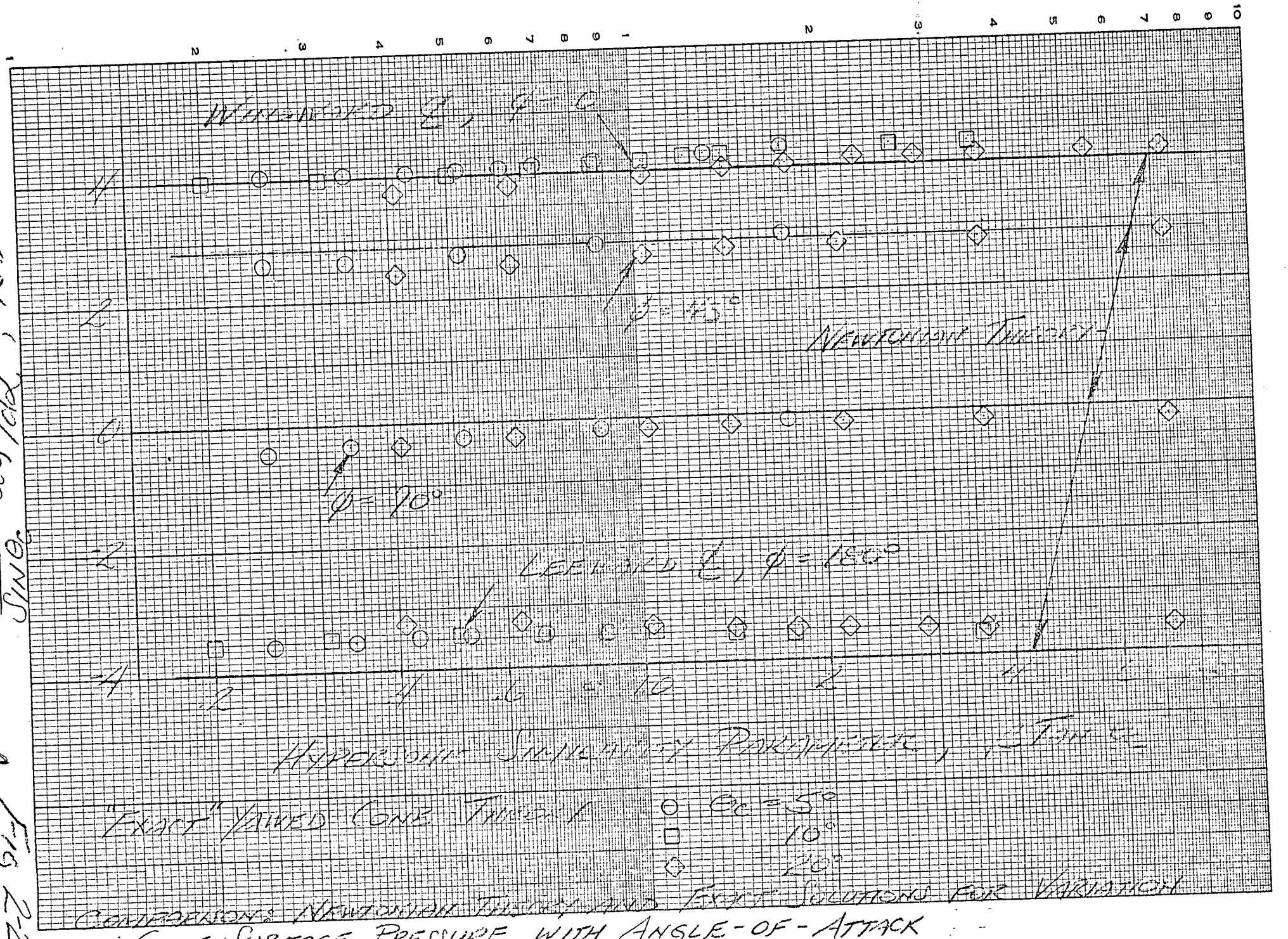

NO. 340-L220 DIETZGEN GRAPH PAPER
SEMI-LOGARITHMIC
2 CYCLES X 20 DIVISIONS PER INCH

EUGENE DIETZGEN CO.
MADE IN U. S. A.

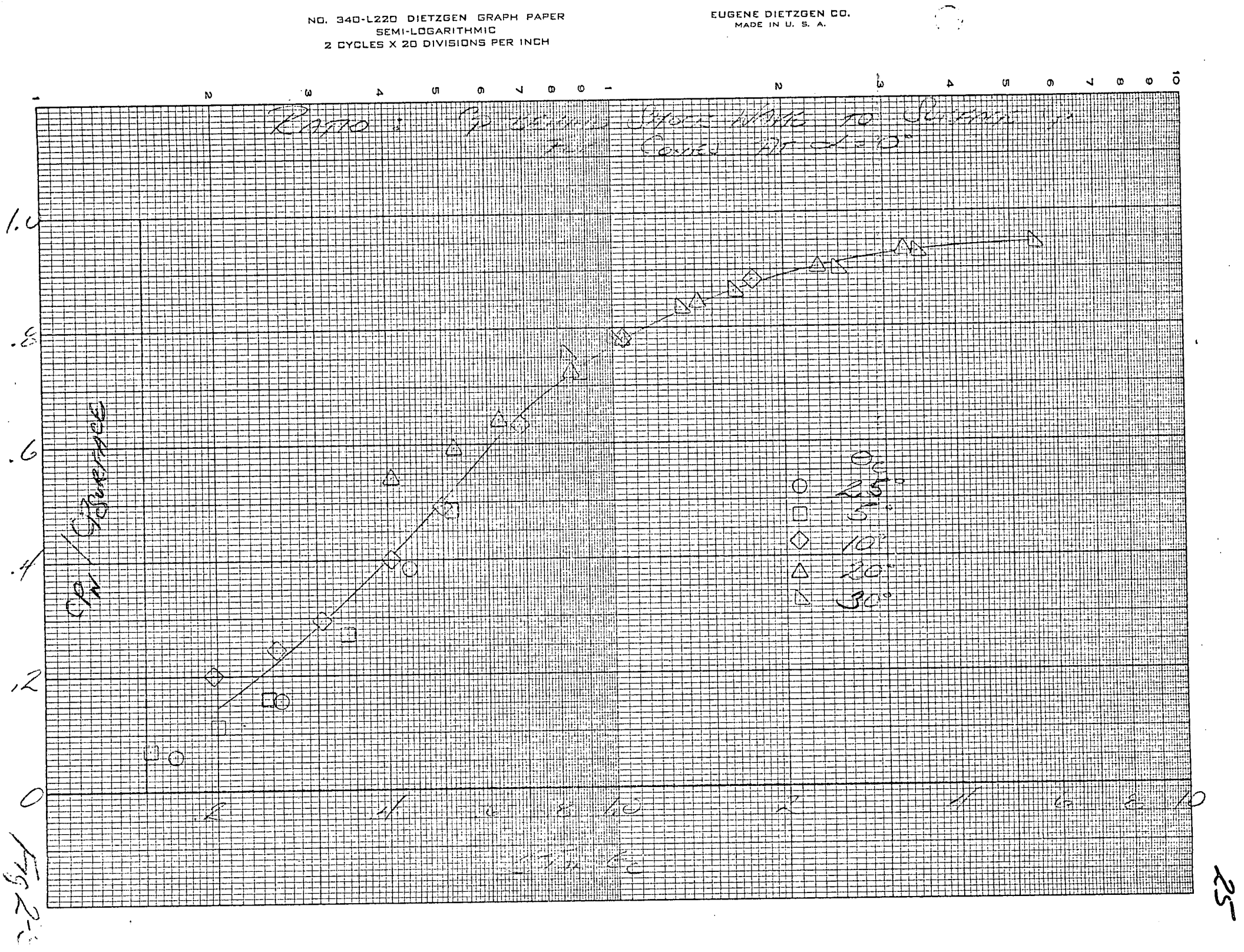

NO. 340-L220 DIETZGEN GRAPH PAPER
SEMI-LOGARITHMIC
2 CYCLES X 20 DIVISIONS PER INCH

EUGENE DIETZGEN CO.
MADE IN U. S. A.

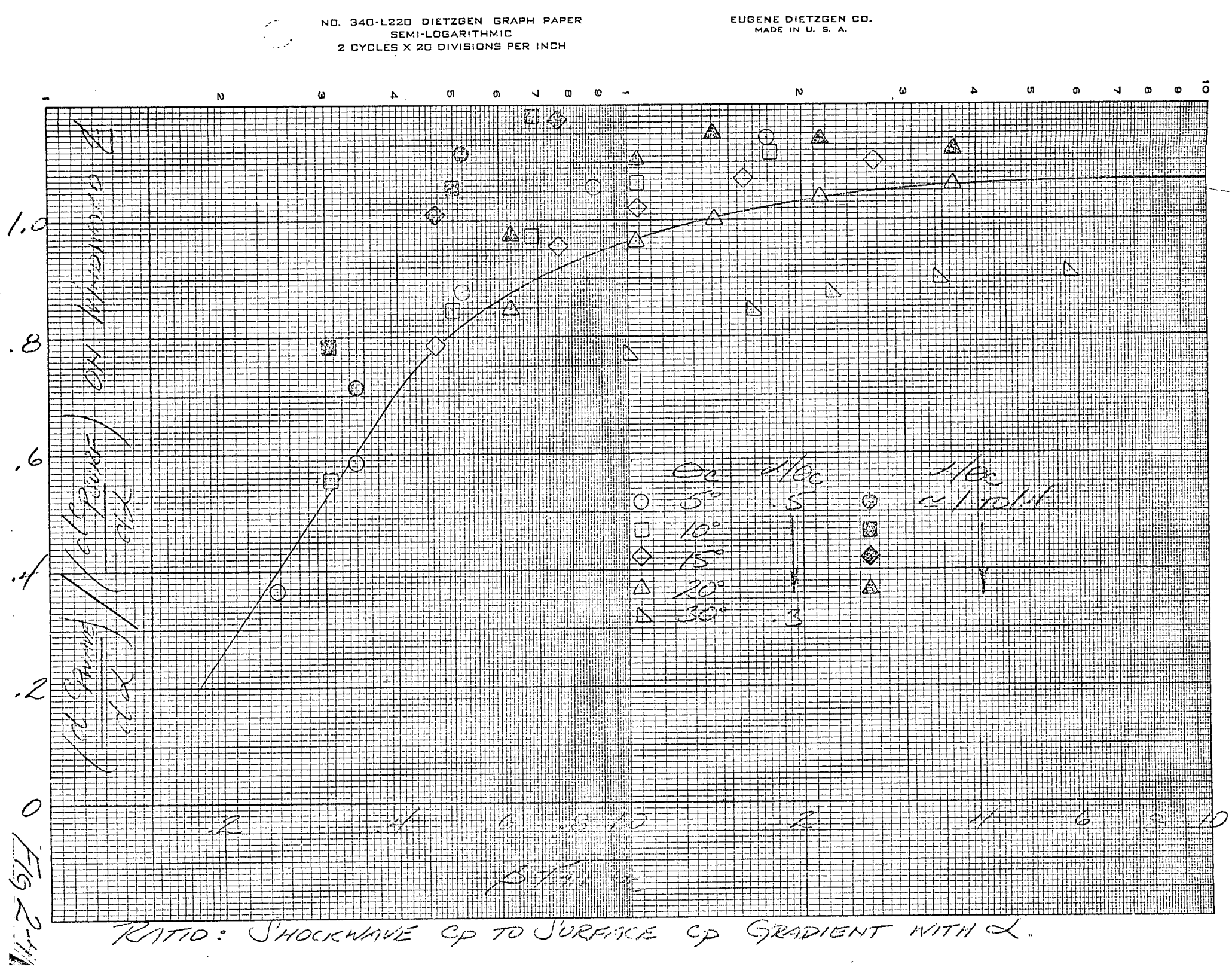

Ratio: Shockwave cp to Surface cp Gradient with L.

Section 3: Isolated Flowfield - General Body Shapes

An engineering method for calculating the isolated flow field surrounding the Shuttle Orbiter fuselage is given below. The general approach is a direct extension of that for the isolated tank and includes the effect of non-circular cross-sections and fuselage camber. The required geometry data are indicated in Sketch 3-A.

The orbiter fuselage "true" inboard profile in Sketch 3-A is taken directly from the configuration lines drawing. AERSEP approximates the true profile by cutting the fuselage into a series of "plugs" with straight line connects between controlling fuselage stations, e.g., FS 155, 250, 450, 600, 800, etc. The following geometrical input data are required at the selected fuselage control stations.

Z_u = Z to upper surface of true inboard profile

Z_ℓ = Z to lower surface of true inboard profile

Z_{e_u} = Z to upper surface of "effective" inboard profile (see Sketch 3-B)

Z_{e_ℓ} = Z to lower surface of "effective" inboard profile (see Sketch 3-B)

W = Fuselage width

These data are used by AERSEP to calculate the following derived geometric information.

$S(x)$ = Cross-sectional area at designated fuselage control station

$$S = W(Z_{e_u} - Z_{e_\ell}) \qquad \text{Eq. 3:1}$$

Z_c = Z distance to centroid of cross-sectional area at designated fuselage control stations

Eq. 3:2

θ_{cn} = Equivalent cone angle for n'th fuselage plug

Eq. 3:3

$$TAN\,\theta_{cn} = \frac{S_{n+1}^{1/2} - S_n^{1/2}}{\pi^{1/2}(x_{n+1} - x_n)}$$

i_{cn} = Equivalent cone incidence for n'th plug

$$TAN\,i_{cn} = \frac{z_{cn} - z_{cn+1}}{x_{n+1} - x_n}$$ Eq. 3:4

$i_{\ell n}$ = Lower surface incidence of n'th plug

$$TAN\,i_{\ell n} = \frac{z_{\ell n} - z_{\ell n+1}}{x_{n+1} - x_n}$$ Eq. 3:5

i_{un} = Upper surface incidence of n'th plug

$$TAN\,i_{un} = \frac{z_{un} - z_{un+1}}{x_{n+1} - x_n}$$ Eq. 3:6

The total fuselage flow is constructed by overlaying the individual flows generated by each fuselage plug. Each plug in turn is considered to be a yawed equivalent cone (at angle-of-attack and incidence) which has been distorted to conform to the actual fuselage cross-sectional. The expression for surface pressure is accordingly made up of three terms;

$$c_{p_s} = c_{p_{o_s}} + \Delta c_{p_{s\alpha^*}} + \Delta c_{p_{s\alpha_t}}$$ Eq. 3:7

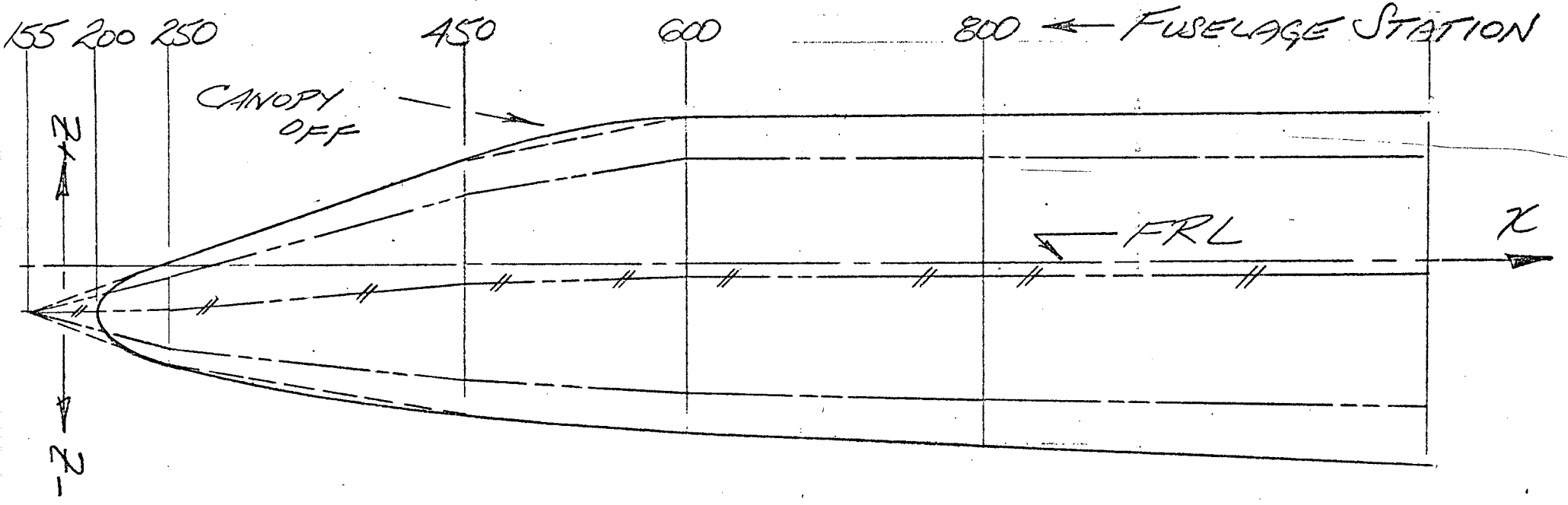

SKETCH 3A: ORBITER FUSELAGE GEOMETRY

TRUE ORBITER FUSELAGE INBOARD PROFILE

AERSEP APPROXIMATE ORBITER FUSELAGE INBOARD PROFILE USED IN FLOW FIELD CALCULATION

AERSEP FUSELAGE MEAN CAMBER LINE

AERSEP "EFFECTIVE" ORBITER FUSELAGE INBOARD PROFILE USED IN EVALUATION OF AERODYNAMIC LOADS

FS 450, CROSS-SECTION

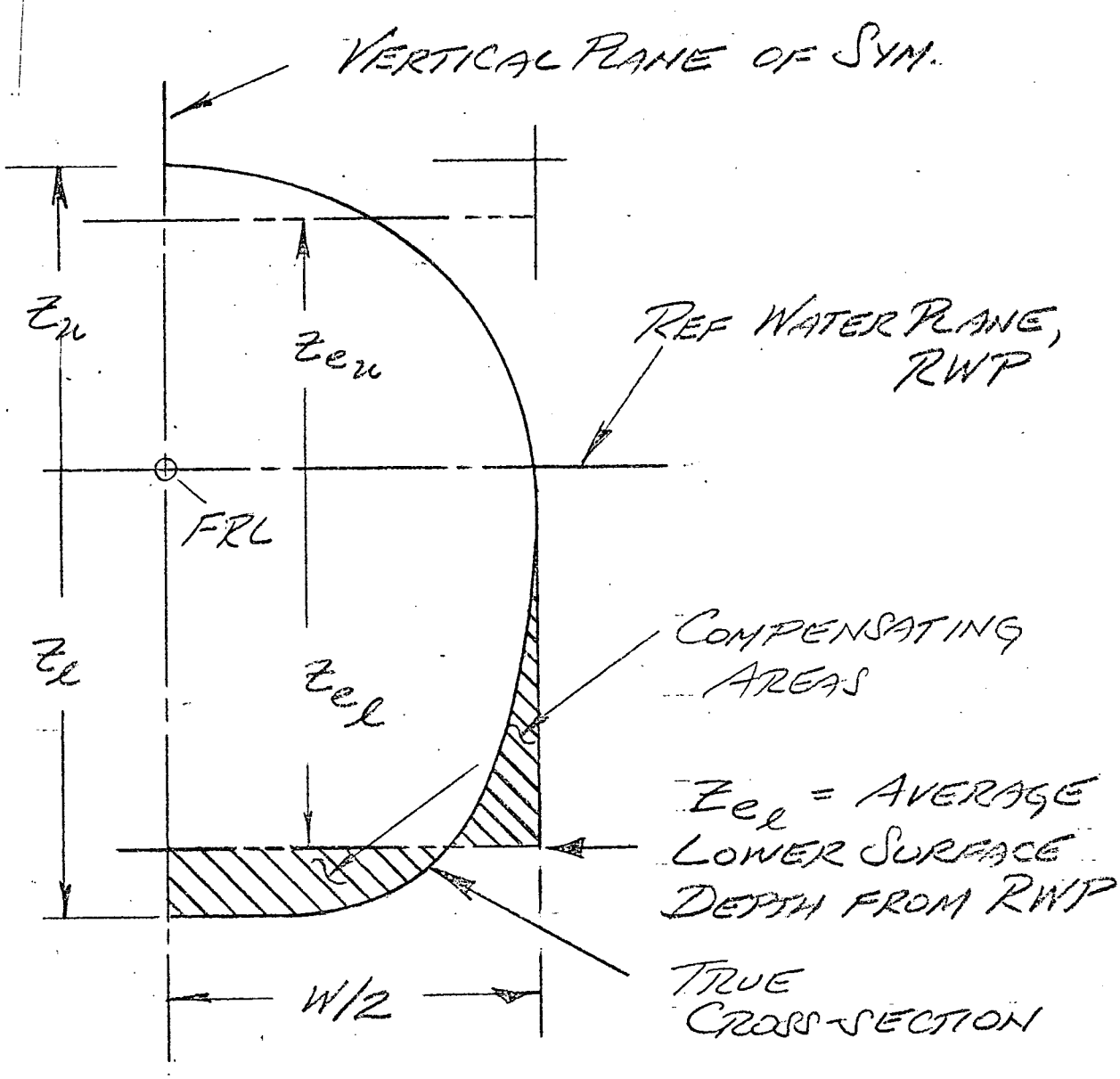

SKETCH 3B TYPICAL CROSS-SECTION AND "EFFECTIVE" HEIGHT

where

$C_{p_{OS}}$ = Surface pressure coefficient on "equivalent" cone at $\alpha = 0$

$\Delta C_{p_{S\alpha^*}}$ = Increment to surface pressure coefficient due to equivalent cone angle-of-attack plus incidence = α^*

$\Delta C_{p_{S\alpha t}}$ = Increment to surface pressure coefficient due to distorting the "equivalent" circular cone to the actual fuselage cross-sectional shape.

These are evaluated as follows:

$C_{p_{OS}}$ — from Figure 2-1

$$\Delta C_{p_{S\alpha^*}} = 2\left(\underbrace{|\sin(\theta_c+\alpha+i_c)|\sin(\theta_c+\alpha+i_c)}_{\text{(lower surface)}} - \sin^2\theta_c\right) \qquad \text{Eq. 3:8}$$

$$\Delta C_{p_{S\alpha^*}} = 2\left(\underbrace{|\sin(\theta_c-\alpha-i_c)|\sin(\theta_c-\alpha-i_c)}_{\text{(upper surface)}} - \sin^2\theta_c\right) \qquad \text{Eq. 3:9}$$

$$\Delta C_{p_{S\alpha t}} = 4\sin\theta_c\cos\theta_c\,\alpha_{t_\ell} \qquad \text{Eq. 3:10}$$

$$\alpha_{t_\ell} = i_\ell - \underbrace{(\theta_c+i_c)}_{\text{LOWER SURFACE}} \qquad \text{Eq. 3-11}$$

$$\Delta C_{p_{S\alpha t}} = 4\sin\theta_c\cos\theta_c\,\alpha_{t_u} \qquad \text{Eq. 3:12}$$

$$\alpha_{t_u} = -i_u - \underbrace{(\theta_c-i_c)}_{\text{UPPER SURFACE}} \qquad \text{Eq. 3-13}$$

The rationale and justification underlying the C_{p_o} and $\Delta C_{p_{\alpha^*}}$ contributions was treated earlier (Eq. 2:1). Justification for the $\Delta C_{p_{\delta t}}$ term as given in Eq. 3:10 and 3:12 paralles that for the $\Delta C_{p_{\alpha^*}}$ contribution, Eq. 3:8 and 3:9. In each case it is assumed that the effect of local panel angle-of-attack changes due to the angle-of-attack, α_{FRL}, incidence, i_c; and distortion to a non-circular cross-section can be evaluated using Newtonian Theory. Figure 2-2 substantiates this assumption for α_{FRL} effects and by inference for i_c effects. Figure 3-1 and 3-2 provide additional justification and demonstrate the suitability of Eqs. 3:7 thru 3:13 as a general method for evaluating the orbiter fuselage surface pressure distribution.

A similar procedure is used to determine the shock wave properties corresponding to a fuselage "plug". The pressure coefficient immediately behind the shock is given by

$$C_{p_W} = C_{p_{o_W}} + \Delta C_{p_{W_{\alpha^*}}} + \Delta C_{p_{W_{\delta t}}} \qquad \text{Eq. 3:14}$$

where

$C_{p_{o_W}}$ = Surface pressure coefficient behind shock wave of "equivalent" cone at $\alpha = 0$

$\Delta C_{p_{W_{\alpha^*}}}$ = Increment to shock wave pressure due to equivalent cone angle-of-attack plus incidence, α^*

$\Delta C_{p_{W_{\alpha_t}}}$ = Increment to shock wave pressure due to distorting the "equivalent" circular cone to the actual fuselage cross-sectional shape.

These terms are evaluated as follows:

$C_{p_{o_W}}$ FROM FIG 2-3

$$\Delta C_{p_{W_{\alpha^*}}} = \left[\frac{dC_{p_W}/d\alpha}{dC_{p_S}/d\alpha}\right] \Delta C_{p_{S_{\alpha^*}(\ell)}} \qquad \text{Eq. 3:15}$$

$\left[\frac{dC_{p_W}/d\alpha}{dC_{p_S}/d\alpha}\right]$ FROM FIG 2-4

(lower surface)

$$\Delta C_{p_{W_{\alpha^*}}} = -\left[\frac{dC_{p_W}/d\alpha}{dC_{p_S}/d\alpha}\right] \Delta C_{p_{S_{\alpha^*}(u)}} \qquad \text{Eq. 3:16}$$

(upper surface)

$$\Delta C_{p_{W_{\alpha_t}}} = \left[\frac{dC_{p_W}/d\alpha_t}{dC_{p_S}/d\alpha_t}\right](dC_{p_S}/d\alpha_t)\alpha_{t_l} \quad \text{Eq. 3:17}$$

$$\alpha_{t_l} = i_l - (\theta_c + i_c) \quad \text{Eq. 3:18}$$

$$dC_{p_S}/d\alpha_t = 4 \sin\theta_c \cos\theta_c \quad \text{Eq. 3:19}$$

$\left[\frac{dC_{p_W}/d\alpha_t}{dC_{p_S}/d\alpha_t}\right]$ FROM FIG 3-3

LOWER SURFACE

$$\Delta C_{p_{W_{\alpha_t}}} = \left[\frac{dC_{p_W}/d\alpha_t}{dC_{p_S}/d\alpha_t}\right](dC_{p_S}/d\alpha_t)\alpha_{t_u} \quad \text{Eq. 3:20}$$

$$\alpha_{t_u} = -i_u - (\theta_c - i_c)$$

UPPER SURFACE

The correlation curve in Figure 3-3 for the ratio of shockwave to surface shape change was obtained by multiplying the correlation in Figure 2-4 by the factor

$$\frac{(\tan\theta_c / \tan\theta_w)_M}{(\tan\theta_c / \tan\theta_w)_{M=\infty}}$$

This formulation agrees with slender body theory at low M which predicts the radial perturbation velocity due to cross-sectional shape change will decay 1/r times more rapidly than the radial velocity due to α. As M $\rightarrow \infty$ the above factor approaches unity which is the appropriate limit for hypersonic flow. With C_{P_S} and C_{P_W} known the remaining flow properties θ_W, S_W, M_W and M_S can be determined from Eqs. 2:5 to 2:10 given earlier.

Expansion fans originating from the juncture of two successive fuselage plugs (at a fuselage control station) are built up in the same manner as the shoulder expansion fan for the HO tank as described in that section. The only new aspect in the present case is that each expansion fan has an i_c and α_t associated with it which are determined by linear interpolation between adjacent plug values.

The preceding analysis applys to all fuselage plugs for which $\beta \tan \theta_c \geq .15$. The general fuselage analysis when $0 \leq \beta \tan \theta_c \leq 0.15$ is a direct generalization of Eqs. 2:11 to 2:18, Eqs 2:20 to 2:26, and Eqs. 2:27 to 2:30 for the isolated tank. Including incidence and boat-tail effects these equations now read.

Lower Surface

IF: $\alpha + i_\ell \leq -M_\infty$ Eq. 3:21

$$C_{P_S} = -2\left(\frac{C_D}{2}\right)\sin^2(-M_\infty)$$

IF: $-M_\infty \leq \alpha + i_\ell \leq 0$ Eq. 3:22

$$C_{P_S} = -2\left(\frac{C_D}{2}\right)\sin^2(\alpha + i_\ell)$$

IF: $0 \leq \alpha + i_\ell \leq M_\infty$ Eq. 3:23

$$C_{P_S} = 0$$

IF: $\mu_\infty \leq \alpha + i_\ell$

$$C_{p_s} = 2\left(\frac{C_D}{2}\right)\left/\left\{2\sin^2(\alpha + i_\ell) - \sin^2\mu_\infty\right.\right\} \qquad \text{Eq. 3:24}$$

UPPER SURFACE

IF: $\alpha + i_u \geq \mu_\infty$

$$C_{p_s} = -2\left(\frac{C_D}{2}\right)\sin^2(\mu_\infty) \qquad \text{Eq. 3:25}$$

IF: $0 \leq \alpha + i_u \leq \mu_\infty$

$$C_{p_s} = -2\left(\frac{C_D}{2}\right)\sin^2(\alpha + i_u) \qquad \text{Eq. 3:26}$$

IF: $-\mu_\infty \leq \alpha + i_u \leq 0$ Eq. 3:27

$$C_{p_s} = 0$$

IF: $\alpha + i_u \leq -\mu_\infty$

$$C_{p_s} = 2\left(\frac{C_D}{2}\right)\left/\left\{\sin^2(\alpha + i_u) - \sin^2\mu_\infty\right.\right\} \qquad \text{Eq. 3:2}$$

The corresponding shock wave properties are given below

Lower Surface

If: $\alpha + i_\ell \leq -\mu_\infty$

$C_{P_W} = 0$, $M_W = M_\infty$

θ_W (REL TO FRL) $= \alpha - \mu_\infty$ Eq. 3:29

θ_{W_f} (REL TO FRL) $= \alpha$

If: $-\mu_\infty \leq \alpha + i_\ell \leq 0$

$C_{P_W} = 0$, $M_W = M_\infty$

θ_W (REL TO FRL) $= \alpha - \mu_\infty$ Eq. 3:30

θ_{S_W} (REL TO FRL) $= \alpha$

If: $0 \leq \alpha + i_\ell \leq \mu_\infty$

$C_{P_W} = 0$, $M_W = M_\infty$ Eq. 3:31

θ_W (REL TO FRL) $= \alpha - \mu_\infty$

θ_{W_f} (REL TO FRL) $= \alpha$

If: $\mu_\infty \leq \alpha + i_\ell$

θ_W (REL TO FRL) $= -i_\ell$ Eq. 3:32

θ_{W_f} (REL TO FRL) $= -i_\ell$

$$C_{P_W} = 2\left(\frac{C_D}{2}\right)\left\{\sin^2(\alpha + i_\ell) - \sin^2\mu_\infty\right\} \quad \text{Eq. 3:33}$$

i.e., $C_{P_W} = C_{P_S}$

$$M_{IN} = \left\{ 1 + \frac{3\gamma}{7} M_\infty^2 C_{P_W} \right\} \qquad \text{Eq. 3:34}$$

$$M_W^2 \frac{36 M_\infty^2 M_{IN}^2 - 5(M_{IN}^2 - 1)(7M_{IN}^2 + 5)}{(7M_{IN}^2 - 1)(M_{IN}^2 + 5)} \qquad \text{Eq. 3:35}$$

Upper Surface

If: $\alpha + i_{2u} \geq M_\infty$

$C_{P_W} = 0$, $M_W = M_\infty$ — Eq. 3:36

θ_W (REL. TO FRL) $= \alpha + M_\infty$

θ_{W_f} (REL. TO FRL) $= \alpha$

If: $0 \leq \alpha + i_{2u} \leq M_\infty$

$C_{P_W} = 0$, $M_W = M_\infty$ — Eq. 3:37

θ_W (REL. TO FRL) $= \alpha + M_\infty$

θ_{W_f} (REL TO FRL) $= \alpha$

If: $-M_\infty \leq \alpha + i_{2l} \leq 0$

$C_{P_W} = 0$, $M_W = M_\infty$ — Eq. 3:38

θ_W (REL TO FRL) $= M_\infty + \alpha$

θ_{W_f} (REL TO FRL) $= \alpha$

If: $\alpha + i_w \leq -\mu_\infty$

θ_w (REL TO FRL) $= -i_w$ Eq. 3:39

θ_{w_f} (REL TO FRL) $= -i_w$

$C_{P_w} = 2\left(\frac{C_D}{2}\right)\left\{\sin^2(\alpha + i_w) - \sin^2\mu_\infty\right\}$

M_w FROM Eq. 3:35

The AERSEP formulation for the tank and orbiter base flowfield at zero angle of attack is based on the simple model shown in Sketch 3-C. The surface Mach No., M_{S_1}, and flow direction, $\theta_{f_{S_1}}$, immediately upstream of the tank base are $M_{S_1} = M_\infty$ and $\theta_{f_{S_1}}$ (Rel to FRL) = 0 if, as done here, we neglect the relatively small boat-tail. Based on simple linear theory the wake streamline direction is given by

$$\theta_{f_{S_2}} = \frac{(M_\infty^2 - 1)^{1/2}}{2} C_{P_{BASE}}$$

where

$$C_{P_{BASE}} = -\frac{1}{M_\infty^2} \qquad \text{Eq. 3:42}$$

The local pressure, $C_{P_{FP}}$, and flow direction, $\Theta_{f_{FP}}$, anywhere behind the Mach wave off the tank shoulder are related to the corresponding wake streamline values by

$$\frac{C_{P_{FP}}}{C_{P_{BASE}}} = \left|\frac{Z_{S_1}}{Z_{FP}}\right| = \frac{\Theta_{f_{FP}}}{\Theta_{f_{WAKE}}} \qquad \text{Eq. 3:43}$$

$$M_{FP} = M_\infty \qquad \text{Eq. 3:45}$$

The base flow analysis for the orbiter lower surface at $\alpha = 0$ is virtually identical, i.e.,

$$\Theta_{f_2} = -\frac{(M_\infty^2 - 1)^{1/2}}{2} C_{P_{BASE}} \qquad \text{Eq. 3:46}$$

$$\frac{C_{P_{FP}}}{C_{P_{BASE}}} = \left|\frac{Z_{S_1} - Z_c}{Z_{FP} - Z_c}\right| = \frac{\Theta_{f_{FP}}}{\Theta_{f_{WAKE}}} \qquad \text{Eq. 3:47}$$

Assuming the base pressure is constant for $\alpha < 10^{\circ}$ it follows that $C_{p_{FP}}$ and $\theta_{s_{FP}}$ (Rel to Free-Stream) are inariant with α. The above power-off base flow representation is invalid beyond, say, one diameter aft of the base at M = 2. AERSEP calculations are inapplicable when far-wake pressures can exert significant interference effects. Any doubt can be resolved by a simple order-of-magnitude analysis accounting for Mach wave sweep, area affected, and interference pressure level determined from Eqs. 3:46 and 3:47.

SKETCH 3-C : BASE FLOWFIELDS

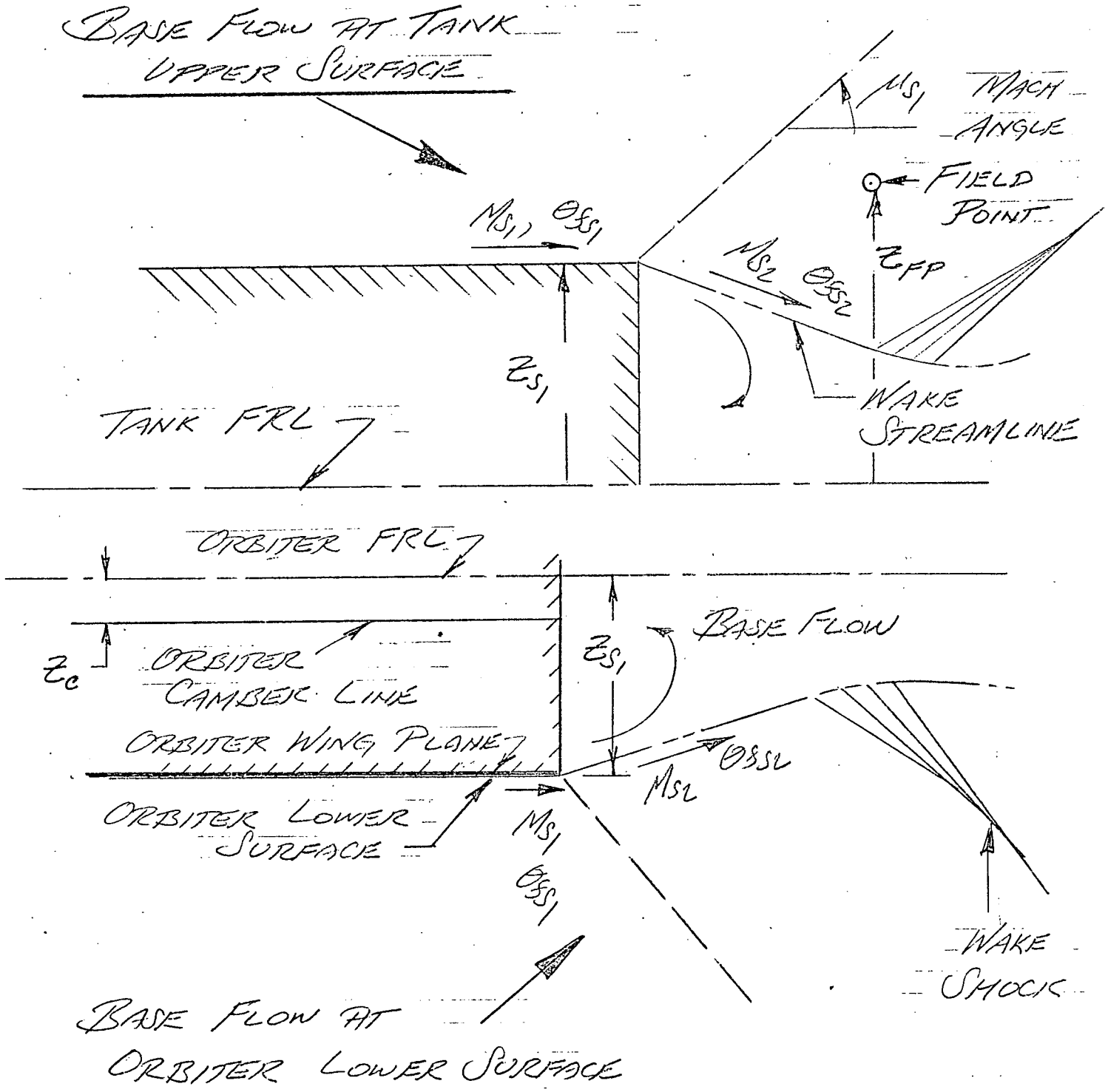

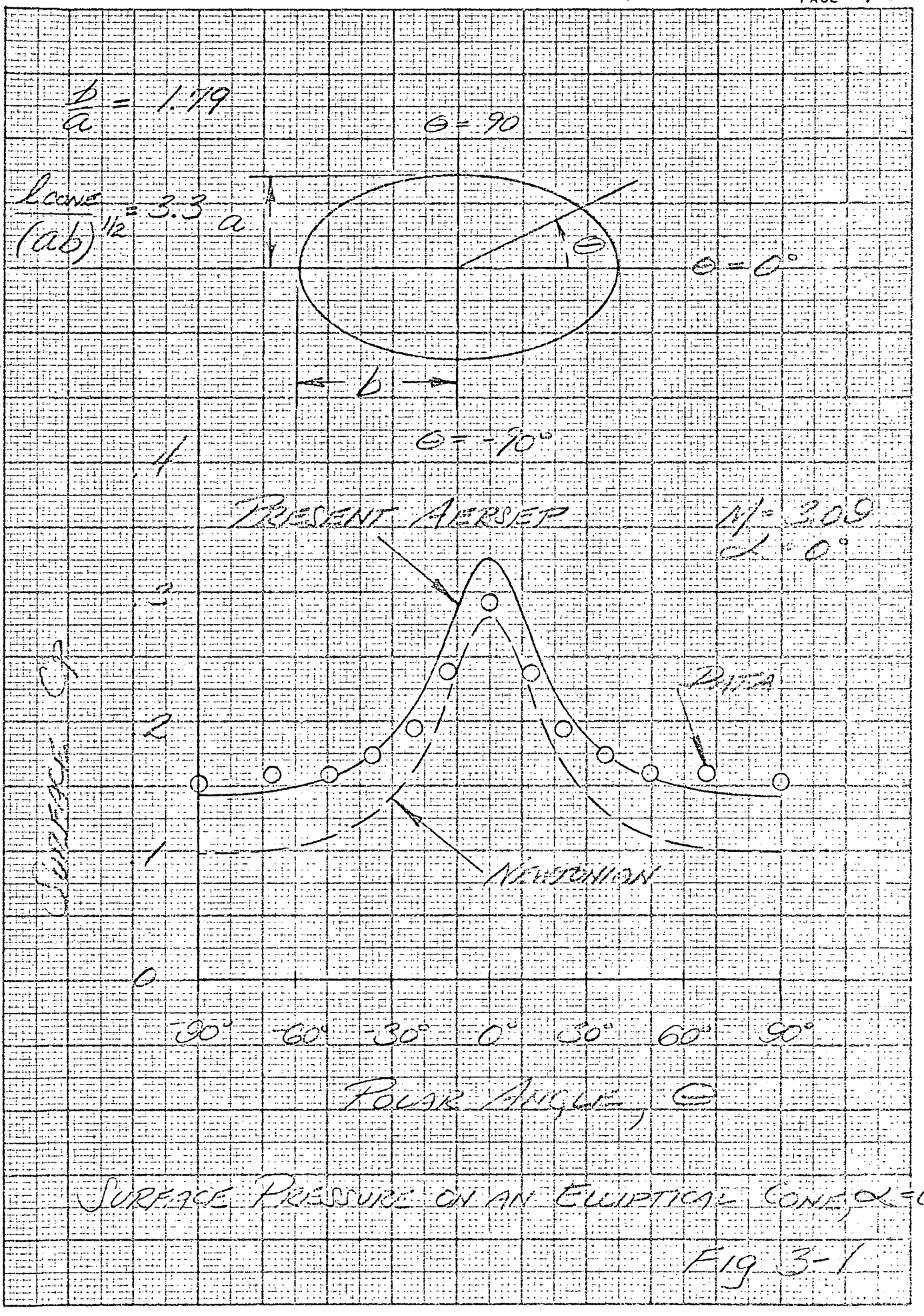

SURFACE PRESSURE ON AN ELLIPTICAL CONE, $\alpha = 0°$

FIG 3-1

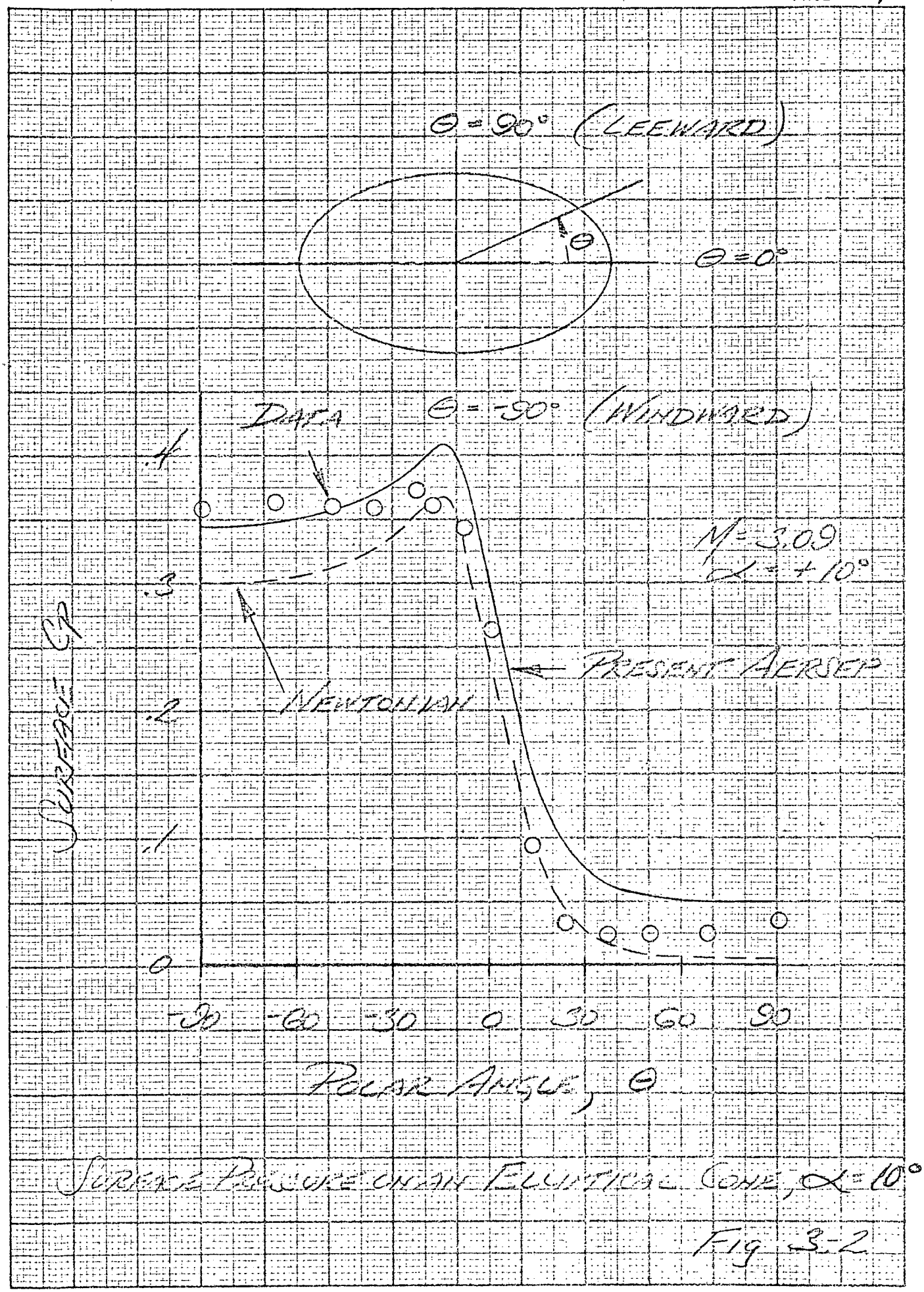

SURFACE PRESSURE ON AN ELLIPTIC CONE, $\alpha = 10°$

FIG 3-2

NO. 340-L220 DIETZGEN GRAPH PAPER
SEMI-LOGARITHMIC
2 CYCLES X 20 DIVISIONS PER INCH

EUGENE DIETZGEN CO.
MADE IN U. S. A.

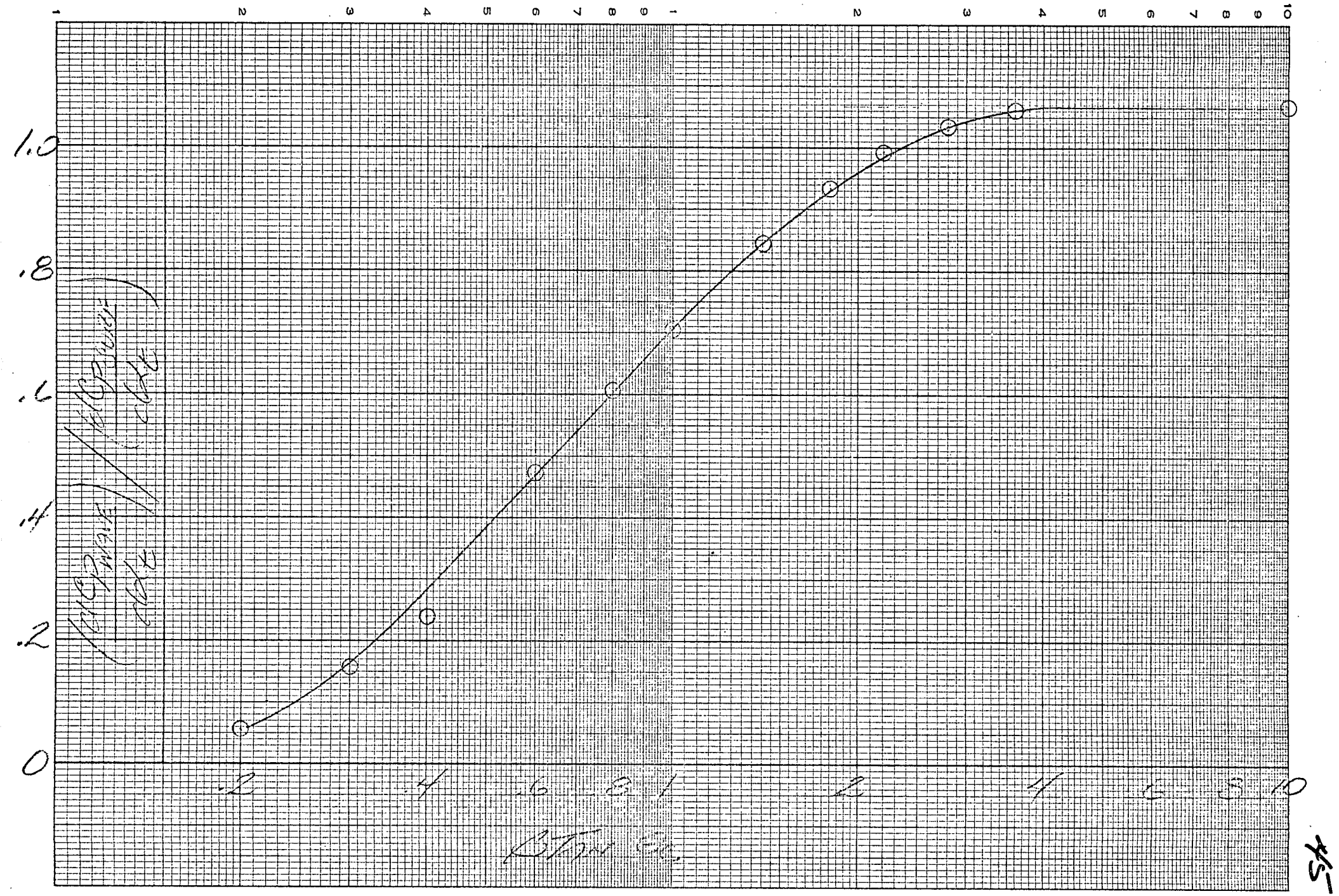

FIG 3-3

Section 4: Isolated Wing-Body Flow Field

For the intended flight envelope, $M \geq 2$, $\alpha \leq \pm 10^{\circ}$, the wing leading edge will be supersonic. In effect a Mach wave drawn from the exposed root chord leading edge at $\alpha = 0$ lies aft of the leading edge and the upper and lower surface flows do not interact except for a small region near the tip. With increasing angle of attack the wing flow, viewed in a plane perpendicular to the leading edge, will appear as shown in Sketch 4-A. For a thin planar wing an oblique shock forms at the underside of the leading edge to redirect the flow parallel to the surface. As α increases the deflection angle δ will eventually equal the shock detachment angle δ_{MAX} corresponding to the normal Mach No., M_N. Any further increase in α results in leading edge shock detachment and significant windward-leeward cross flow, i.e., three dimensional flow. Below this critical α an essentially two dimensional flow field description is adequate. Sketch 4-A gives the variation in α-for-shock-detachment with M_∞ for various Λ_{LE}.

A profile view of the AERSEP lower wing surface flow is shown in Sketch 4-B. The flow deflection due to the wing is

$$\delta_W = K_{W(B)}\alpha + i_W \qquad \text{Eq. 4:1}$$

where i_W is the exposed root chord incidence and $K_{W(B)}$ the body upwash factor. Wing thickness, camber, and twist are neglected. When $\delta_W > 0$ the streamwise shock wave angle θ_W (Rel. to freestream) can be determined by iterative solution of the equation.

$$\tan\delta_W = \frac{5\cot\theta_W\left(M_\infty^2\sin^2\theta_W - 1\right)}{5 + M_\infty^2\left(6 - 5\sin^2\theta_W\right)} \qquad \text{Eq. 4:2}$$

SKETCH 4-A: WING FLOWFIELD STRUCTURE

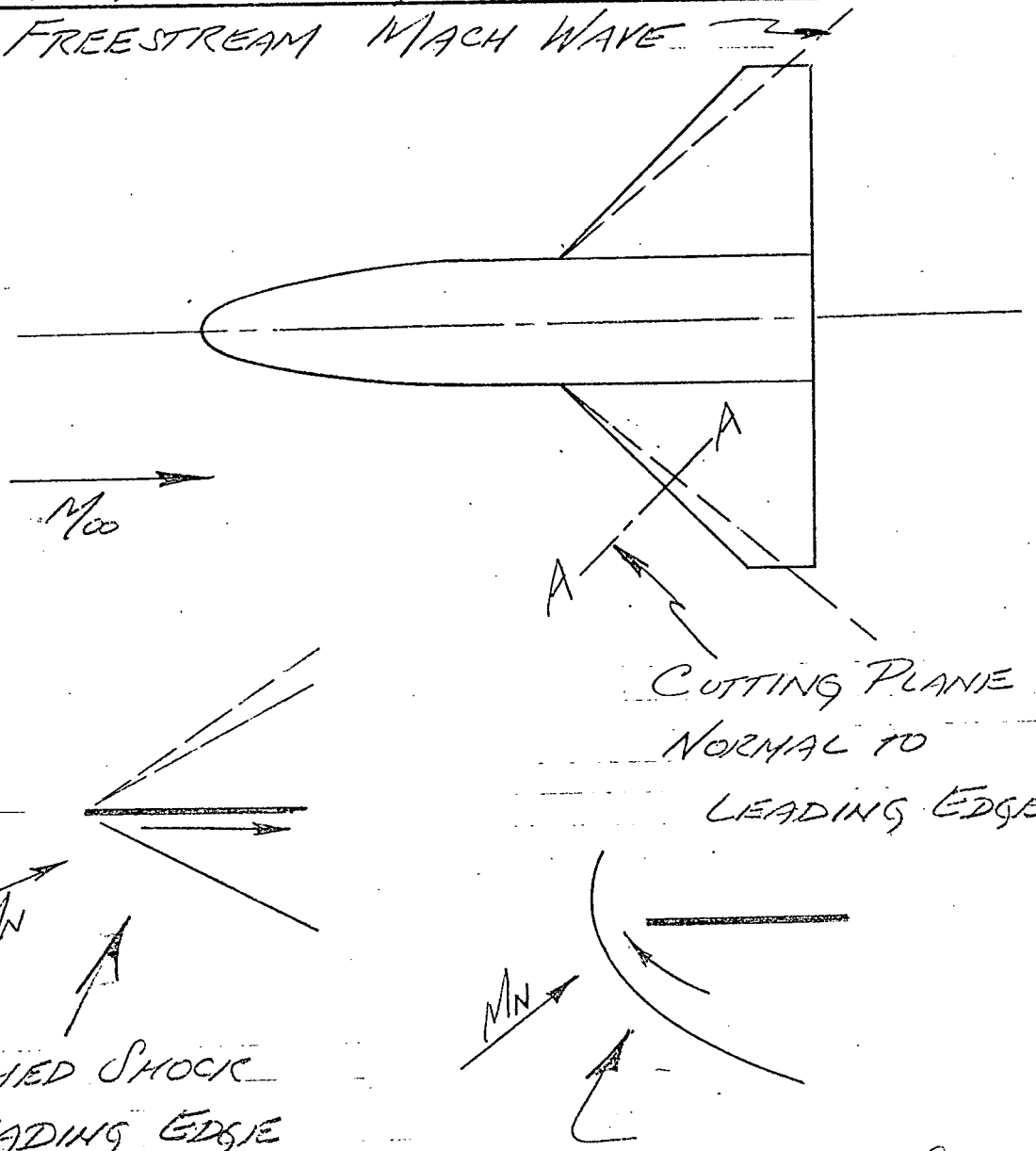

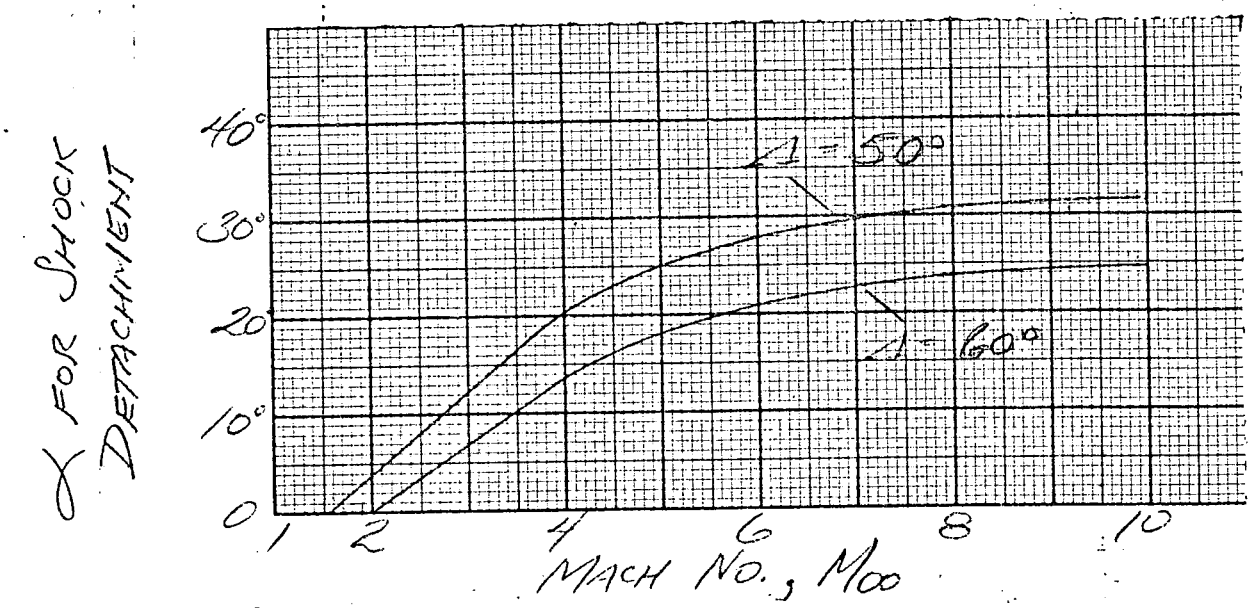

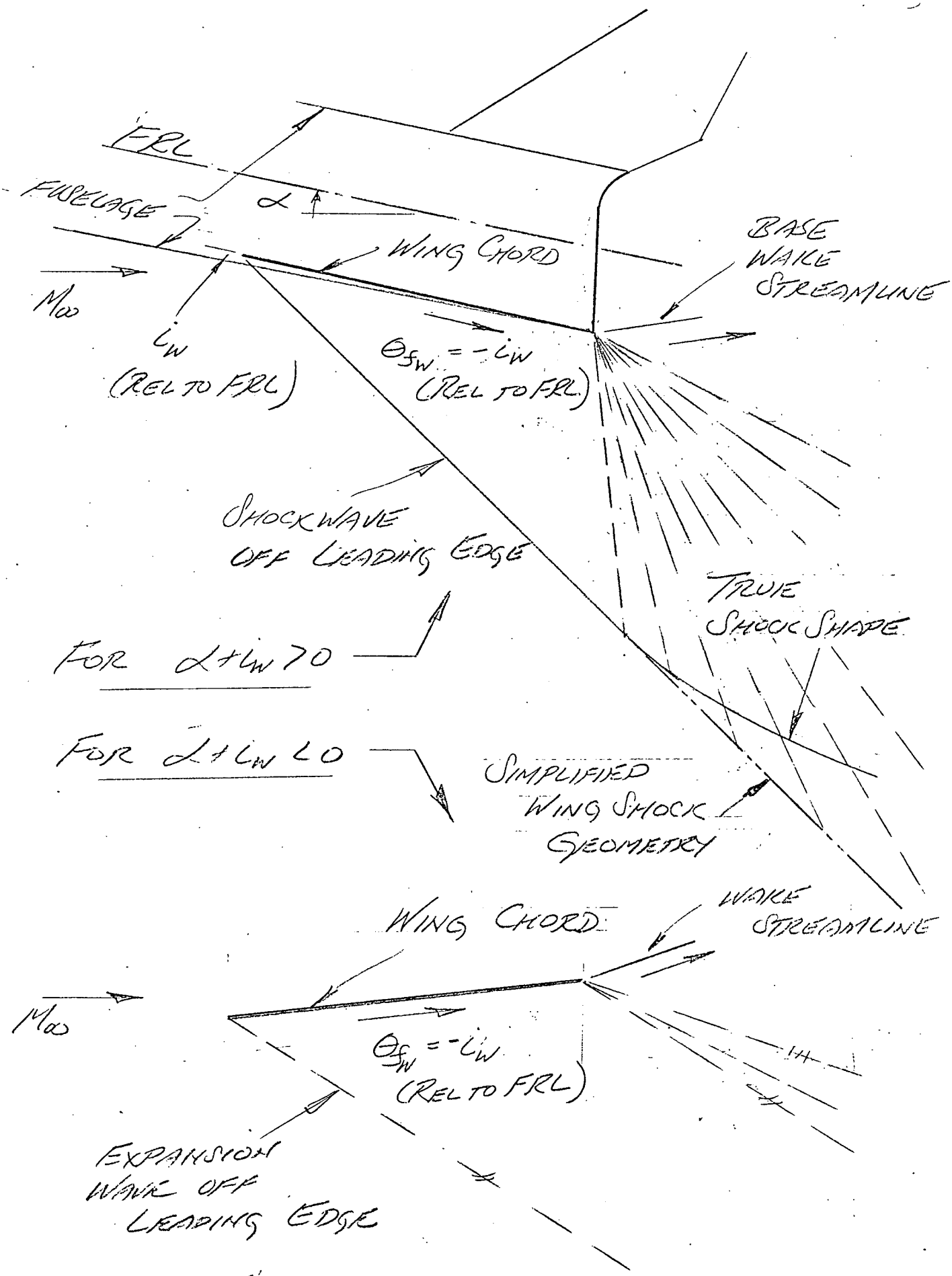

SKETCH 4-B: LOWER SURFACE FLOW PAST WING

Mach No. behind the wing shock, M_W , is calculated from

$$M_N = M_\infty \sin \theta_W \qquad \text{Eq. 4:3}$$

$$M_W^2 = \frac{36 M_\infty^2 M_N^2 - 5(M_N^2-1)(7M_N^2+5)}{(7M_N^2-1)(M_N^2+5)} \qquad \text{Eq. 4:4}$$

The corresponding surface pressure is given by

$$\frac{P_S}{P_\infty} = \frac{7M_N^2-1}{6}, \quad C_{P_S} = \frac{(P_S/P_\infty)-1}{\frac{1}{2}\gamma M_\infty^2} \qquad \text{Eq. 4:5}$$

At negative orbiter angle-of-attack the bottom of the wing can become a leeward surface, i.e., $\delta_W < 0$. For the small negative angles of interest the pressure can be calculated from the linearized expression

$$C_{P_S} = \frac{2\delta_W}{(M_\infty^2-1)^{1/2}} = C_{P_W} \qquad \text{Eq. 4:6}$$

(also require $C_{P_S} \geq -1/M_\infty^2$ always)

$$M_W^2 = 5\left\{\left(1+\frac{M_\infty^2}{5}\right)\left(\frac{P_W}{P_\infty}\right)^{-2/7} - 1\right\} \qquad \text{Eq. 4:7}$$

Since the Shuttle wing trailing edge is coincident with the orbiter base, the flow at the trailing edge will re-expand to the base pressure level $C_{P_b} = -1/M_\infty^2$. For $\delta_W > 0$ the Prandtl-Meyer relations at the trailing edge are written as

$$\frac{P_S - P}{\frac{1}{2}\gamma P_S M_S^2} = \frac{2}{(M_S^2 - 1)^{1/2}} (\theta_f - \theta_{fs}) \qquad \text{Eq. 4:8}$$

where θ_{fs}, P_S and θ_f, P are the flow direction (relative to FRL, measured positive up) and pressure on the wing lower surface and a point in the expansion fan respectively. Mach No. M, at a point in the fan is given by

$$M^2 = 5\left\{\left(1 + \frac{M_S^2}{5}\right)\left(\frac{P}{P_S}\right)^{-2/7} - 1\right\} \qquad \text{Eq. 4:9}$$

To further simplify AERSEP logic the shock wave curvature introduced by the trailing edge expansion waves is neglected and the shock wave location approximated by a straight line.

When $\delta_W < 0$ the trailing edge expansion fan relations are

$$C_p = \frac{P/P_\infty - 1}{\frac{\gamma}{2} M_\infty^2} = \frac{2}{(M_\infty^2 - 1)^{1/2}} (\delta_W - (\theta_f - \theta_{fs})) \qquad \text{Eq. 4:10}$$

and

$$M^2 = 5\left\{\left(1 + \frac{M_\infty^2}{5}\right)\left(\frac{P}{P_\infty}\right)^{-2/7} - 1\right\} \qquad \text{Eq. 4:11}$$

An additional feature included in AERSEP to partially account for three dimensional orbiter wing-body interference effects is illustrated in Sketch 4-C. Spillover of the wing lower surface pressure onto the fuselage is confined to a region aft of the Mach waves from the root chord leading

edge. For supersonic leading edges linear theory predicts the average wing carry-over pressure, $\bar{C_p}$, across the fuselage width, W, will vary from zero at the root leading edge, Station "A", to the exposed wing pressure level at Station "C" located two fuselage Mach wave crossings aft of "A". Theory also indicates the longitudinal variation is approximately linear as indicated in the lower part of Sketch 4-C. AERSEP approximates this distribution over the orbiter fuselage with a "step" loading at Station "B", one Mach-wave-crossing aft of the exposed root leading edge.

Sketch 4-D gives a planview of the orbiter wing-body overlaid on the tank. The hatched region indicates the extent of tank plan area blanketed by wing pressures. For simplicity this irregular area is converted to an equivalent rectangle extending from B* to the orbiter base, i.e.,

$$X_B - X_{B^*} = \frac{(D-W)(X_B - X_{LE})}{D} \qquad \text{Eq. 4-12}$$

The net orbiter lower surface wing-body flow field is thus given by the isolated fuselage flow field everywhere forward of the wing shock from Station B* and by the two dimensional wing flow downstream. A representative AERSEP calculation for the NASA 040-A orbiter is plotted to scale in Sketch 4-E.

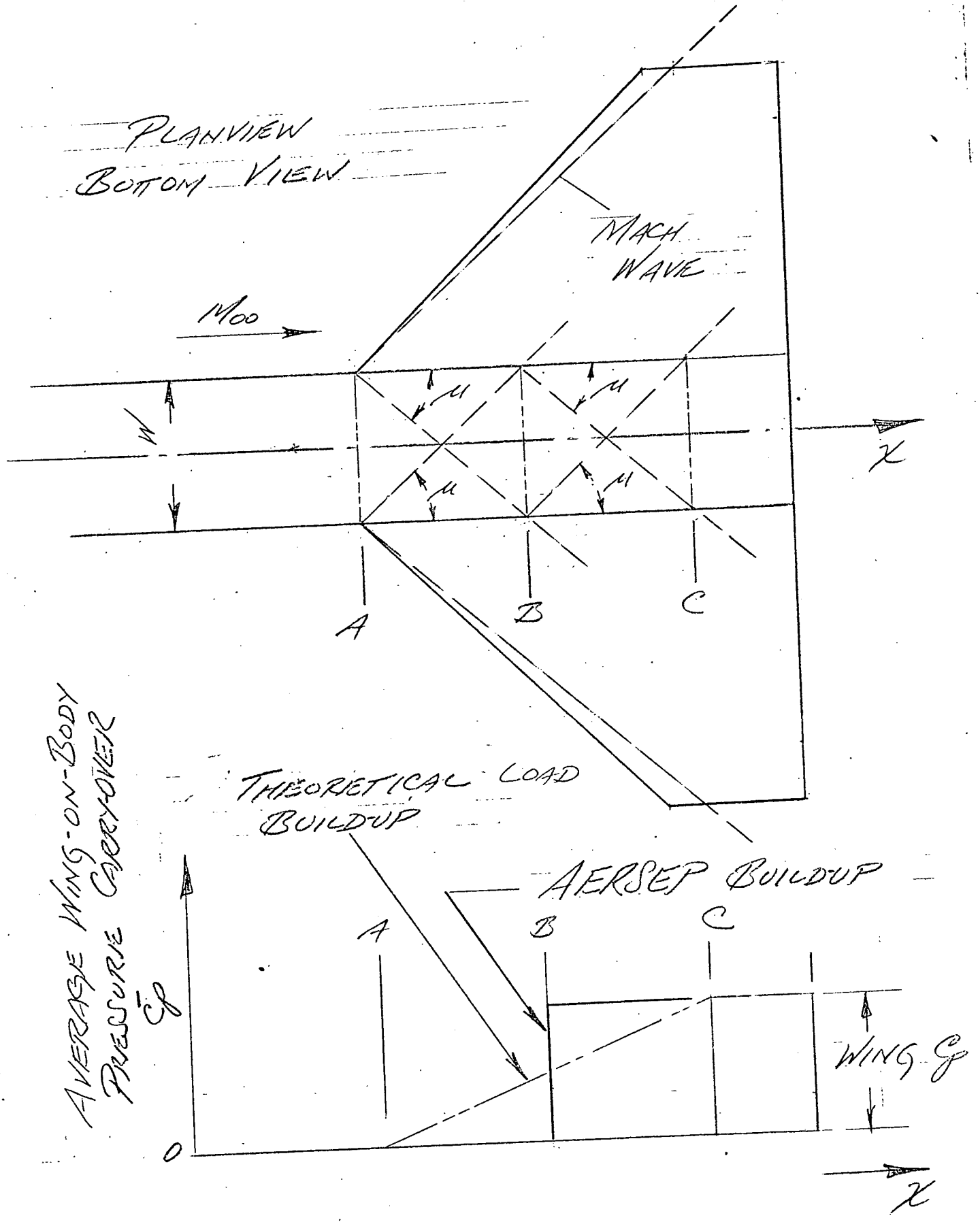

SKETCH 4-C, WING-ON-BODY LOAD CARRYOVER

E

SKETCH 4-D: ORIGIN OF ORBITER WING SHOCK

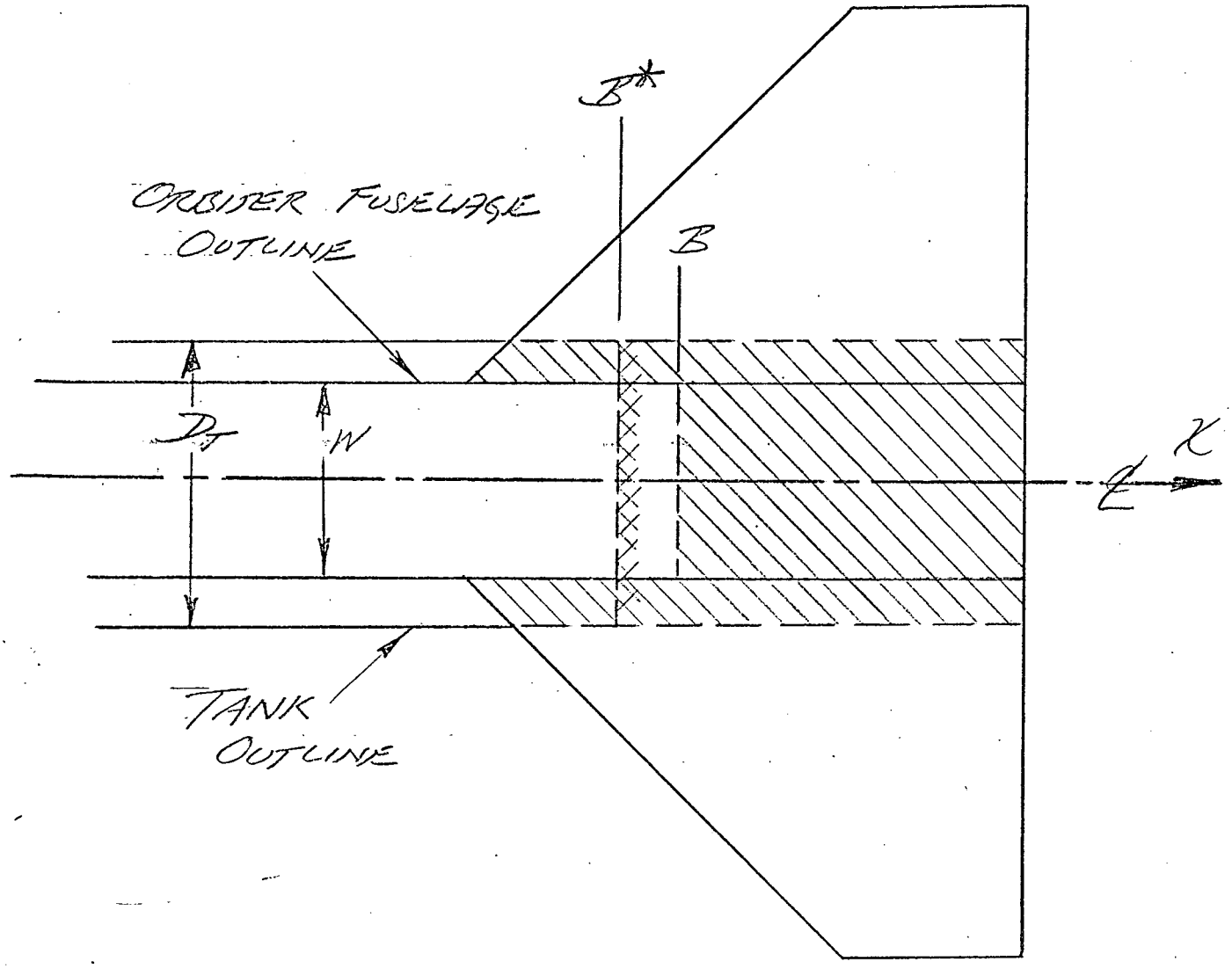

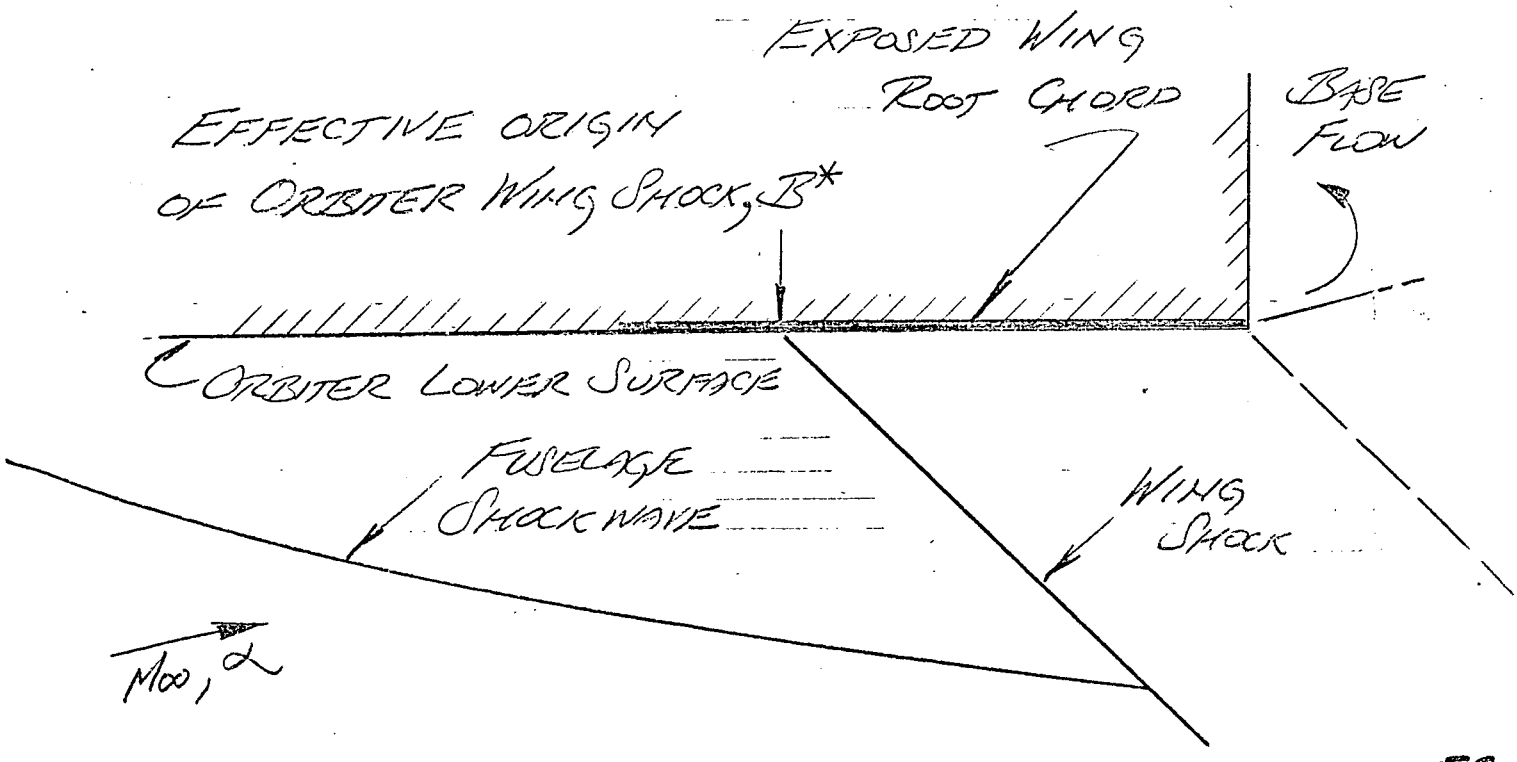

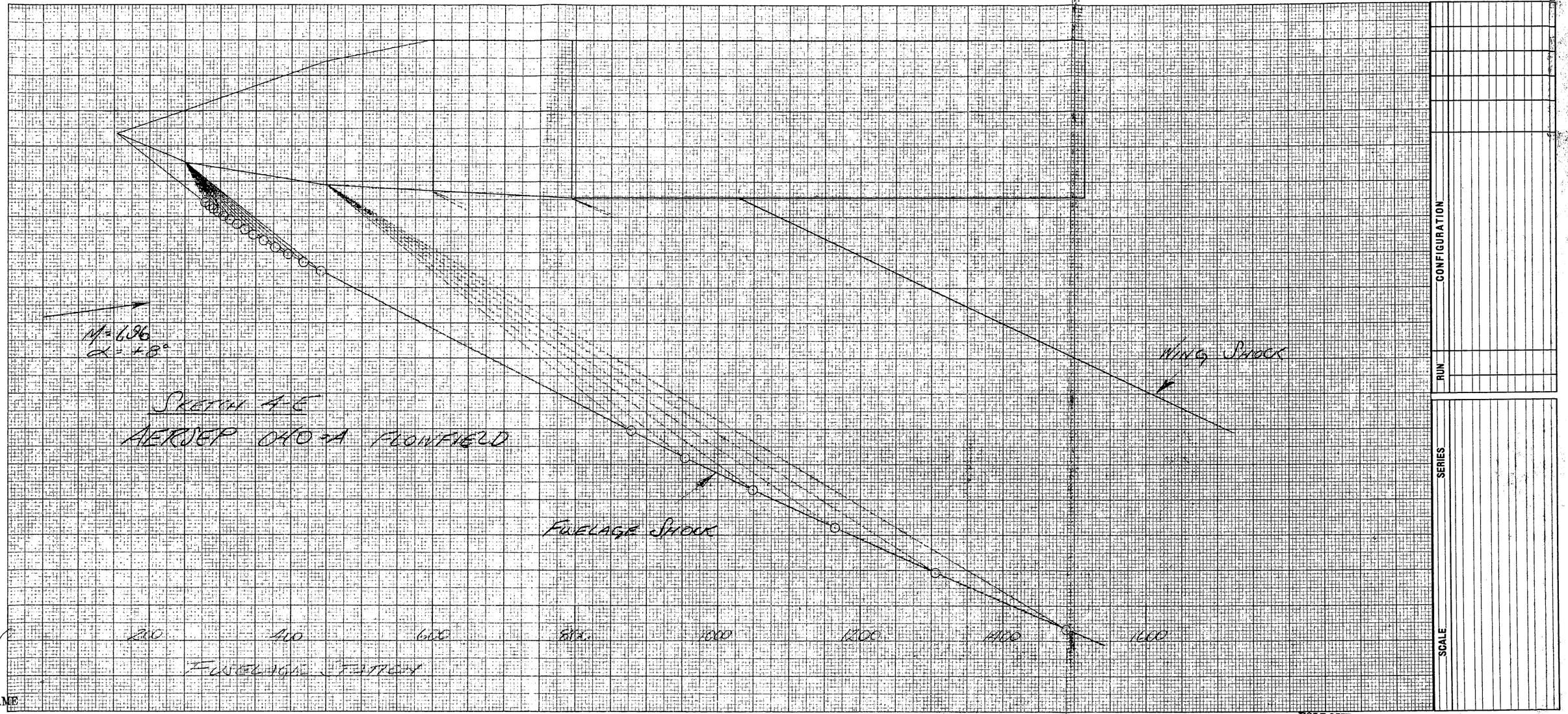

SKETCH A-E

AEROSP 040-A FLOWFIELD

PAGE
FIGURE
CONFIGURATION
RUN
SERIES
SCALE

FOLDOUT FRAME 1

ENG-126 K-E ALBANENE® TRACING PAPER 54137 N.Y. GRUMMAN AEROSPACE CORPORATION

FOLDOUT FRAME 2

FOLDOUT FRAME 3

REPORT
DATE

Section 5: Primary Interference Loads on Bodies

Perhaps the most critical step in the entire AERSEP analysis is the evaluation of body loads in a non-uniform interference flow field. "Primary" refers to the aerodynamic loading on the orbiter when placed in the isolated tank flow field. "Reflected" interferences due to orbiter shockwave reflections off the tank back onto the orbiter are accounted for separately.

The geometry for the primary load evaluation on the orbiter fuselage is indicated in Sketch 5-A. The tank and upper half of its flow field are shown underneath the "effective" outline of the orbiter. As discussed in Section 3 the "effective" outline measures from the FRL to the average fuselage height as seen in cross-section. Local flow properties evaluated along the "effective" orbiter outline are more representative for load evaluation than those along the true geometric profile.

The average primary interference pressure across the fuselage width of the orbiter lower surface at some station X is given by

$$\frac{p_s^*}{p_\infty} = \frac{p}{p_\infty}\left\{1 + \frac{\gamma}{2} M^2 c_p^*\right\} \qquad \text{Eq. 5:1}$$

where

$$c_p^* = K\left(\frac{c_p}{2}\right) 2 \sin^2 \alpha^* \qquad \text{IF } \alpha^* \geq 0$$

$$c_p^* = 0 \qquad \text{IF } \alpha^* < 0$$

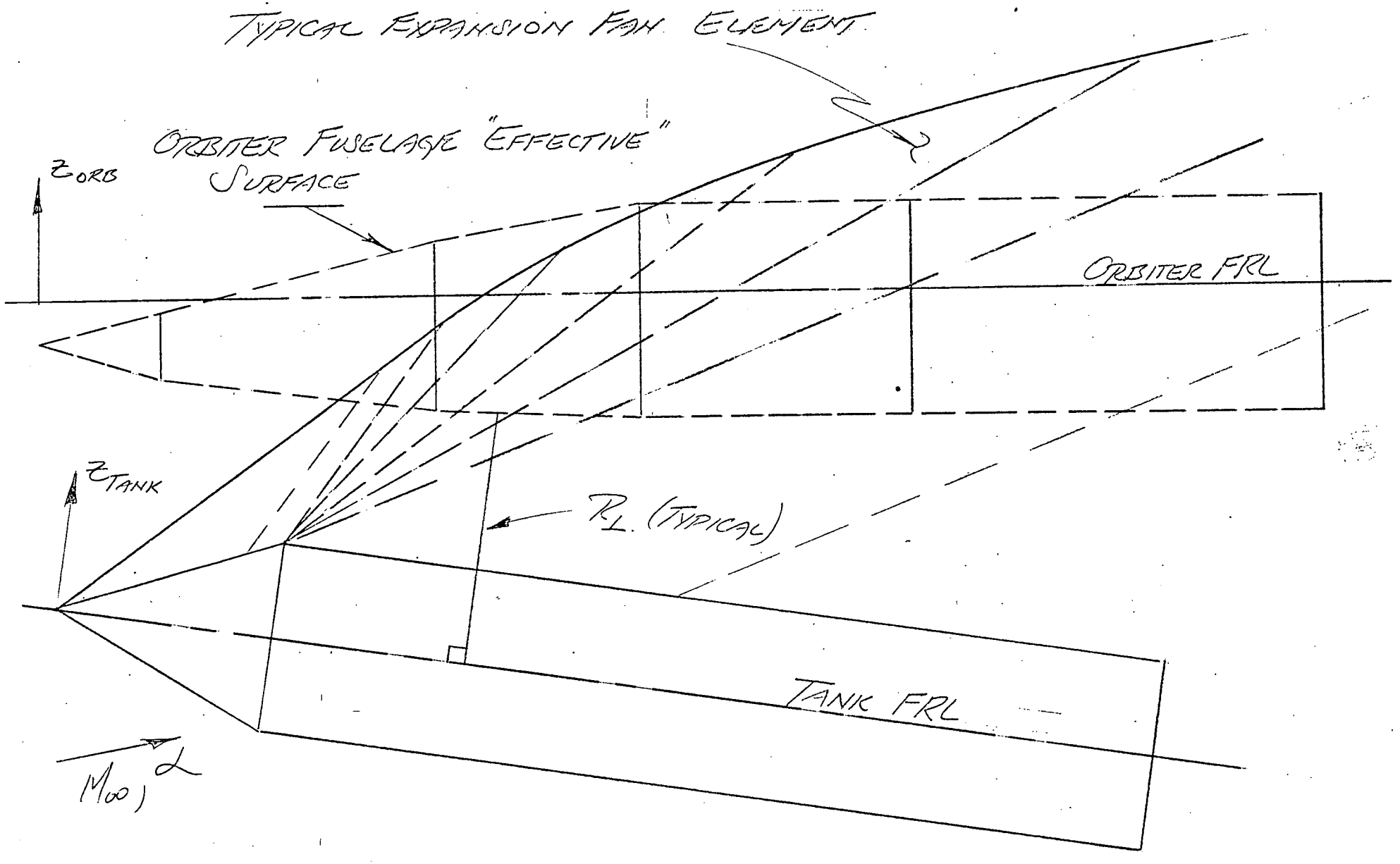

SKETCH 5-A: ORBITER PRIMARY LOAD EVALUATION IN TANK FLOWFIELD

$C_D/2$ ~ Ratio, cross-flow drag coefficient of orbiter fuselage lower surface to that of a flat plate

K ~ A cross-flow drag factor that accounts for the quasi-axisymmetric nature of the tank interference flow field; a function of R_L/W, W = fuselage width at station X

α^* = Angle-of-attack between orbiter "effective" lower surface at station X and the local flow direction in the tank interference flow field

P, M = Local static pressure and Mach No. in the tank flow field along orbiter "effective" lower surface

To evaluate Eq. 5:1 α^* is calculated from

$$\alpha^* = (\alpha_{ORB} - \alpha_T) + i_{le_{ORB}} + \theta_f \qquad \text{Eq. 5:2}$$

where θ_f is the flow direction in the tank flow field relative to the tank FRL. Both α_{ORB} and α_T are measured relative to their respective FRL's. The orbiter effective lower surface incidence, $i_{le_{ORB}}$, is given by

$$i_{le} = TAN^{-1}\left\{\frac{Z_{le,n} - Z_{le,n+1}}{X_{n+1} - X_n}\right\} \qquad \text{Eq. 5:3}$$

where "n" denotes "at the n'th" fuselage control station. Appropriate values for $C_D/2$ and the decay constant "C" (which determines K) can be read from Figure 5-1 and 5-2 for each fuselage plug. Average upper "effective" surface loading is determined in exactly the same manner and the resulting force and moment determined by numerical integration.

Isolated orbiter fuselage force and moment are calculated in a similar manner. The appropriate equations for the orbiter lower surface are:

$$\frac{P^*_\infty}{P_\infty} = 1 + \frac{\gamma}{2} M_\infty^2 C^*_{P_\infty} \qquad \text{Eq. 5:4}$$

$$C^*_{P_\infty} = \left(\frac{C_D}{2}\right) 2 \sin^2 \alpha^* \quad \text{IF } \alpha^* \geq 0$$
$$= 0 \quad \text{IF } \alpha^* < 0 \qquad \text{Eq. 5:5}$$

$$\alpha^* = \alpha_{ORB} + i_{e,ORB} \qquad \text{Eq. 5:6}$$

Equation 5:5 for $C^*_{P_\infty}$ is nothing more than the familiar Newtonian expression for surface pressure coefficient multiplied by a cross-flow drag ratio to account for the cross-sectional shape.

In light of the opening remarks to this section it might seem unlikely that Eq. 5:1 would be adequate for load evaluation over the Mach number range 2 to 10. In point of fact, however, the integrated force and moment predicted by this equation are identical to slender body theory when α^* is small and Newtonian-Crossflow results when nonlinear α^* effects are significant. These theoretical anchor points are vital and assure reasonable AERSEP predictions over the intended Mach spectrum.

FIGURE 5-1 EFFECT OF FUSELAGE CROSS-SECTION ON C_{D_2}

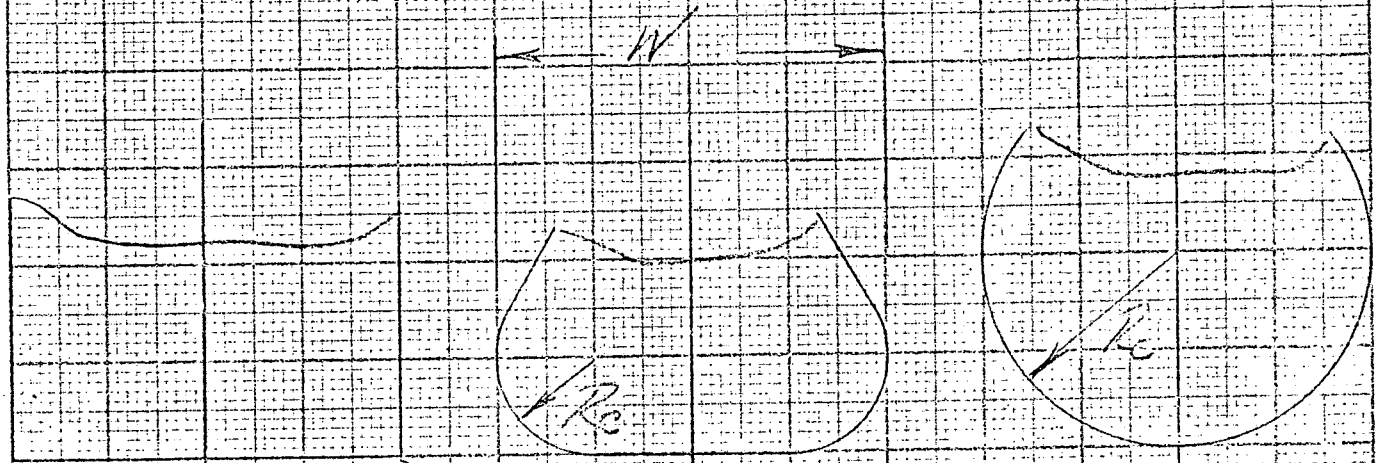

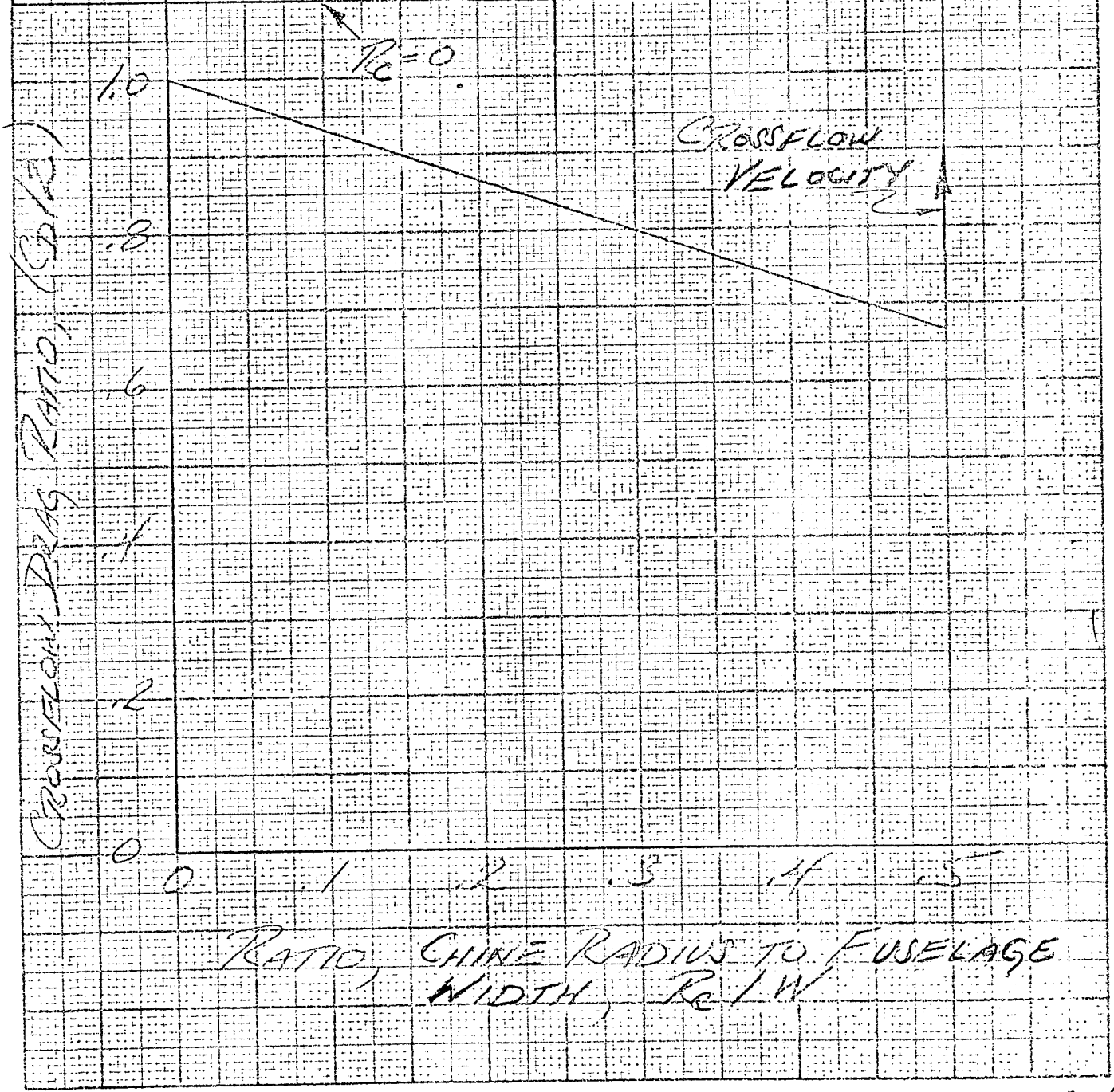

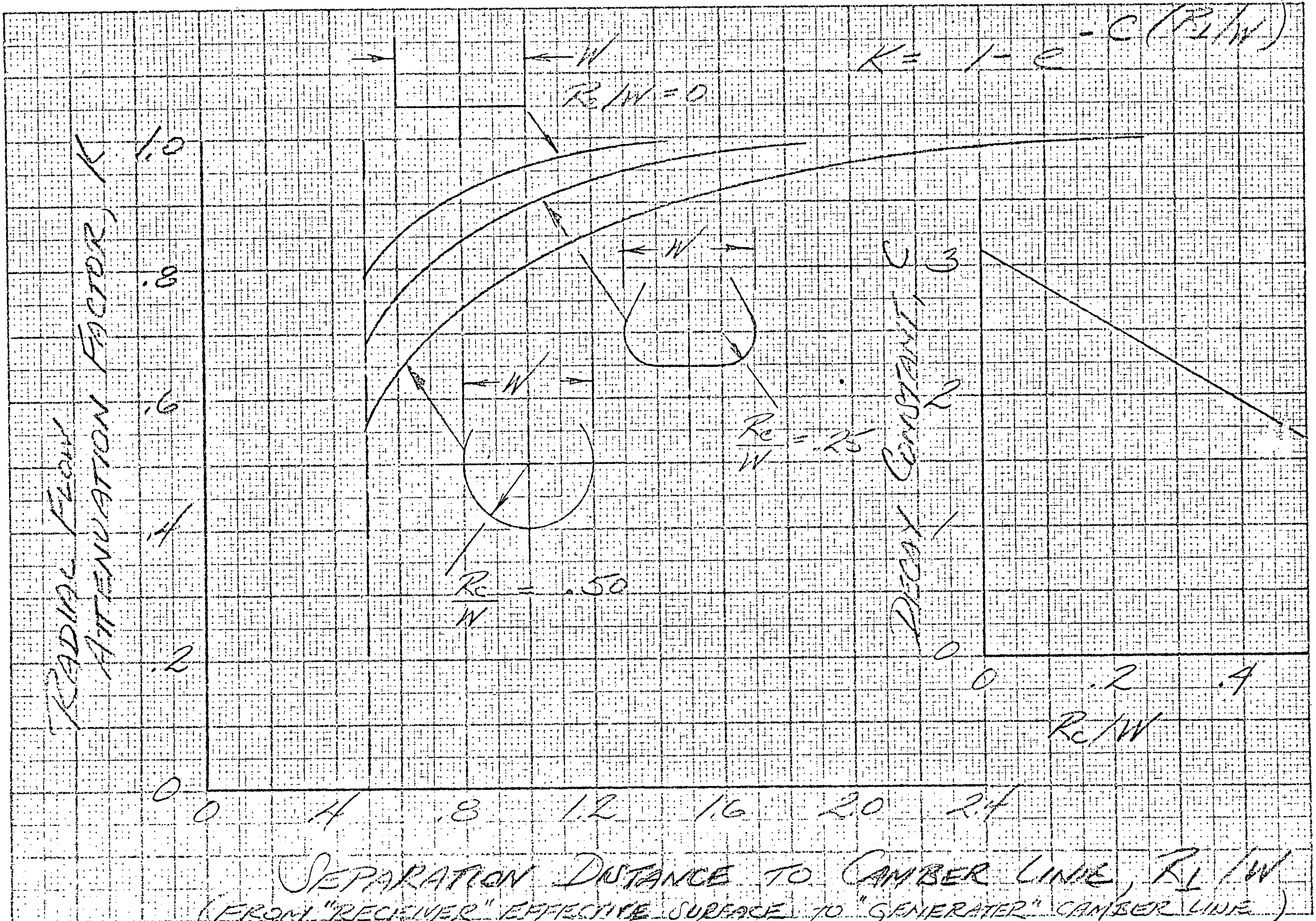

FIGURE 5-2: RADIAL FLOW EFFECT ON CROSSFLOW DRAG

Section 6: Primary Interference Loads, on Wing-Body Configurations

The total lift on the Shuttle Orbiter in free air can be expressed as

$$C_{L_{WB}} = C_{L_B} + (K_{W(B)} + K_{B(W)}) C_{L_{\alpha_W}} \alpha + (K_{W(B)} + K_{B(W)}) C_{L_{\alpha_W}} i_W \qquad \text{Eq. 6:1}$$

where

C_{L_B} = Lift of isolated body at α

$C_{L_{\alpha_W}}$ = Lift curve slope of exposed wing panels when joined together to form an isolated wing

$K_{W(B)}$ = Interference factor which accounts for the lift increment on the exposed wing due to fuselage induced upwash at α

$K_{B(W)}$ = Interference factor which accounts for lift carry over from the exposed wing at α onto the fuselage

$K_{W(B)}$ = Interference factors due to wing incidence; similar to $K_{W(B)}$ and $K_{B(W)}$

For configurations with supersonic leading edges and no fuselage aft of the wing trailing edge Eq. 6:1 can be simplified to

$$C_{L_{WB}} \cong C_{L_B} + K_{W(B)} C_{L_{\alpha_W}} \alpha + C_{L_{\alpha_W}} i \qquad \text{Eq. 6:2}$$

$K_{W(B)}$ depends on the body width to wing span ratio, w/b, as shown in Figure 6-1 from Ref. 5.

Equation 6:2 can be adapted to the present case for evaluating the orbiter loading in the interference flow field generated by the tank. Primary interference on the fuselage, corresponding to C_{L_B}, can be calculated by

the method obtained in the previous section. The additional loading on the orbiter due to wing and wing-body contributions is determined from the loading integral

$$C_{L_{WB}} - C_{L_B} = \frac{1}{S_{REF}} \int_{S_{WING\ EXPOSED}} \left\{ K_{W(B)} \alpha_{l_W} + i_W \right\} \frac{\Delta C_p}{\alpha^*} \frac{q_l}{q_\infty} dS \quad \text{Eq. 6:3}$$

where

$$\frac{\Delta C_p}{\alpha^*} = \frac{4}{(M_l^2 - 1)^{1/2}}$$

q_l = Local dynamic pressure

ΔC_p = Differential pressure coefficient across wing surface referred to the local dynamic pressure

α^*_W = Total angle-of-attack between wing surface and the local flow direction in the tank flow field

i_W = Orbiter wing incidence (relative to orbiter FRL)

$\alpha_{l_W} = \alpha^* - i_W$

The integrand in Eq. 6:3 is evaluated assuming that the tank interference flow field is approximately axisymmetric (about the wind axis) in the region of the wing. Sketches 6-A and 6-B illustrate the procedure for determining the off-centerline local flow properties in the wing Mean Reference Plane, MRP. Consider the transverse plane A-A which intersects the centerline shock envelope at "S" in Sketch 6-A. A circle swung through "S" as in Sketch 6-B intersects the wing at span station "S*" along W-W, the trace of A-A in

the MRP. Successive calculation of "S*" for a range of fuselage stations defines the shock trace on the exposed wing. Flow properties in each meridian plane, ϕ = constant, are assumed to be the same as in the plane of symmetry. The total angle-of-attack, α^*, between the local flow and the wing at some point "P*" is calculated from

$$\alpha_W^*(P^*) = \alpha_{ORB} + i_W + \theta_{SF} \quad (\text{REL TO FS AT } P) \qquad \text{Eq. 6:4}$$

In performing the load integration, Eq. 6:3, the exposed wing is divided into regions internal and external to the shockwave trace. The tank flow field defines the local flow within the trace while free stream conditions prevail outside. The wing contribution to C_m is given by

$$C_{m_W} = -\frac{1}{S_{REF}\, \ell_{REF}} \int_{S_{WING\ EXPOSED}} \left\{ K_{W(B)} \alpha_{\ell_W} + i_W \right\} \times \left\{ \frac{\Delta C_p}{\alpha^*} \frac{q_\ell}{q_\infty} \right\} (x - x_{cg})\, dS \qquad \text{Eq. 6:5}$$

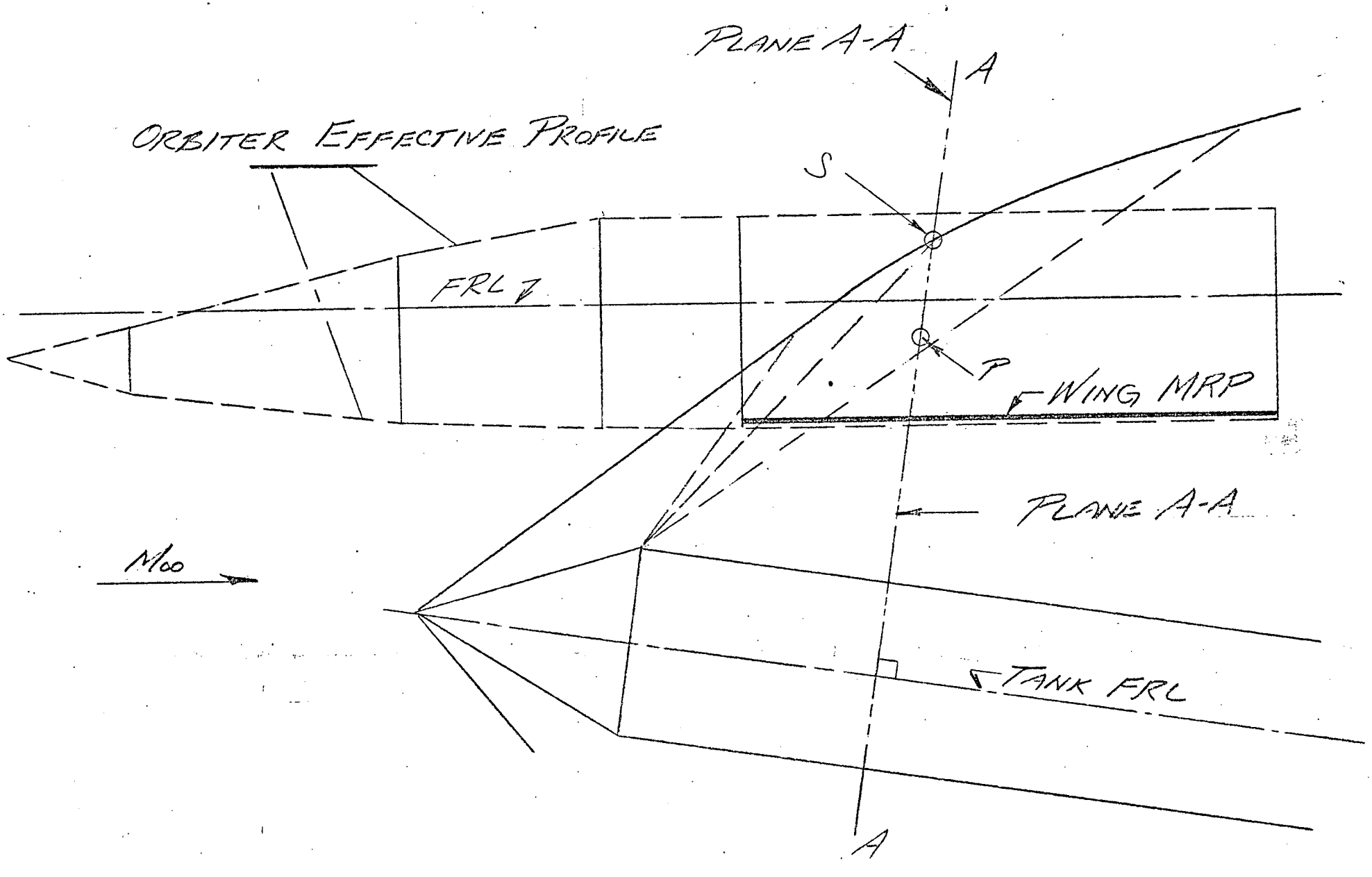

SKETCH 6-A1 : CONSTRUCTION OF LOCAL FLOW IN WING MEAN REFERENCE PLANE, MRP; PROFILE

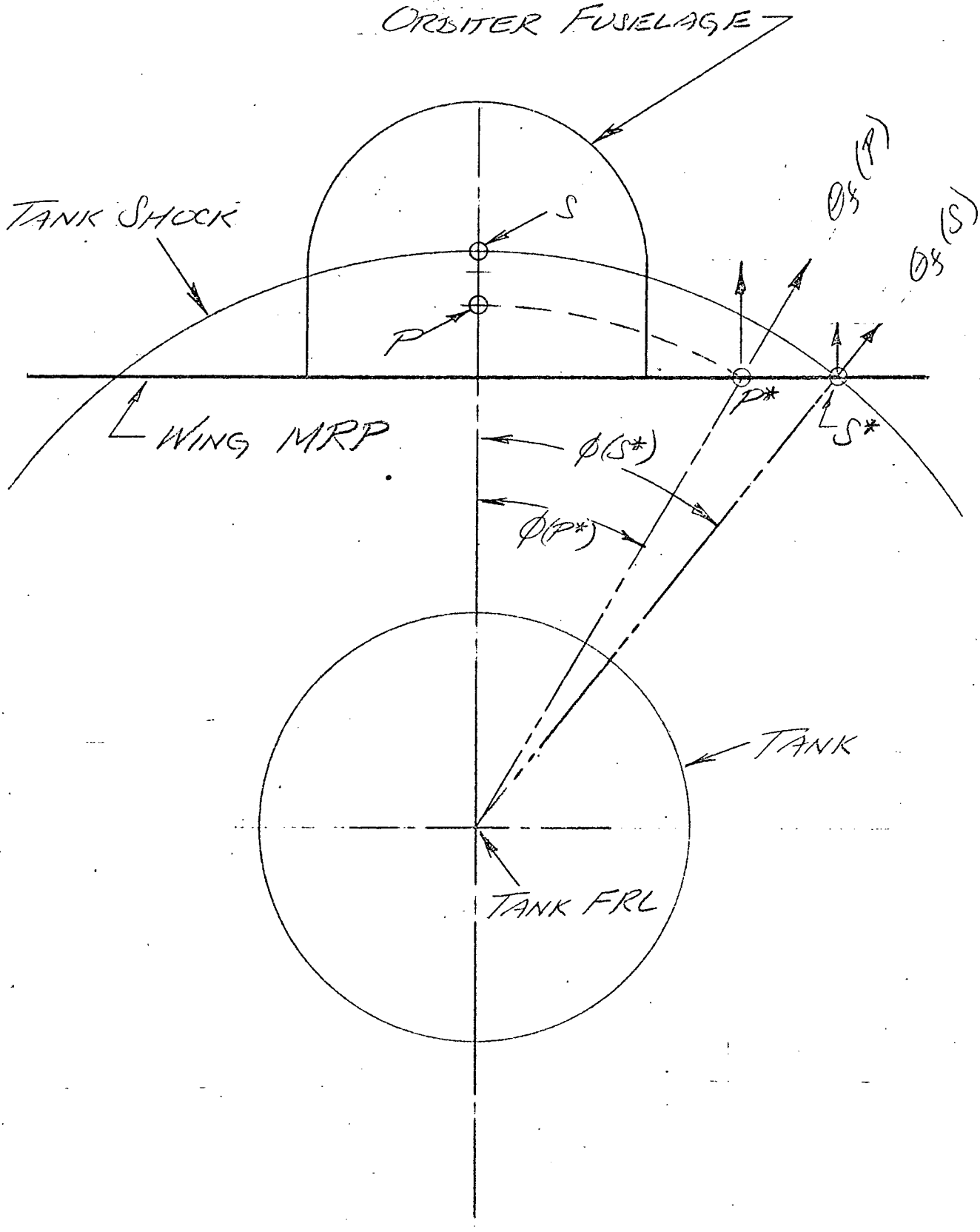

SKETCH 16-B: CONSTRUCTION OF LOCAL FLOW IN WING MRP; CROSS-SECTIONAL VIEW IN PLANE A-A.

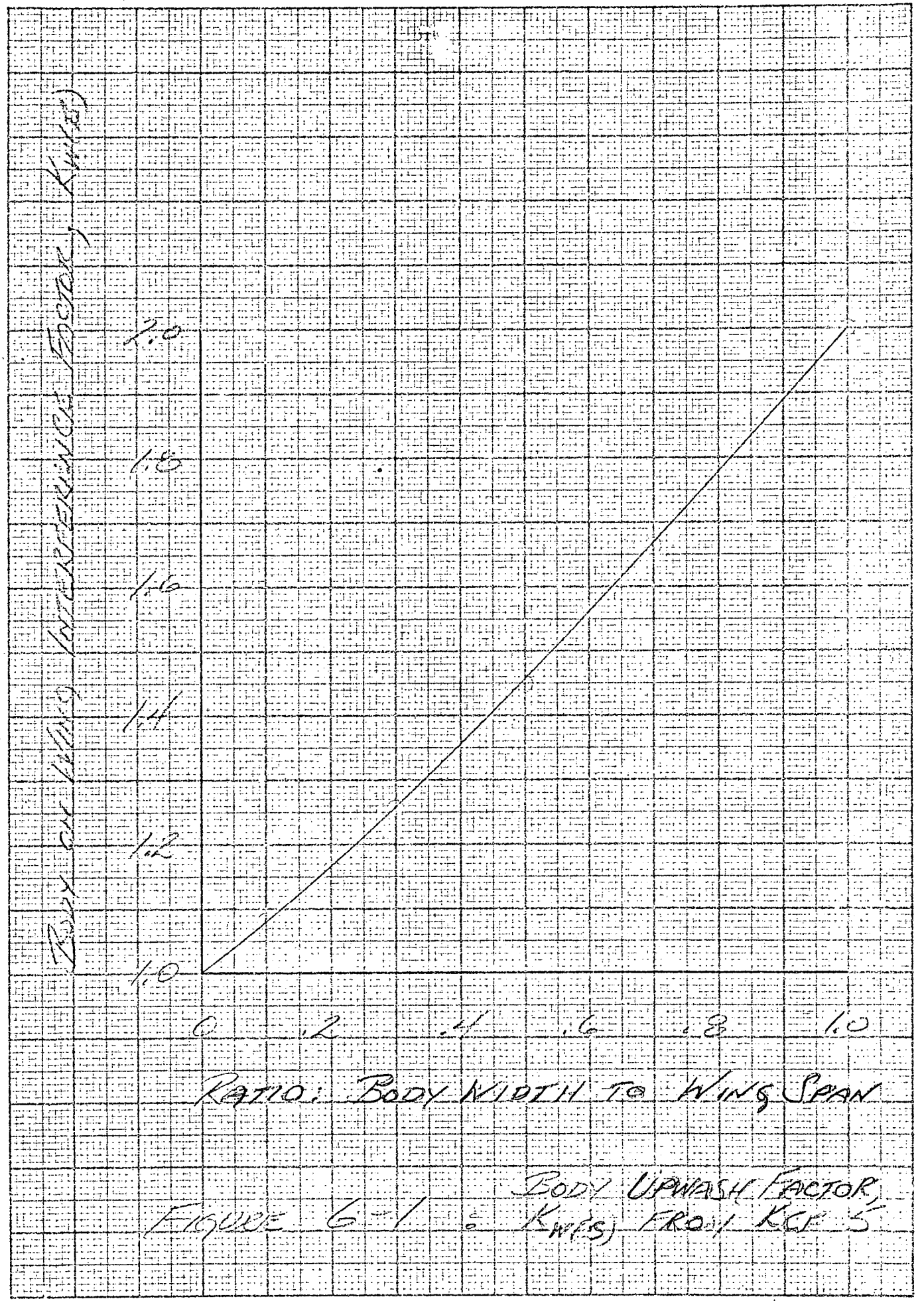

FIGURE 6-1 BODY UPWASH FACTOR, $K_{WF(S)}$ FROM KCF 5

Section 7: Wave Reflections from Bodies

It will be recalled from Sections 5 and 6 that the "Primary Interference" loads determined thus far do not account for shockwave reflections. A representative situation is illustrated in Sketch 7-A. In general the strength of the reflected flow field will be proportional to the primary interference loading and, for bodies, will decay with distance from the reflecting surface. Reflected intererences will be subordinate to the primary loading and slender body theory should be adequate for its evaluation.

For simplicity consider the special case of orbiter wave reflections off the HO tank at $\alpha_{TANK} = 0$. Let the primary interference loading on the tank over the length ΔX at station X_1 be shown in Sketch 7-B and zero elsewhere. According to slender body theory the potential function for the perturbation flow field associated with this incremental load is

$$\Omega(x,r) = -\frac{a(x)}{r}\cos\phi \qquad \text{Eq. 7:1}$$

where x, r are the cylindrical coordinates of an arbitrary field point. Equation 7:1 describes the induced flow due to a lineal dipole singularity distribution of strength $a(x)$ stretched out along the tank x axis (FRL). The local strength factor $a(x)$ can be evaluated by equating the dipole normal force to the tank primary interference loading over the interval x_1 to $x_1 + \Delta x$. Thus

$$\int_{x_1}^{x_1+\Delta x} d\left(\frac{N}{q}\right) dx = \int_0^{2\pi}\left[\int_{x_1}^{x_1+\Delta x} -c_p\, dx\right] R_{TANK}\cos\phi\, d\phi$$

$$= \int_0^{2\pi}\left[\int_{x_1}^{x_1+\Delta x} \frac{2}{V_\infty}\frac{\partial\Omega}{\partial x}\, dx\right] R_{TANK}\cos\phi\, d\phi$$

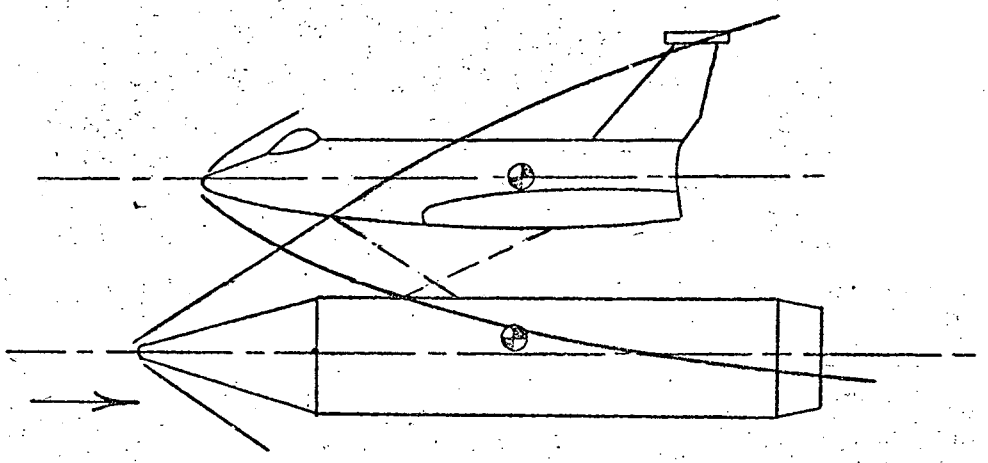

SKETCH 7-A: WAVE REFLECTIONS

——— SHOCKS

- - - - REFLECTIONS

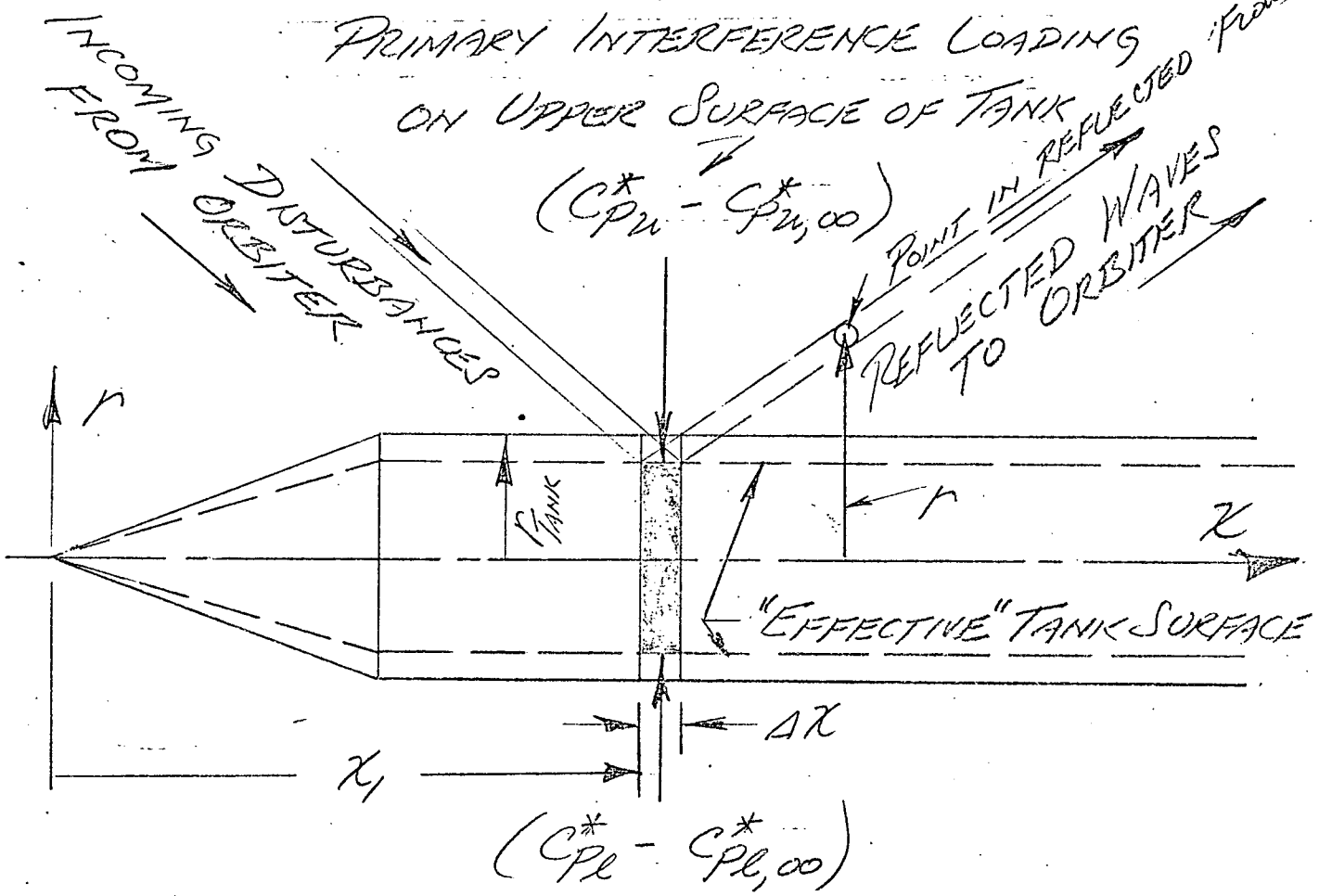

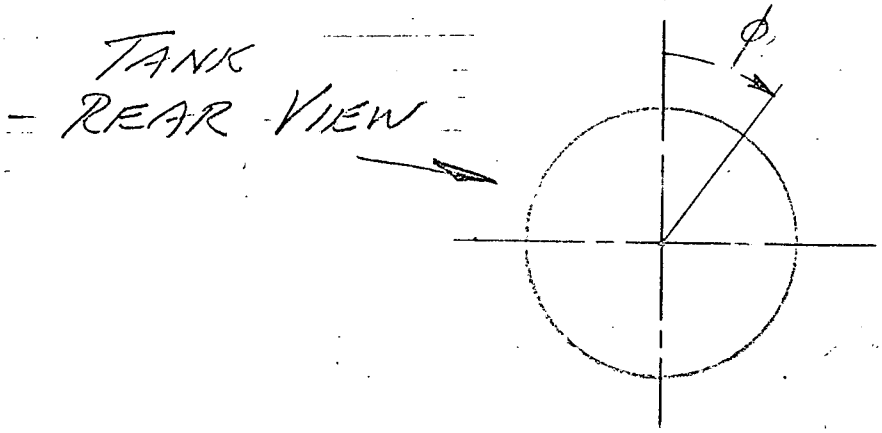

SKETCH 7-B: PRIMARY INTERFERENCE LOADING & REFLECTED WAVES

$$= -\int_0^{2\pi} \left[\int_{x_1}^{x_1+\Delta x} \frac{2}{V_\infty} \frac{1}{R_{TANK}} \frac{d\,a(x)}{dx} \cos\phi \, dx \right] R_{TANK} \cos\phi \, d\phi$$

$$= -\frac{2}{V_\infty} \left[a(x_1+\Delta x_1) - a(x_1) \right] \int_0^{2\pi} \cos^2\phi \, d\phi$$

$$= -\frac{2\pi}{V_\infty} \left\{ a(x_1+\Delta x) - a(x) \right\} \qquad \text{Eq. 7:2}$$

The normal force due to the primary interference loading can be written as

$$-W \left\{ \left(C_{p_u}^* - C_{p_{u_\infty}}^* \right) - \left(C_{p_\ell}^* - C_{p_{\ell_\infty}}^* \right) \right\} \Delta x \qquad \text{Eq. 7:3}$$

Hence, from Eq. 7:2 and 7:3

$$a(x_1+\Delta x) - a(x_1) = \frac{V_\infty}{2\pi} W \left\{ \left(C_{p_u}^* - C_{p_{u_\infty}}^* \right) - \left(C_{p_\ell}^* - C_{p_{\ell_\infty}}^* \right) \right\} \qquad \text{Eq. 7:4}$$

Substituting back into Eq. 7:1 for the potential it follows that

$$\Omega(x_1+\Delta x, r) - \Omega(x, r) = \qquad \text{Eq. 7:5}$$
$$-\frac{V_\infty}{2\pi} \frac{W}{r} \left\{ \left(C_{p_u}^* - C_{p_{u_\infty}}^* \right) - \left(C_{p_\ell}^* - C_{p_{\ell_\infty}}^* \right) \right\} \cos\phi$$

or

$$= -\frac{1}{\pi} \frac{(W/2)}{r} \left\{ \left(C_{p_u}^* - C_{p_{u_\infty}}^* \right) - \left(C_{p_\ell}^* - C_{p_{\ell_\infty}}^* \right) \right\} \qquad \text{Eq. 7:6}$$
$$\times \cos\phi$$

The left hand side of Eq. 7:6 may be rewitten as follows

$$\frac{1}{V_\infty}\left\{\Omega(x_1+\Delta x, r) - \Omega(x_1, r)\right\} = \frac{1}{V_\infty}\int_{x_1}^{x_1+\Delta x} \frac{\partial \Omega}{\partial x}\, dx$$

$$= \frac{-1}{2}\int_{x_1}^{x_1+\Delta x} \frac{-2}{V_\infty}\frac{\partial \Omega}{\partial x}\, dx$$

$$= -\frac{1}{2}\int_{x_1}^{x_1+\Delta x} c_p\, dx$$

$$= -\frac{1}{2}\,\bar{c}_p \qquad \text{Eq. 7:7}$$

where $\bar{c}_p$ is the average reflected c_p, i.e., $\bar{c}_{p_R}$ over the interval x_1 to $x_1+\Delta x$. The final expression for $\bar{c}_{p_R}$ is

$$\bar{c}_{p_R}(x_1, r) = \frac{W}{\pi r}\left\{\left(c_{p_u}^* - c_{p_{u_\infty}}^*\right) - \left(c_{p_\ell}^* - c_{p_{\ell_\infty}}^*\right)\right\} \times \cos\phi \qquad \text{Eq. 7:8}$$

On the tank surface in the plane of symmetry, $r = W/2$, $\phi = 0$,

$$\bar{c}_{p_R}(x_1, R_{TANK}) = \frac{2}{\pi}\left\{\left(c_{p_u}^* - c_{p_{u_\infty}}^*\right) - \left(c_{p_\ell}^* - c_{p_{\ell_\infty}}^*\right)\right\} \qquad \text{Eq. 7:9}$$

For $r > R_{TANK}$ the reflected wave strength varies inversely with r, i.e.,

$$\frac{\bar{c}_{p_R}(x_1, r)}{\bar{c}_{p_R}(x_1, R)} = \frac{R_{TANK}}{r} \qquad \text{Eq. 7:10}$$

Simple slender body theory (above) implies that the flow in the crossflow plane through x_1 is completely determined by the body cross-sectional shape and loading at x_1. In actual fact reflections off the tank surface will be swept aft along the local Mach wave as shown in Sketch 7-B. The AERSEP code carries this one step further and propagates the tank reflections along the characteristic structure (Mach wave net) of the isolated tank flow field.

Once the reflected wave $\bar{c}_{p_R}$ is known the remaining reflected flow properties are determined from the relations

$$\frac{p_R}{p_\infty} = 1 + \frac{\gamma}{2} M_\infty^2 \bar{c}_{p_R} \qquad \text{Eq. 7:11}$$

$$M_R = M_\infty \qquad \text{Eq. 7:12}$$

$$\bar{\theta}_{f_r} = \frac{(M_\infty^2 - 1)^{1/2}}{2} \bar{c}_{p_R} \qquad \text{Eq. 7:13}$$

It should be noted that $\bar{\theta}_{f_r}$, the average flow direction defined above, is in a sense fictitious. The reflected disturbance from the tank at x_1 influences the entire flow field aft of the Mach cone from x_1 and is not confined to the Δx wide ray indicated in Sketch 7-B. The net effect of this assumption results in only minor error in the calculated linear reflected

loading since the integrated $\bar{\theta}_{f_r}$ and the centroid of its distribution are well predicted. Nonlinear loads, which depend on local $\theta_{f_r}^2$, would be unreliable, however, and are ignored in the AERSEP reflected load calculation. Order of magnitude analysis indicates these non-linear loads will be small.

Tank shockwave and flow field reflections off the orbiter fuselage are handled in the same way as reflections off the tank. The appropriate equations for the orbiter, corresponding to Eq. 7:9 and 7:10 for the tank, are

$$\bar{C}_{p_R} = \frac{2}{\pi}\left\{\frac{W/2}{|z_\ell - z_c|}\right\}\left\{(C_{p_\ell}^* - C_{p_{\ell\infty}}^*) - (C_{p_u}^* - C_{p_{u\infty}}^*)\right\} \qquad \text{Eq. 7:14}$$

and

$$\frac{\bar{C}_{p_R}\,(\text{IN FIELD})}{\bar{C}_{p_R}\,(\text{ON SURF})} = \left|\frac{z_\ell - z_c}{z - z_c}\right| \qquad \text{Eq. 7:15}$$

where z_ℓ, z_c, z are the z coordinates of the orbiter lower surface, orbiter camber line, at x_1 and a field point on the same orbiter characteristic (Mach ray) as z_ℓ, the surface point.

Reflected loads are determined using the same AERSEP computer routines as for the primary interference load calculation where, now, the reflected flow field is substituted for the isolated flow field. The only significant change is a modification to Eq. 6:4 which, for reflected loads on the wing, now reads.

$$\alpha_{\ell_W} = \alpha_{ORB} + \theta_{f_T}\,(\text{REL TO FS AT } P)\cos^2\phi \qquad \text{Eq. 7:16}$$

The added $\cos\phi$ factor is due to the $\cos\phi$ dependence of the reflected dipole flow field.

Section 8: Wave Reflections from Wing-Bodies

The reflected flow field from the orbiter wing lower surface is defined in much the same way as the isolated wing flow field in Section 4. The primary interference load or normal force on the exposed wing panel may be written as

$$\int_{S_{WING\ EXPOSED}} \left(\Delta C_{p_W}^{*} - \Delta C_{p_{W_\infty}}^{*} \right) dS \qquad \text{Eq. 8:1}$$

In Eq. 8:1 $\Delta C_{p_W}^{*}$ and $\Delta C_{p_{W_\infty}}^{*}$ are the differential C_p across the wing (C_p lower minus C_p upper) in the isolated tank flow field and the freestream respectively. These terms can be identified with the loading integral, Eq. 6:3. Approximately one half of the primary interference loading in Eq. 8:1 is due to the primary loading on the lower surface. Thus, the refected wave strength from the wing onto the tank can be approximated by

$$\bar{C}_{p_R} = \frac{1}{2 C_R} \int_{LE}^{TE} \left(\Delta C_{p_W}^{*} - \Delta C_{p_{W_\infty}}^{*} \right) dx \qquad \text{Eq. 8:2}$$

The integral in Eq. 8:2 extends over the inboard exposed wing root chord.

The reflected flow field geometry is taken to be identical to the isolated orbiter wing-body flow field. Orbiter fuselage reflections define the flow back to the wing shock as in Sketch 4-B. The wing reflected flow prevails aft of the shock emanating from point "B" in Sketch 4-C.

Section 9: Summary and AERSEP Input Data Requirements

AERSEP input data requirements are modest as may be seen by the following NASA MSC 040-A data-set. Sketch 9-A portrays the 040-A orbiter "True", "Approximate", and "Effective" profiles (see Section 3 for definitions) used to generate the AERSEP predictions appearing in Sections 10.2 to 10.7. Vertical ordinate data and fuselage width at each control station are indicated in Sketch 9-B. Effective crossflow drag ratios, $C_D/2$, and decay constants, C, for each fuselage plug are also noted. Both parameters are determined by the local cross-sectional shape using Figures 9-1 and 9-2 except in nose regions where $C_D/2 = 1.0$. In addition AERSEP's fuselage representation is stereotyped as constant-section from the exposed root chord leading edge aft.

Input data for the wing is limited to a specification of the leading edge location (Fuselage Station) at the exposed root and tip, the reference wing semi-span, and wing root incidence, i_W. The present code assumes a simple trapazoidal planform with an unswept trailing edge terminating at the fuselage base. Where some (modest) fuselage extension beyond the wing and/or trailing edge sweep is encountered ignore the extended fuselage length and substitute an equivalent exposed wing panel with the same root chord, area, and 50% MGC location. The effects of orbiter fuselage upwash on the wing is accounted for by a $K_{W(B)}$ factor (see Figure 6-1) which, within reason, may alternately be selected to match isolated orbiter predicted C_{m_α} with data.

HO Tank data appear in Sketch 9-C which parallels the orbiter fuselage presentation. Both orbiter and tank moment reference center locations are specified in their individual body axis system.

AERSEP nomenclature and sign convention for the relative orbiter-tank positioning is indicated in Sketch 9-D. The primary data are X, Z, α_i, and α. Tank angle of attack, α_T, is a derived quantity. More detailed information concerning the AERSEP code is given in the users manual, Reference 7.

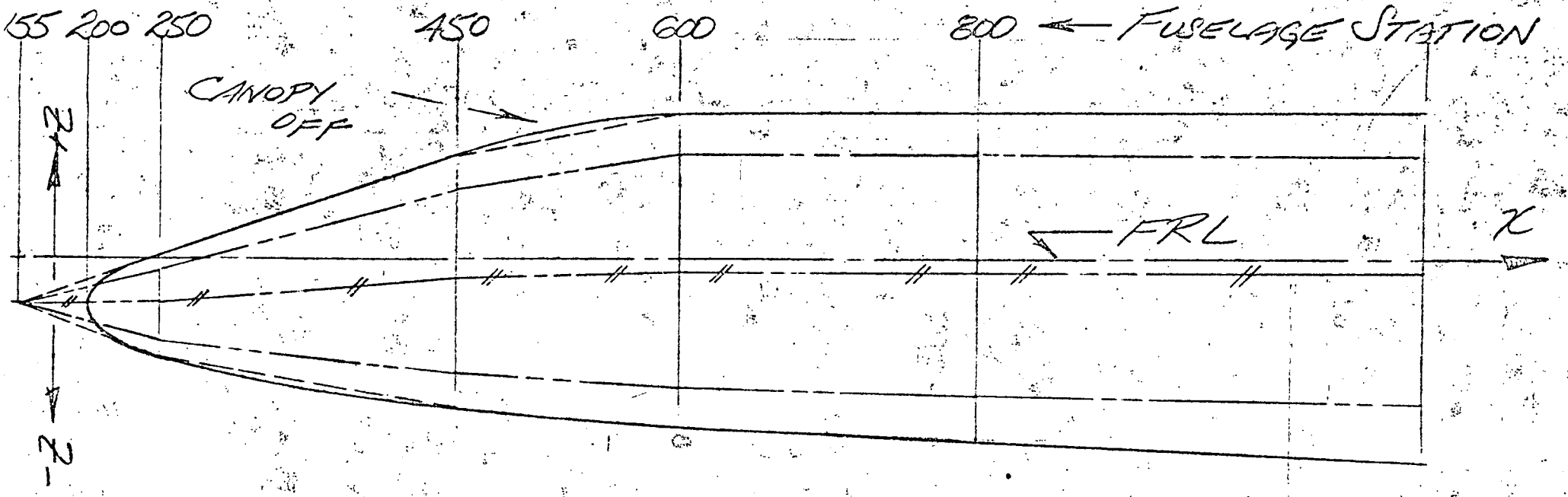

SKETCH 9-A ORBITER FUSELAGE GEOMETRY

TRUE ORBITER FUSELAGE INBOARD PROFILE

AERSEP APPROXIMATE ORBITER FUSELAGE INBOARD PROFILE USED IN FLOW FIELD CALCULATION

AERSEP FUSELAGE MEAN CAMBER LINE

AERSEP "EFFECTIVE" ORBITER FUSELAGE INBOARD PROFILE USED IN EVALUATION OF AERODYNAMIC LOADS

C 78

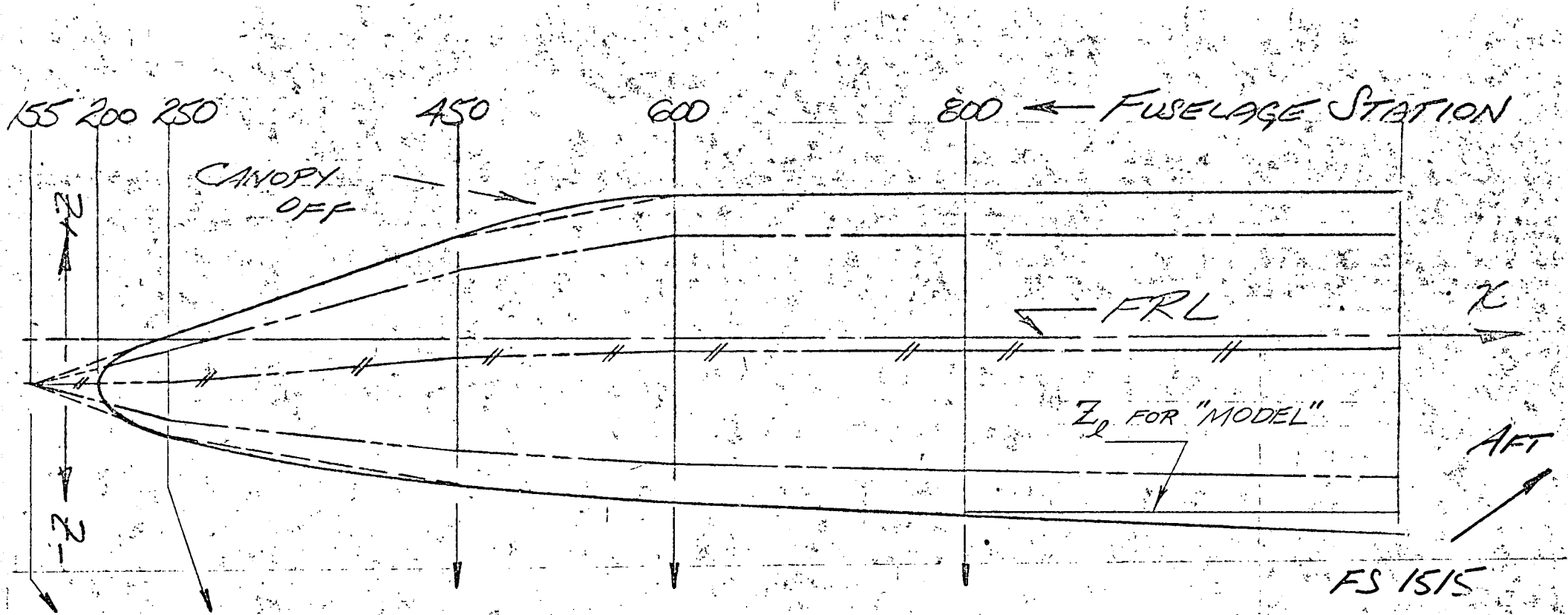

$Z_u = -31$	$Z_u = +1$	$Z_u = +71$	$Z_u = +100$	$Z_u = +100$	$Z_u = +100$
$Z_{eu} = -31$	$Z_{eu} = -5$	$Z_{eu} = +57$	$Z_{eu} = +84$	$Z_{eu} = +84$	$Z_{eu} = +84$
$Z_{e\ell} = -31$	$Z_{e\ell} = -64$	$Z_{e\ell} = -87$	$Z_{e\ell} = -99$	$Z_{e\ell} = -122$	$Z_{e\ell} = -122$
$Z_\ell = -31$	$Z_\ell = -71$	$Z_\ell = -103$	$Z_\ell = -111.5$	$Z_\ell = -122$	$Z_\ell = -122$
$W = 0$	$W = 68$	$W = 171$	$W = 204$	$W = 204$	$W = 204$
$\frac{C_D}{2} = 1$	$\frac{C_D}{2} = 1$	$\frac{C_D}{2} = 1$	$\frac{C_D}{2} = .93$	$\frac{C_D}{2} = 1$	
$C = 1.65$	$C = 1.95$	$C = 2.25$	$C = 2.75$	$C = 3.1$	

SKETCH 9-B: AERSEP INPUT DATA FOR 040-A ORBITER FUSELAGE

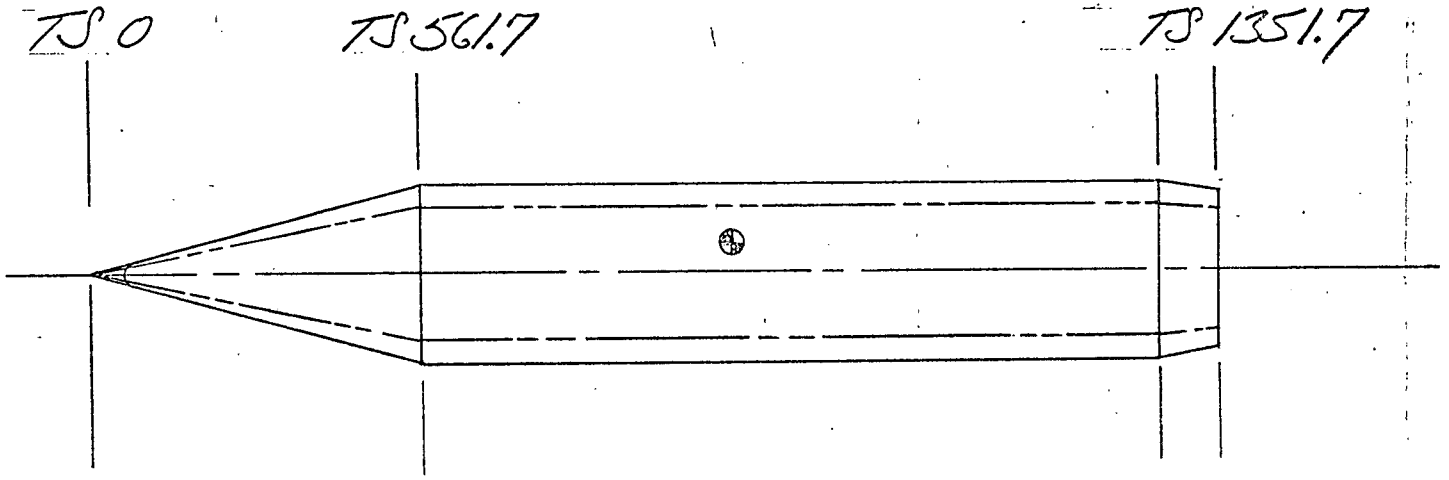

FS 0	FS 561.7	FS 1351.7
$z_u = 0$	$z_u = 150$	$z_u = 150$
$z_{e_u} = 0$	$z_{e_u} = 118$	$z_{e_u} = 118$
$z_{e_\ell} = 0$	$z_{e_\ell} = -118$	$z_{e_\ell} = -118$
$z_\ell = 0$	$z_\ell = -150$	$z_\ell = -150$
$W = 0$	$W = 300$	$W = 300$
$\frac{C_D}{2} = 1$	$\frac{C_D}{2} = .667$	
$c = 1.65$	$c = 1.65$	

SKETCH 9-C: AERSEP INPUT DATA FOR HO TANK

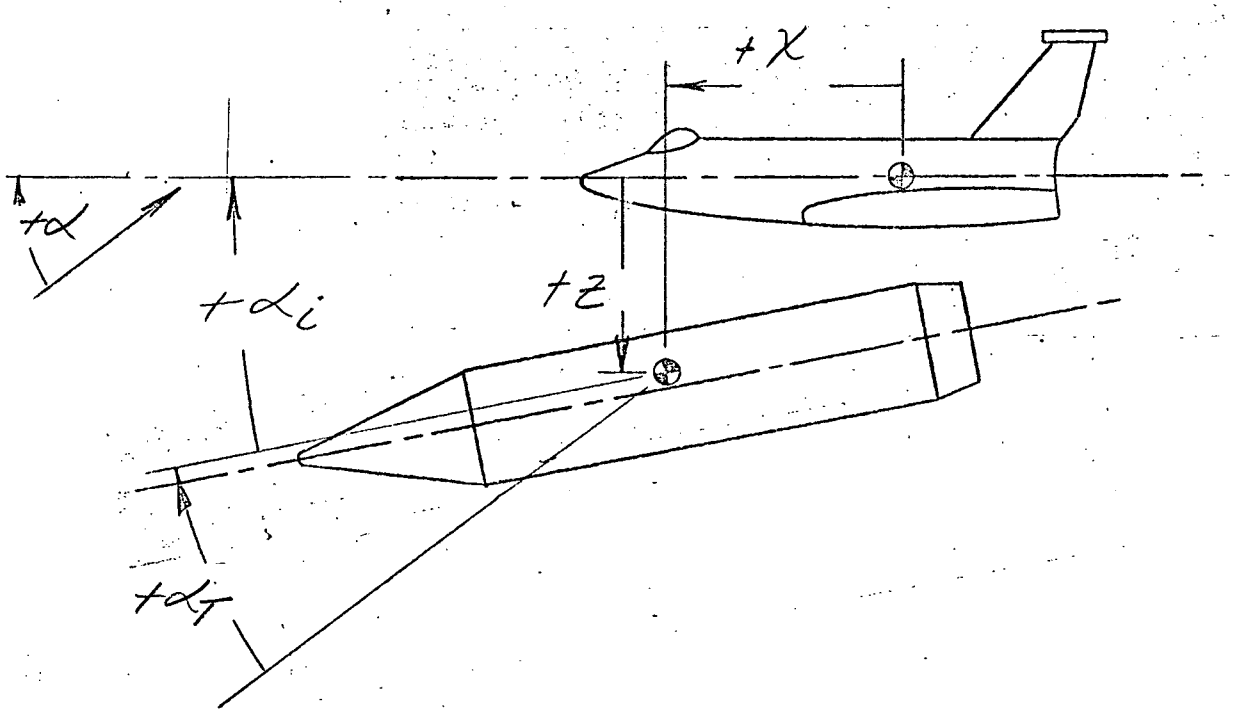

SKETCH 9-D: AERSEP NOMENCLATURE FOR RELATIVE POSITIONING OF SHUTTLE ORBITER - HO TANK

FIGURE 5-1 EFFECT OF FUSELAGE CROSS-SECTION ON C_{D_2}

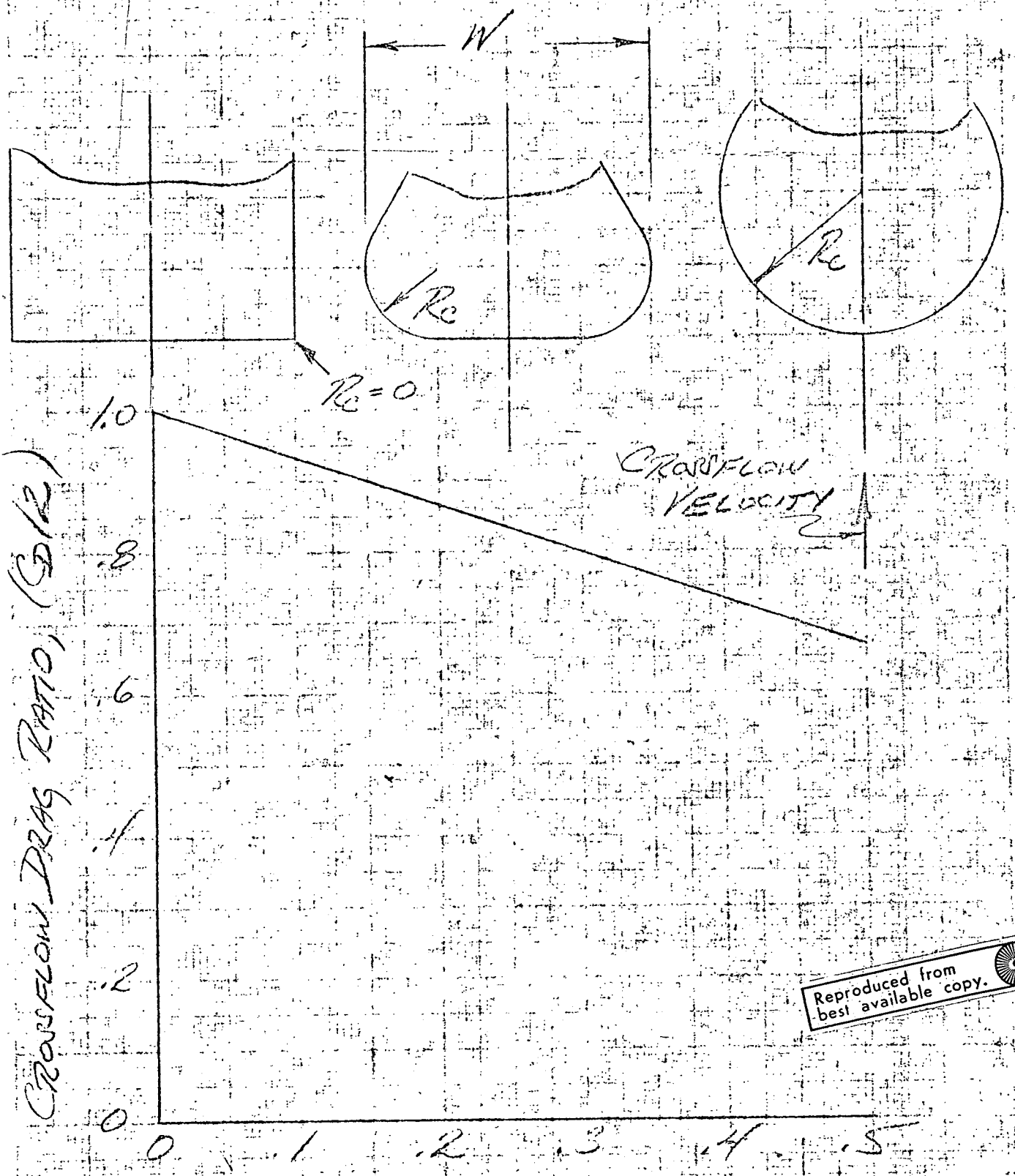

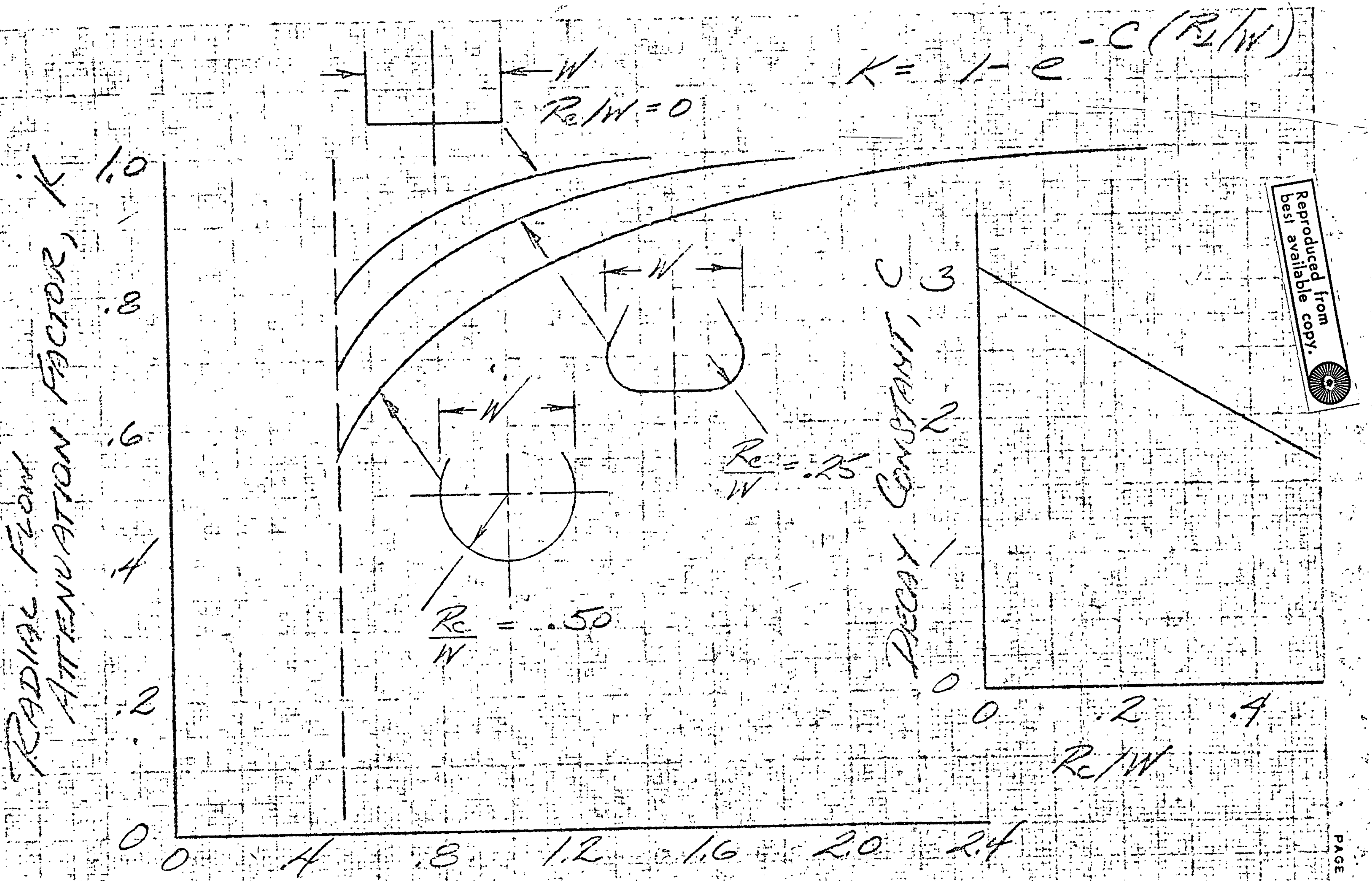

SEPARATION DISTANCE TO CAMBER LINE, R_L/W
(FROM "RECEIVER" EFFECTIVE SURFACE TO "GENERATER" CAMBER LINE)

~~Fig. 9~~-2: RADIAL FLOW EFFECT ON CROSSFLOW DRAG

Fig 9-2

NASA MSC 040-A

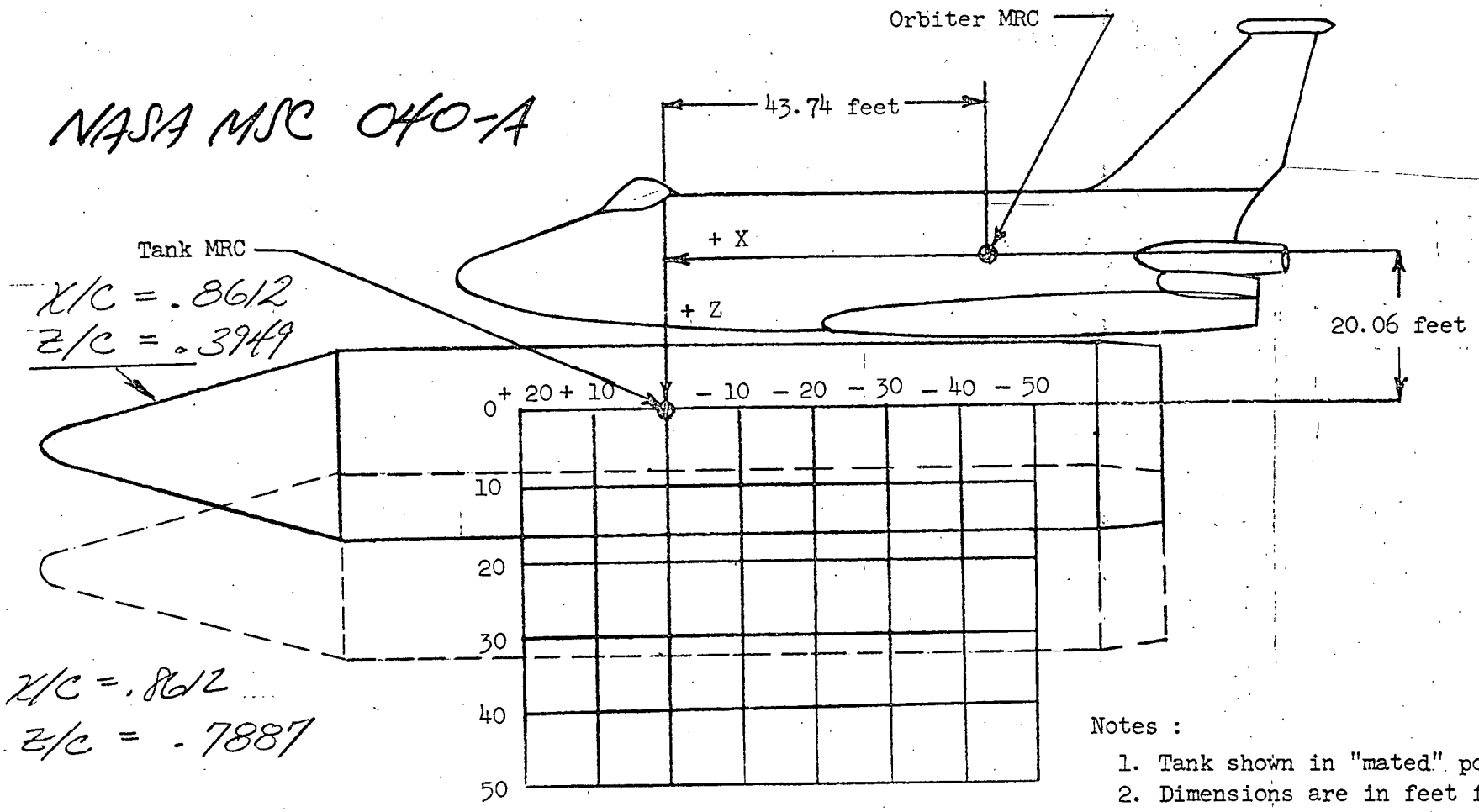

Notes :

1. Tank shown in "mated" position.
2. Dimensions are in feet full scale.

X, full scale, ft measured from "mated" position	$X/\bar{c}$ measured from Orbiter MRC to tank MRC	Z, full scale, ft measured from "mated" position	$Z/\bar{c}$ measured from Orbiter MRC to tank MRC
-50	-.1232	0	.3949
-30	.2705	8	.5525
-25	.3690	10	.5918
-20	.4674	12	.6312
-10	.6629	18	.7493
0	.8612	20	.7887
10	1.0580	30	.9856
20	1.2549	40	1.1825
		50	1.3754

$609.5'' = \bar{c}$

Figure 7 .- Separation Variable Grid.

Section 10: Data Comparisons - General Results

AERSEP predictions for representative configurations are compared with wind tunnel data in Figures 10.1 through 10.7. In all figures the experimental data are denoted by open symbols and AERSEP predictions by heavy crosses. All test data have been plotted to as large a scale as warrented by reading accuracy from the original source.

AERSEP results and data for parallel staged tanks at M = 2,5 and 10 are compared in Figures 10.1-1 through 10.1-9. The zero stagger side by side arrangement results in high levels of interference. For the closest spacing at M = 2 the nose shock from each impinges on the forebody of the other resulting in extreme surface pressures and undoubtedly some local ~~shock~~ reflected shock detachment. Despite this the interference moment is reasonably well predicted at all α. The normal force correlation is less satisfactory.

Pitching moment and normal force predictions at M = 5 show good agreement with data barring the normal force at α = 8? At M = 10 an extreme sensitivity to small variations in separation distance is noted and the AERSEP results are slightly displaced from the available data. It is clear, however, that the heavy nose-down moment at the close spacing must reverse to a strong nose-up as the tanks separate and the impinging shock "walks" back. The high M results imply that the analysis is sensitive to the precise selection of receiver "effective height" at which average incident flow properties for determining Tank "2" loads are evaluated. The need to select an "average" point can be avoided by employing a three dimensional receiver surface subdivided into small panels for local loads evaluation. This alternative was considered when formulating the present code but was ruled out by schedule limitations.

AERSEP calculations and isolated 040-A Tank data at M = 1.96 and 4.0 are compared in Figures 10.2-1, 10.2-2. The predicted results are independent of Mach No., underestimate the lift at low angle-of-attack, and underestimate the pitching moment at M = 1.96. In common with contemporary engineering programs AERSEP ignores fuselage forebody-on-afterbody lift carry-over effects. The carry-over lift aerodynamic center is near the shoulder at low Mach No. and moves aft at high Mach No. which accounts for the pitching moment discrepancy at M = 1.96. Nonetheless the agreement with data indicates that AERSEP's loading analysis is adequate for the present purposes.

Isolated 040-A orbiter characteristics and AERSEP predictions are compared in Figure 10.3-1 and 10.3-2. AERSEP does not account for wing twist or camber effects, hence, the C_{M_o} prediction should be ignored. This simplification has virtually no effect on predicted interference levels and does not compromise AERSEP's utility for this purpose in practical abort-separation cases. Lift curve slope and longitudinal stability show excellent correlation with data at M = 1.96 and M = 4.0.

Representative NASA 040-A Orbiter/Tank wind tunnel data (Ref. 6) and AERSEP interference predictions are compared in Figures 10.4 through 10.7. No simple generalization of these data is possible except to note that in a majority of cases the AERSEP results are within ΔC_N, $\Delta C_M \leq .015$ of the test data, i.e., within the accuracy level of contemporary arbitrary body computer programs limited to interference-free configurations.

Earlier in this section it was noted that the present code uses a minimum of information to describe the Orbiter/Tank geometry. Instead AERSEP employs cross flow drag coefficients, radial flow factors, a body upwash factor, and "effective" fuselage upper/lower heights to determine average values which summarize the principal configuration effects. Preliminary 040-A AERSEP correlations indicated

that an alternative technique for calculating average flow direction in the tank (Orbiter) afterbody flowfield gave better results than the method prescribed in Section 3 and 5. Instead of using the flow direction in the vertical plane of symmetry (Eq. 3:29-3:39) the average direction is now related to the local C_p. Spacifically where the generator $\beta \tan \theta_c \leq .15$ the average local flow direction is given by:

Lower Surface

$$\theta_f \text{ (REL. TO FREESTREAM)} = -\frac{(M_\infty^2-1)^{1/2} C_p}{2}$$

Upper Surface

$$\theta_f \text{ (REL. TO FREESTREAM)} = +\frac{(M_\infty^2-1)^{1/2} C_p}{2}$$

With the advantage of hindsight the explanation is almost obvious. At angle of attack the subsonic crossflow velocity distribution around, say, the tank will vary betweeen twice the freestream value at the maximum breadth to zero (rel. to FRL) in the vertical plane of symmetry. Moving away from the tank surface there is a strong tendency for the average crossflow to return to the freestream value, θ_f(rel to freestream) $\approx \alpha_{FRL}$, so that in effect at small $+\alpha$ the adjacent orbiter fuselage is not shielded by the belly mounted tank.

With regard to the selection of other AERSEP parameters the following should be noted. Extensive experience with delta wing shuttle orbiter configurations has consistently shown that selecting $K_{W(B)} = 1$ gives the best isolated orbiter predictions. The same proves true for predicting interference effects. Slightly better correlation was also observed when the AERSEP wing shock was defined to originate from the exposed root chord leading edge instead of the B* location prescribed in Section 4. This choice partially compensates for wing thickness effects not included in the AERSEP analysis.

In reviewing various 040-A AERSEP calculations and laying out the computed flowfield structure it was noted that at no time did the HO Tank lower surface reflections impinge onto the orbiter. The code was modified accordingly so that only orbiter-lower-surface/tank-upper-surface primary loads were used to determine the reflected wave strength.

All AERSEP results in this section were calculated using the procedural modifications noted above. In summary the data correlations suggest that extending the present AERSEP code to incorporate a three dimensional model of the orbiter-tank geometry would result in consistently better estimates particularly at $M \geq 4$. As it is, by judicious averaging, the present AERSEP code prediction accuracy (with interference) approaches that expected for interference-free situations.

CONCLUSION

An engineering analysis and AERSEP computer code for predicting NASA Shuttle Orbiter - HO Tank longitudinal aerodynamic characteristics during abort separation has been developed. Computed results are applicable at Mach number above 2 for angle-of-attack between $\pm$ 10 degrees. No practical restrictions on orbiter-tank relative positioning are indicated for tank-under-orbiter configurations. AERSEP is also compatible with the NASA JSC UNIVAC 1108 Executive System. Input data requirements and running time are minimal facilitating its use for parametric studies, test planning, and trajectory analysis. In a majority of cases AERSEP Orbiter-Tank predictions with interference are comparable in accuracy with state-of-the-art estimates for interference-free configurations.

Further generalization and/or refinement of the present AERSEP formulation to expand the applicable flight envelope is feasible. Extending AERSEP to incorporate a detailed three dimensional orbiter-tank geometry model would result in improved estimates throughout the present flight envelope $M \geq 2$, $\alpha \pm 10^{o}$.

REFERENCES

1. Sims, Joseph L.; Tables for Supersonic Flow Around Right Circular Cones at Zero Angle-of-Attack, NASA SP 3004, 1964.
2. Jones, D. J.; Tables of Inviscid Supersonic Flow About Circular Cones at Incidence, $\gamma = 1.4$, Vol. I and II, AGARDograph 137, 1969.
3. Ames Research Staff; Equations, Tables, and Charts for Compressible Flow, NACA TR 1135.
4. Hoerner, Sighard H.; Fluid-Dynamic Drag, 1958.
5. Pitts, William C., Nielsen, Jack N., and Kaattari, George E.; Lift and Center of Pressure of Wing-Body-Tail Combinations at Subsonic, Transonic, and Supersonic Speeds, NACA Rep. TR 1307.
6. Fossler, Ivy and Cole, Paul; Abort Staging Characteristics of an External Oxygen Tank Separating from the Space Shuttle 040-A Orbiter at Mach Numbers of 0.6, 2.0, and 4.0, NASA DMS DR-1241, June 1972.
7. Vachris, A.; AERSEP Users Manual

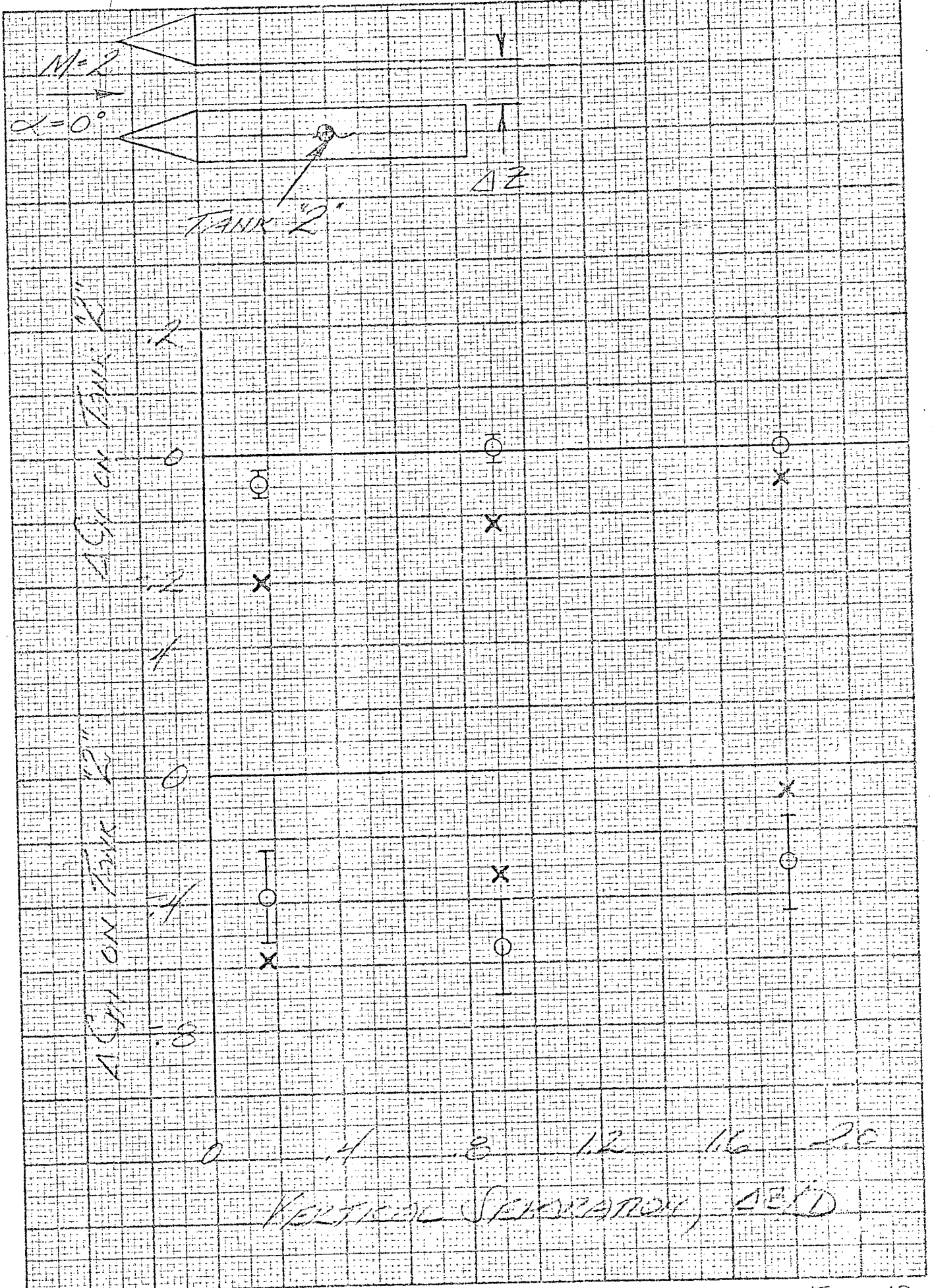
M=2
α=0°
Δz
TANK "2"
TANK "2" ON TANK "1"
TANK "1" ON TANK "2"
0
.4
.8
1.2
1.6
2.0
KEYSTONE SEPARATION, AERO

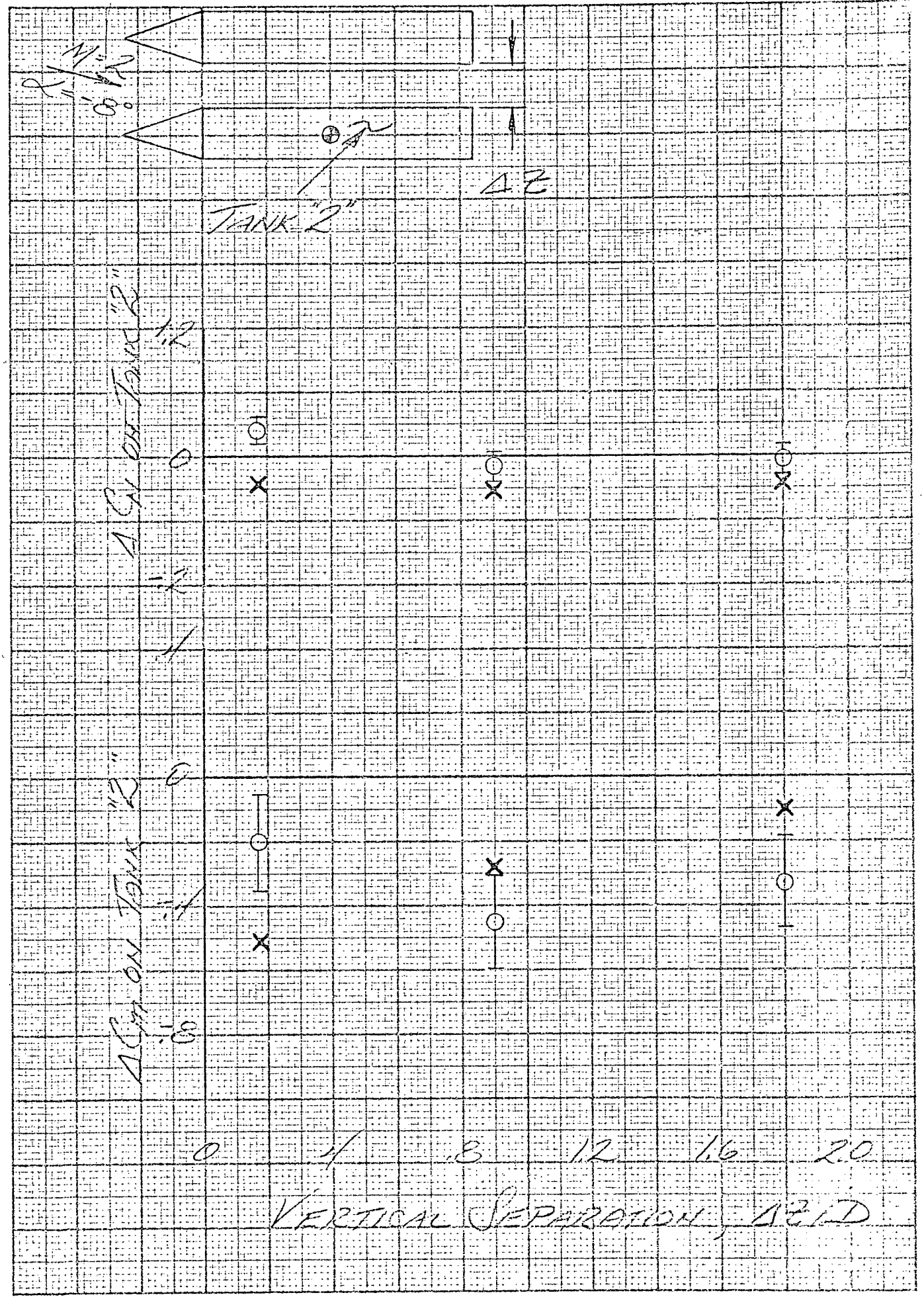
N
Δ Z
TANK "2"
Δ Z ON TANK "2"
Δ Z ON TANK "2"
0
.4
.8
1.2
1.6
2.0
VERTICAL SEPARATION, Δ Z IN

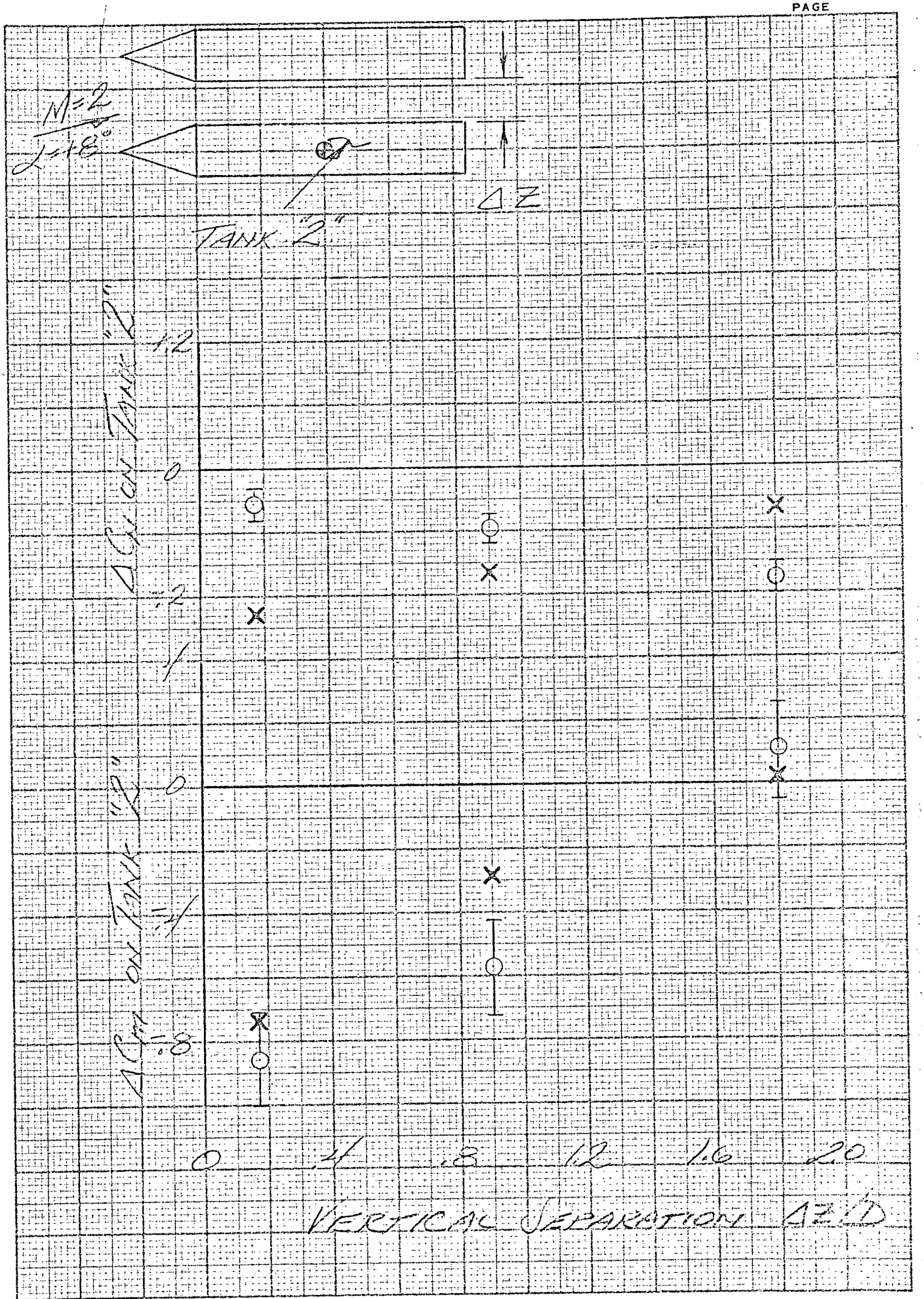
M=2
α=8°
ΔZ
TANK "2"
ΔCp on Tank "2"
1.2
1.0
.8
.6
.4
.2
0
ΔCp on Tank "1"
.4
.2
0
-.2
-.4
-.6
-.8
0
.4
.8
1.2
1.6
2.0
VERTICAL SEPARATION ΔZ/D

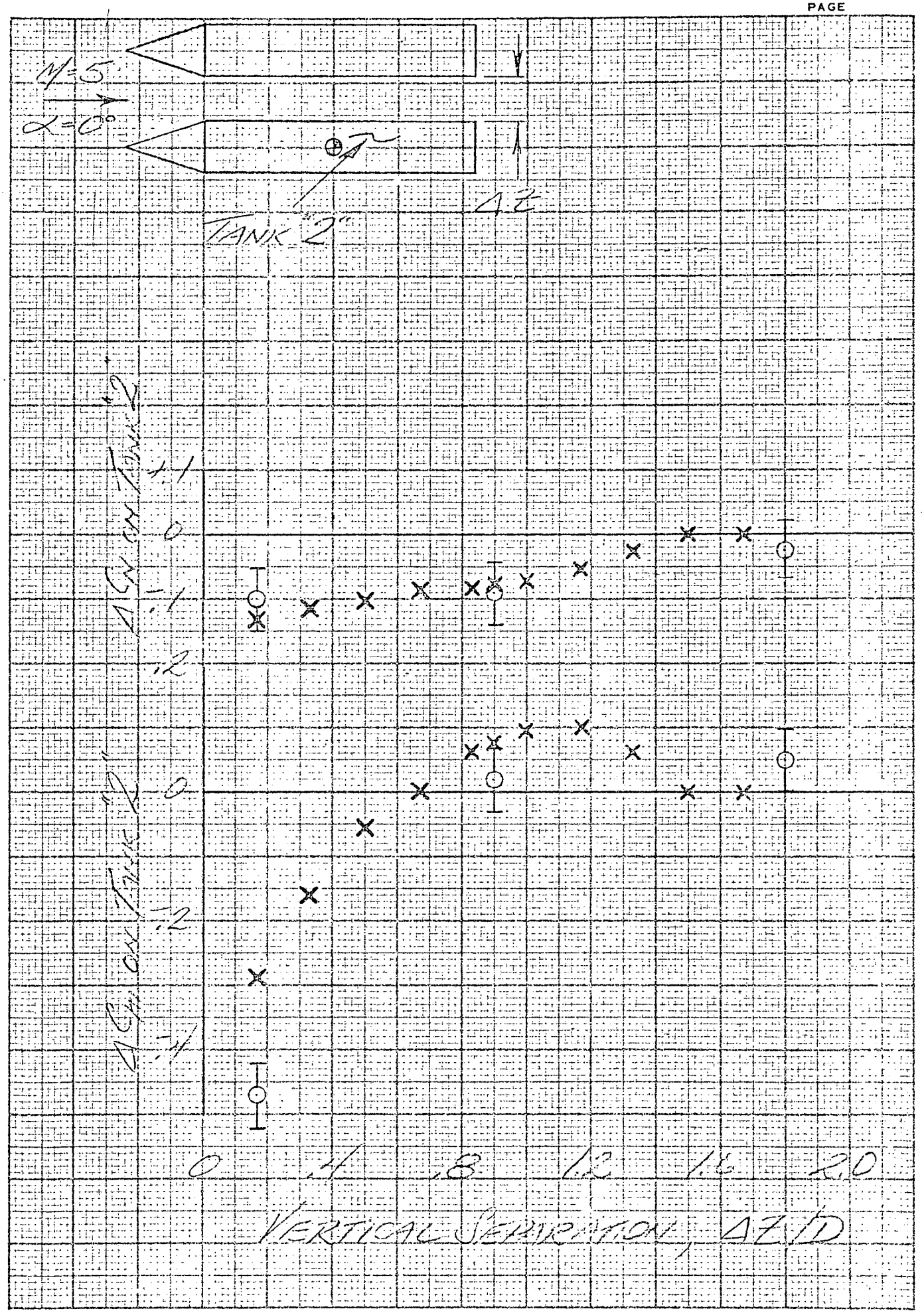
M=5.
α=0°
ΔZ
TANK "2"
ΔC_M Tank #2
ΔC_M Tank #1
+.1
0
-.1
-.2
-.1
-.2
0
.4
.8
1.2
1.6
2.0
VERTICAL SEPARATION, ΔZ/D

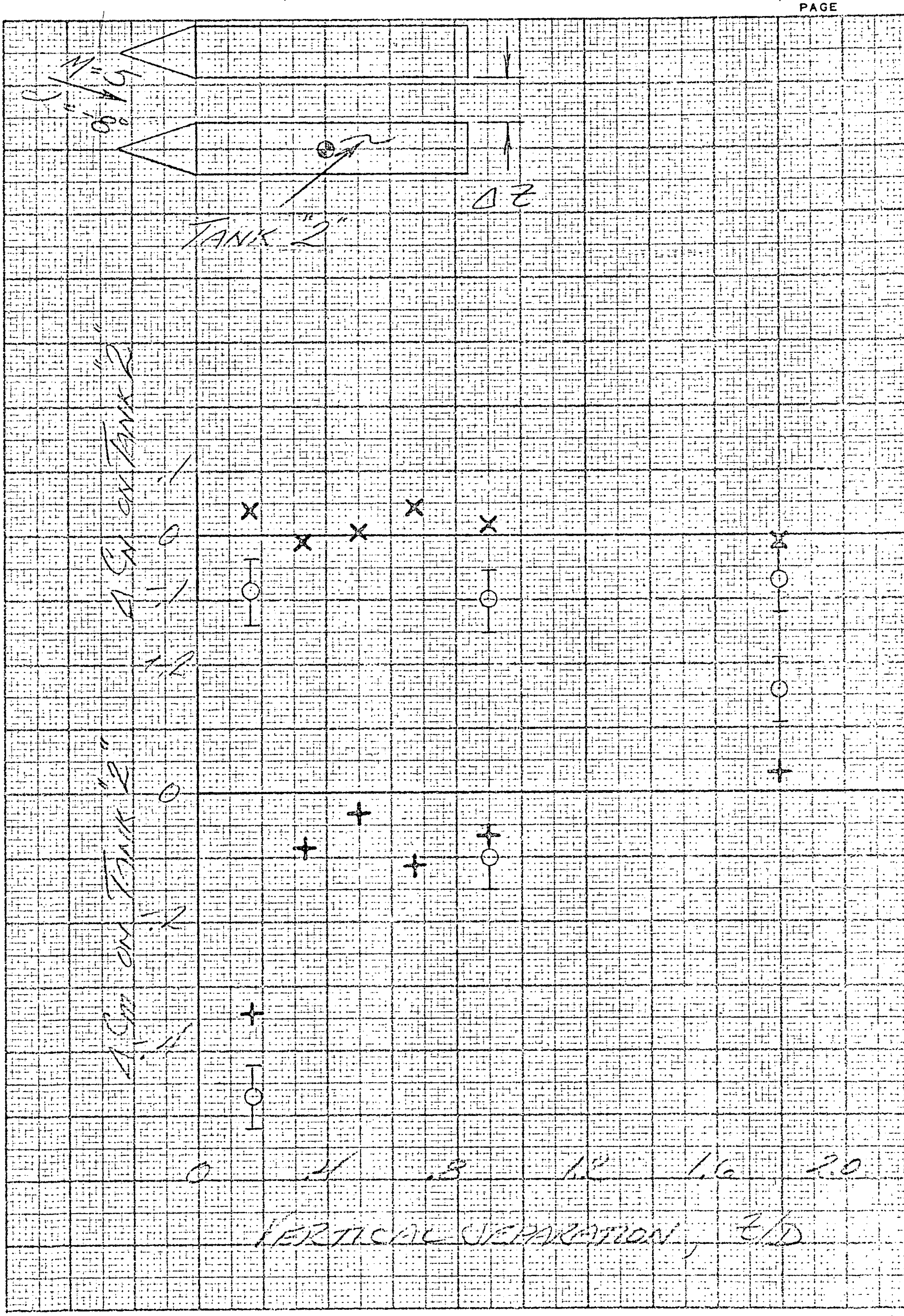
M = 5
C/L
.8"
ΔZ
TANK "2"
ΔCN on TANK 2
.1
0
-.1
-.2
ΔCm on TANK "2"
0
-.2
-.4
0
.4
.8
1.2
1.6
2.0
VERTICAL SEPARATION, Z/D

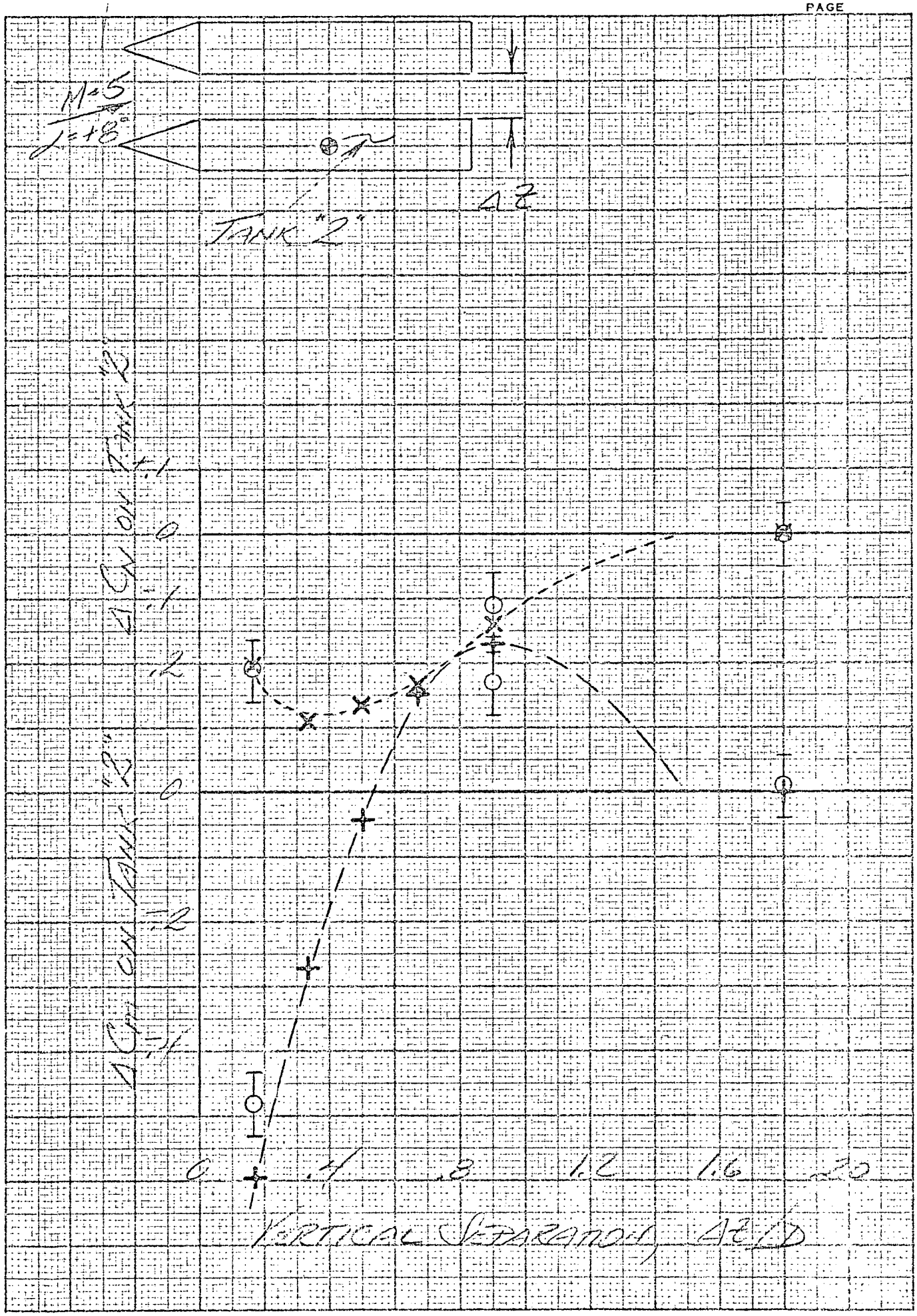
M=5
α=+8°
Δz
TANK "2"
ΔC_N on TANK "2"
ΔC_N on TANK "1"
0
-.1
-.2
0
-.2
-.1
0
.4
.8
1.2
1.6
2.0
VERTICAL SEPARATION, Δz/D

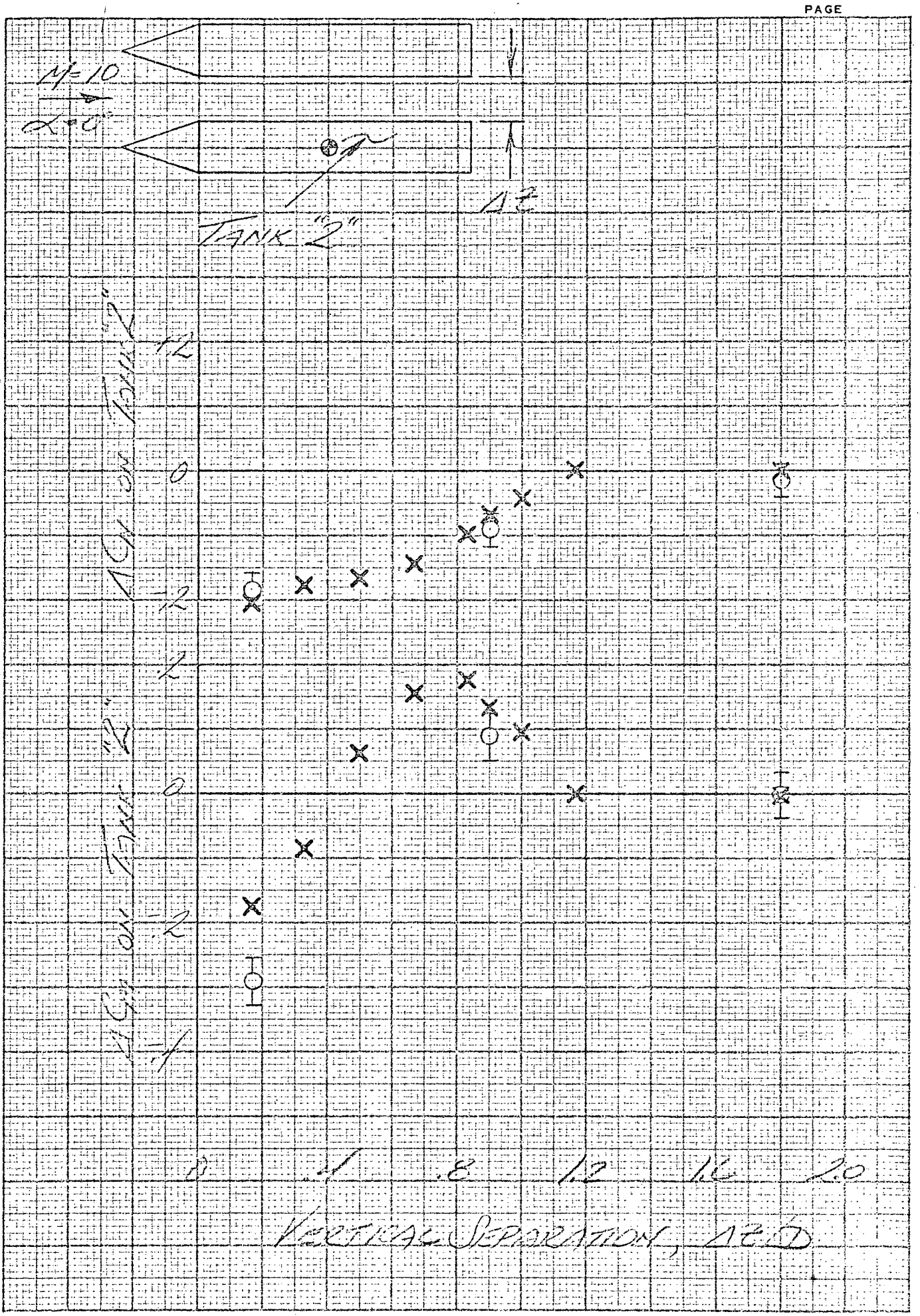
M=10
α=0°
TANK "2"
ΔCN on Tank "2"
1.2
0
-.2
.2
ΔCN on Tank "1"
0
-.2
-.4
0
.4
.8
1.2
1.6
2.0
VERTICAL SEPARATION, Δz/D

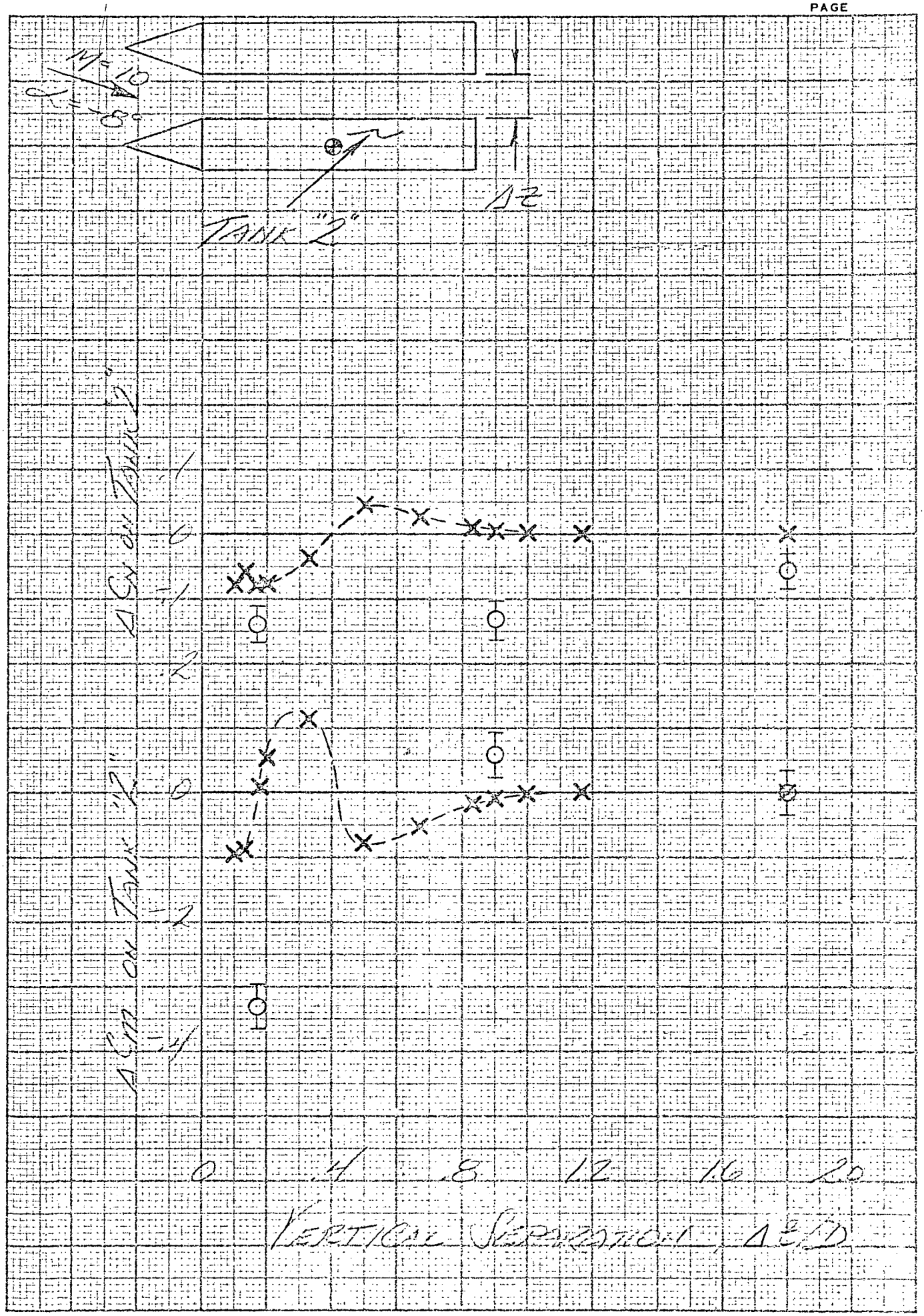
M = 1.0
α = 0°
Δz
Tank "2"
ΔCN on Tank "2"
Tank "1"
ΔCm on Tank "1"
0
4
8
12
16
20
Vertical Separation, Δz/D

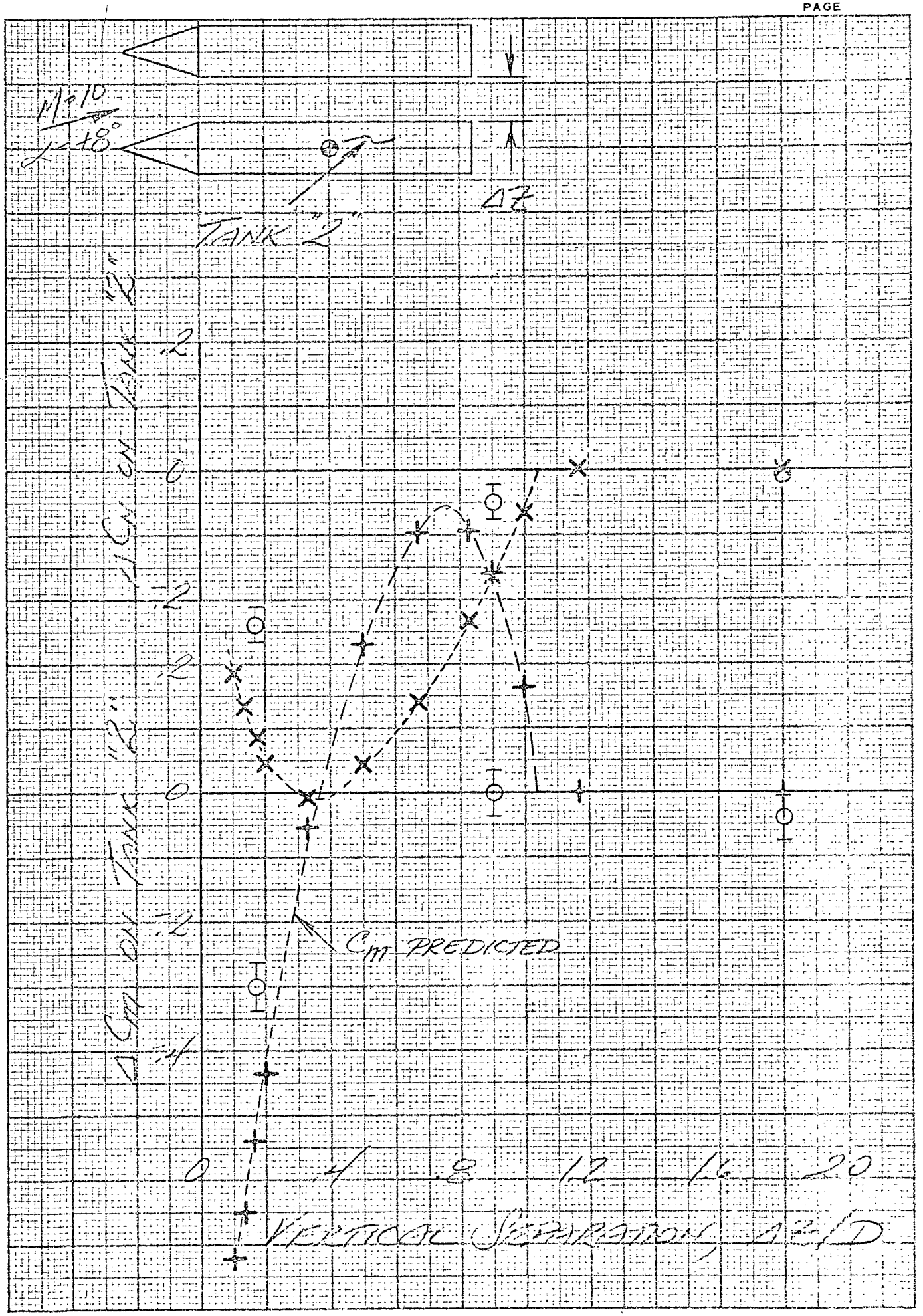
M=10
α=±0°
ΔZ
TANK "2"
ΔCm ON TANK "2"
ΔCm ON TANK "1"
Cm PREDICTED
VERTICAL SEPARATION, Z/D
0
4
8
12
16
20
2
1
0
-1
-2

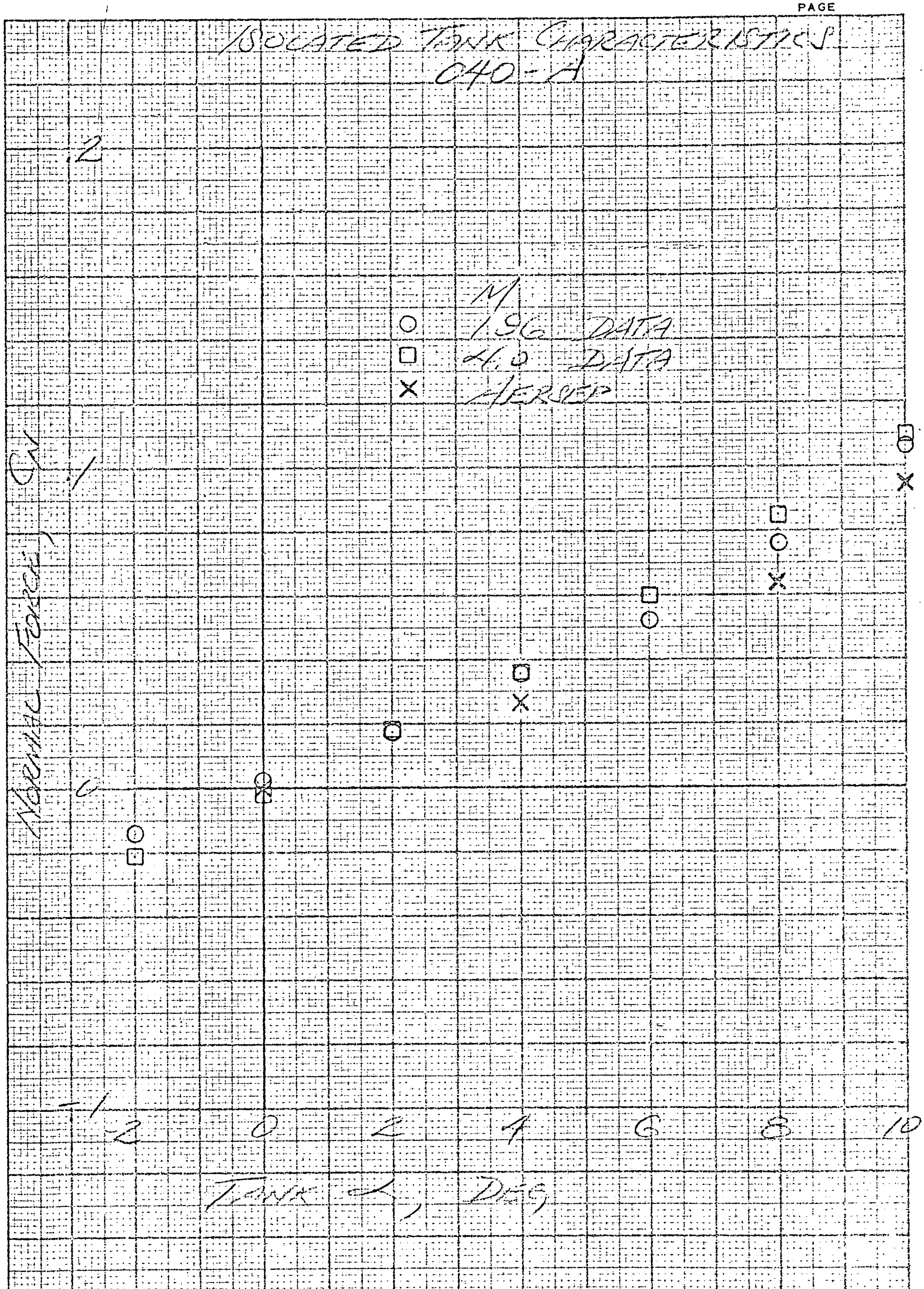
ISOLATED TANK CHARACTERISTICS
040-A
M
1.96 DATA
4.0 DATA
HERSEP
Normal Force, CN
.2
.1
0
-.1
-2
0
2
4
6
8
10
Tank α, Deg

FIG. 10.2-1

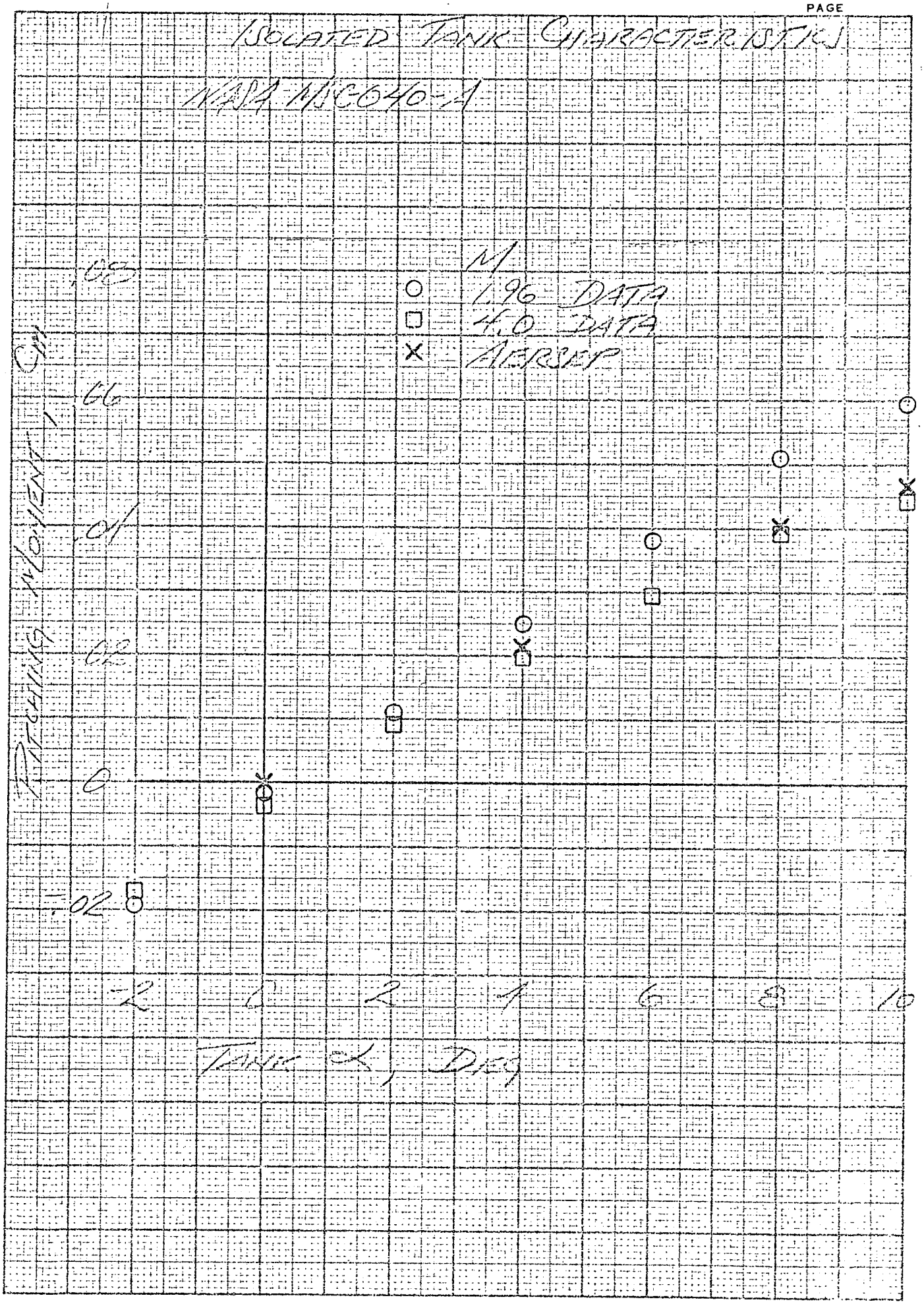
ISOLATED TANK CHARACTERISTICS
NASA MSC040-A
M
1.96 DATA
4.0 DATA
AEDC
PITCHING MOMENT, Cm
.08
.06
.04
.02
0
-.2
0
.2
.4
.6
.8
1.0
TANK CL, DEG

Fig. 10.2-2

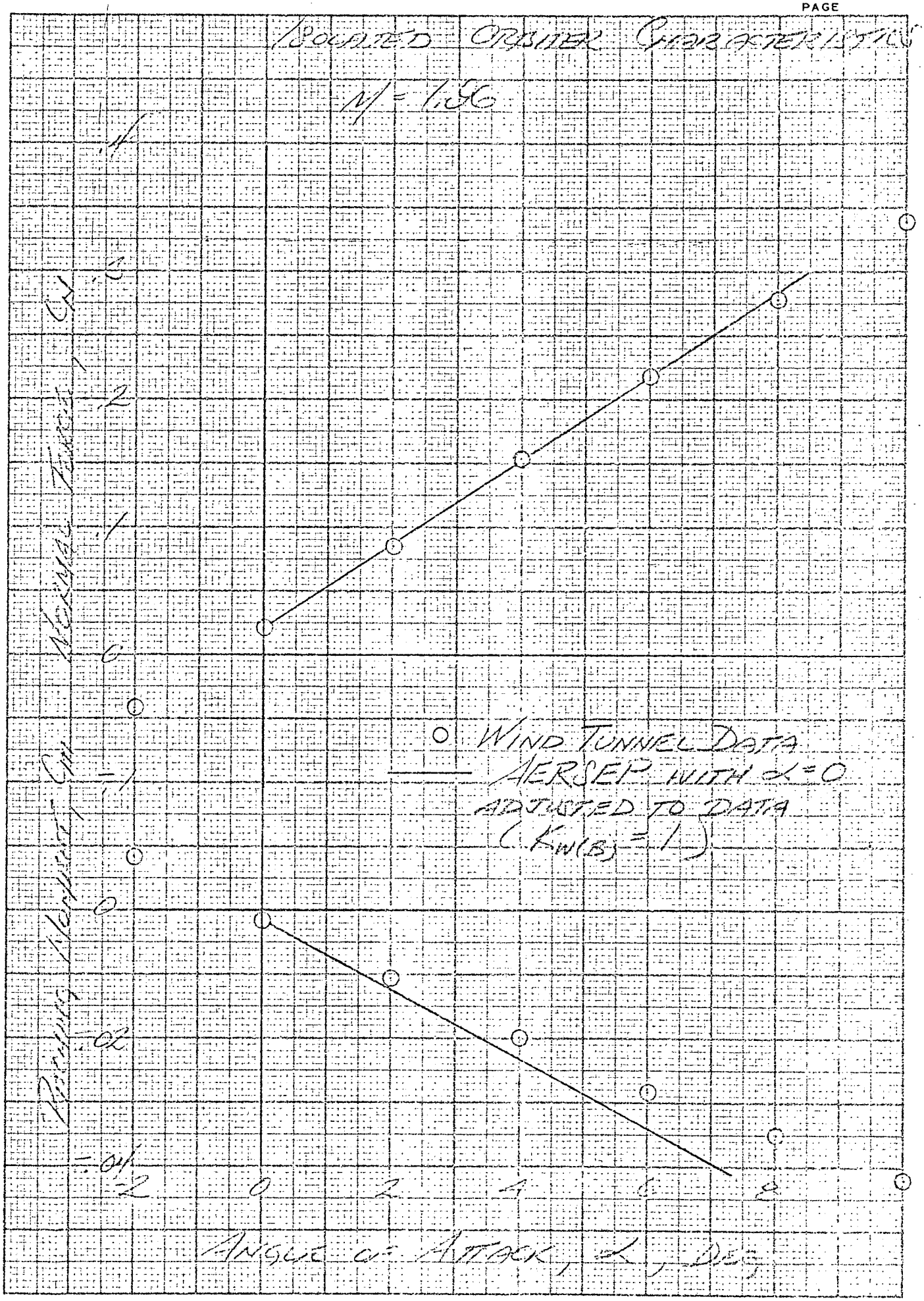
COUPLED ORBITER CHARACTERISTICS
M = 1.56
ROLLING MOMENT, C_{ℓ_w}
.4
.2
0
-.2
-.4
WIND TUNNEL DATA
AERSET WITH $\alpha = 0$ ADJUSTED TO DATA ($K_{W(B)} = 1$)
-2
0
2
4
6
8
ANGLE OF ATTACK, α, DEG

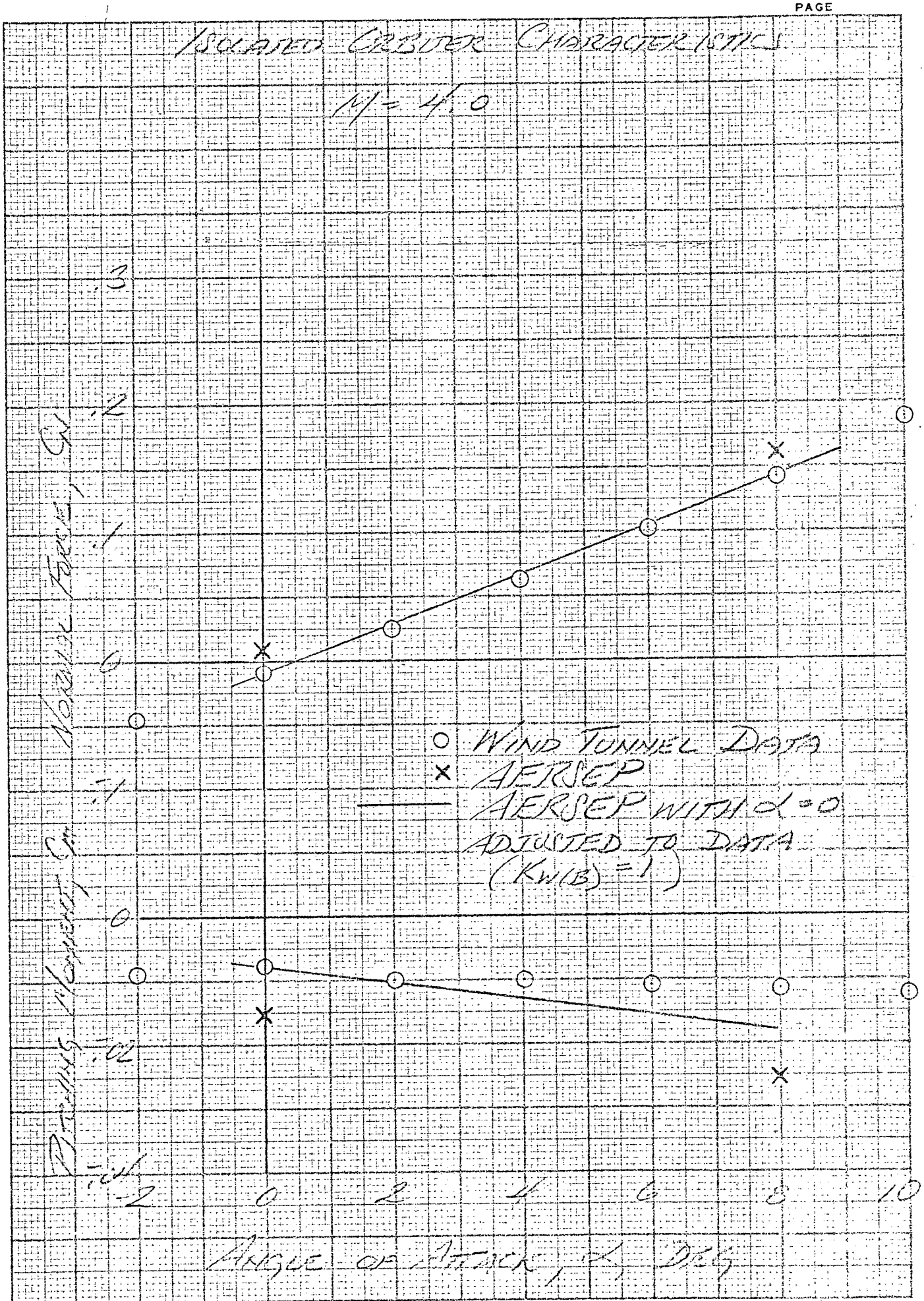
ISOLATED CANARD CHARACTERISTICS
M = 4.0
NORMAL FORCE, C_N
PITCHING MOMENT, C_m
.3
.2
.1
0
-.1
-.2
-2
0
2
4
6
8
10
ANGLE OF ATTACK, α, DEG
○ WIND TUNNEL DATA
× AERSP
AERSP WITH α = 0 ADJUSTED TO DATA (K_W(B) = 1)

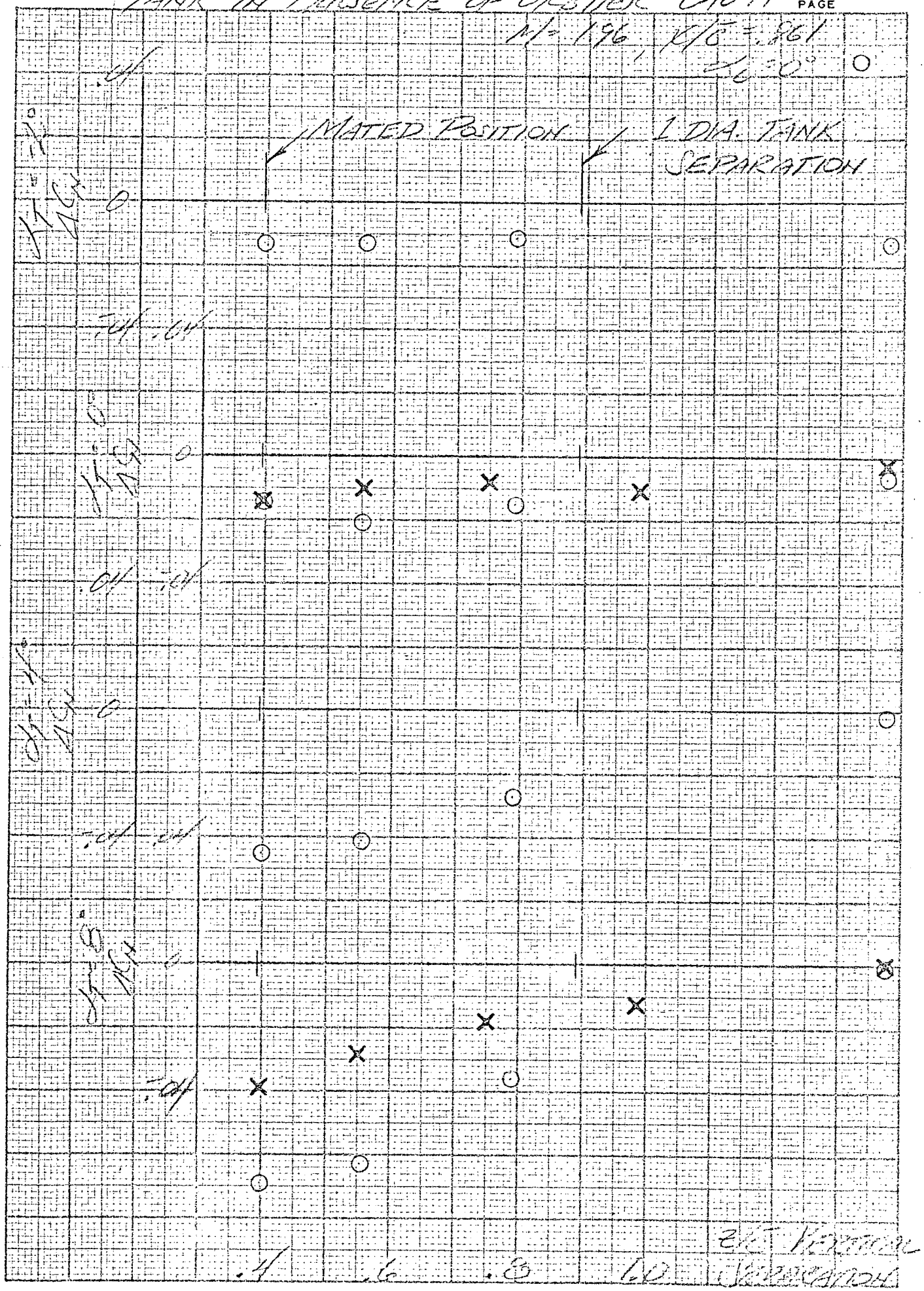
TANK IN PRESENCE OF ORBITER 040-A
M = 1.96
K/D = .961
α = 0°
MATED POSITION
1 DIA. TANK SEPARATION
ET NOSE
SEPARATION

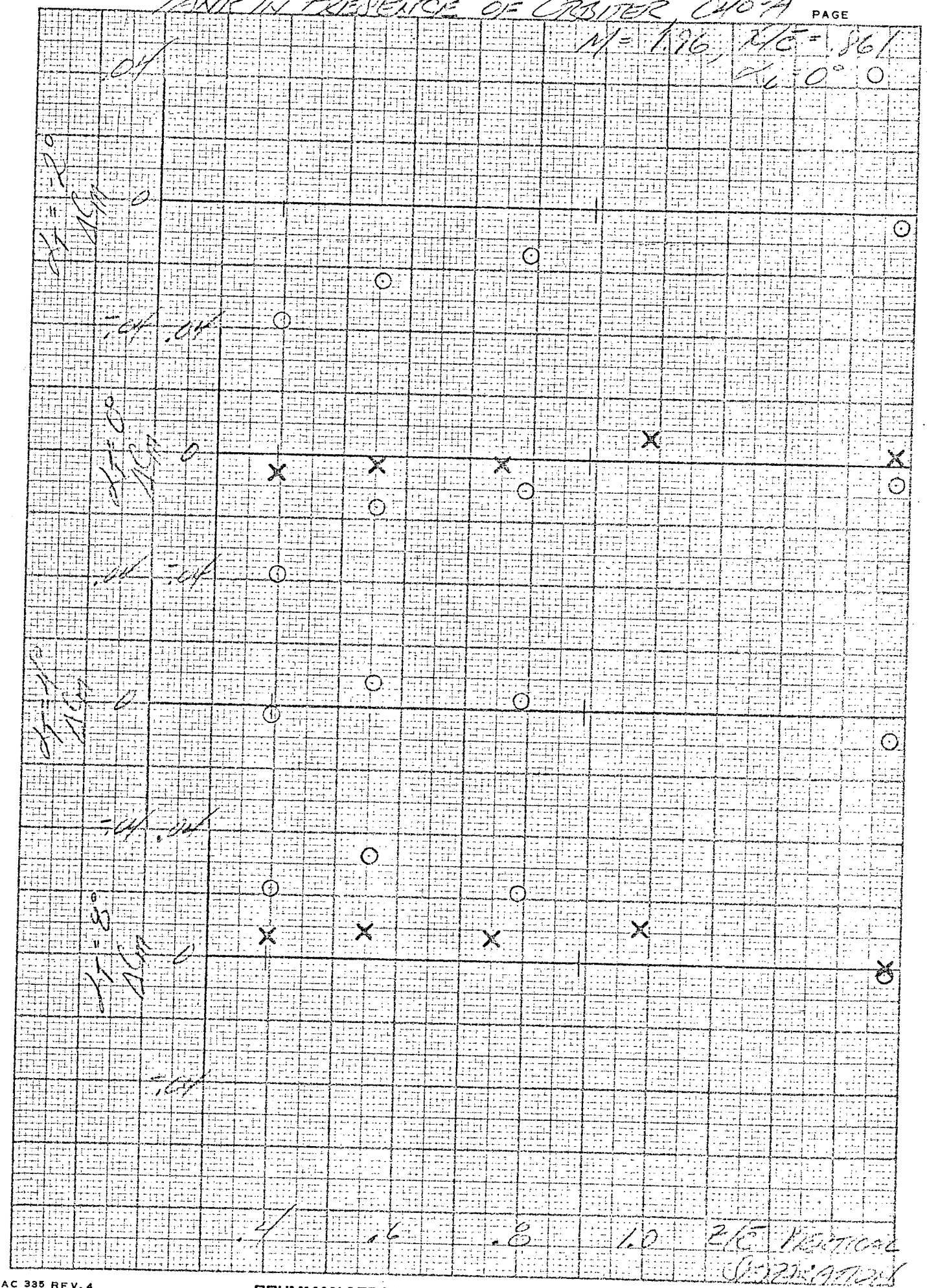
TANK IN PRESENCE OF ORBITER, C/O-A
M = 1.26, R/C = .861
α = 0°
-.04
-.04
-.04
-.04
-.04
-.04
-.04
.4
.6
.8
1.0
2R̄ VERTICAL
SEPARATION

TANK IN PRESENCE OF ORBITER C/O-A

$M = 4.0$, $R/C = .861$, $\alpha_c = 0°$

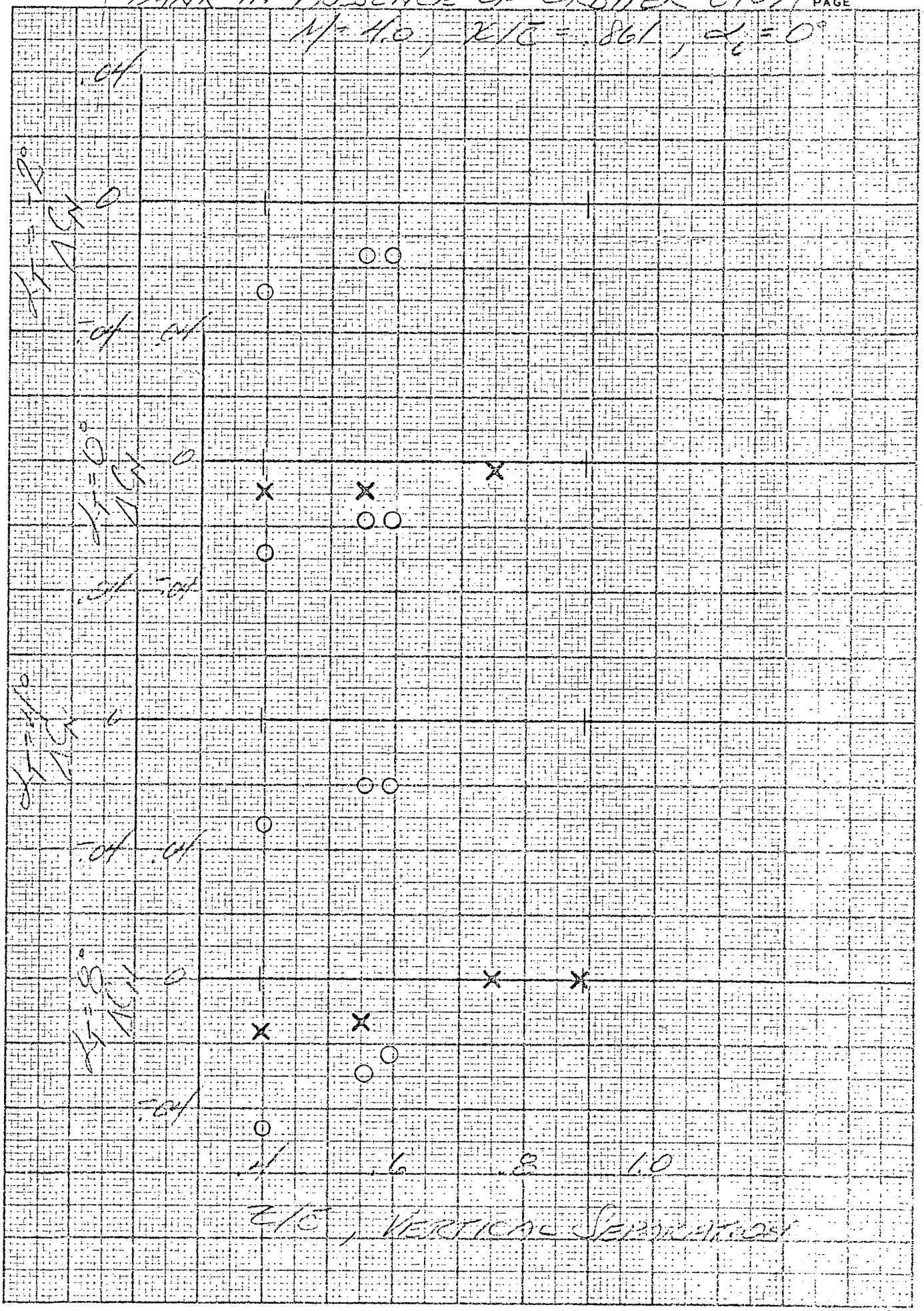

TANK IN PRESENCE OF ORBITER

$M = 4.0$, $Z/\ell = .861$, $\alpha_\ell = 0°$

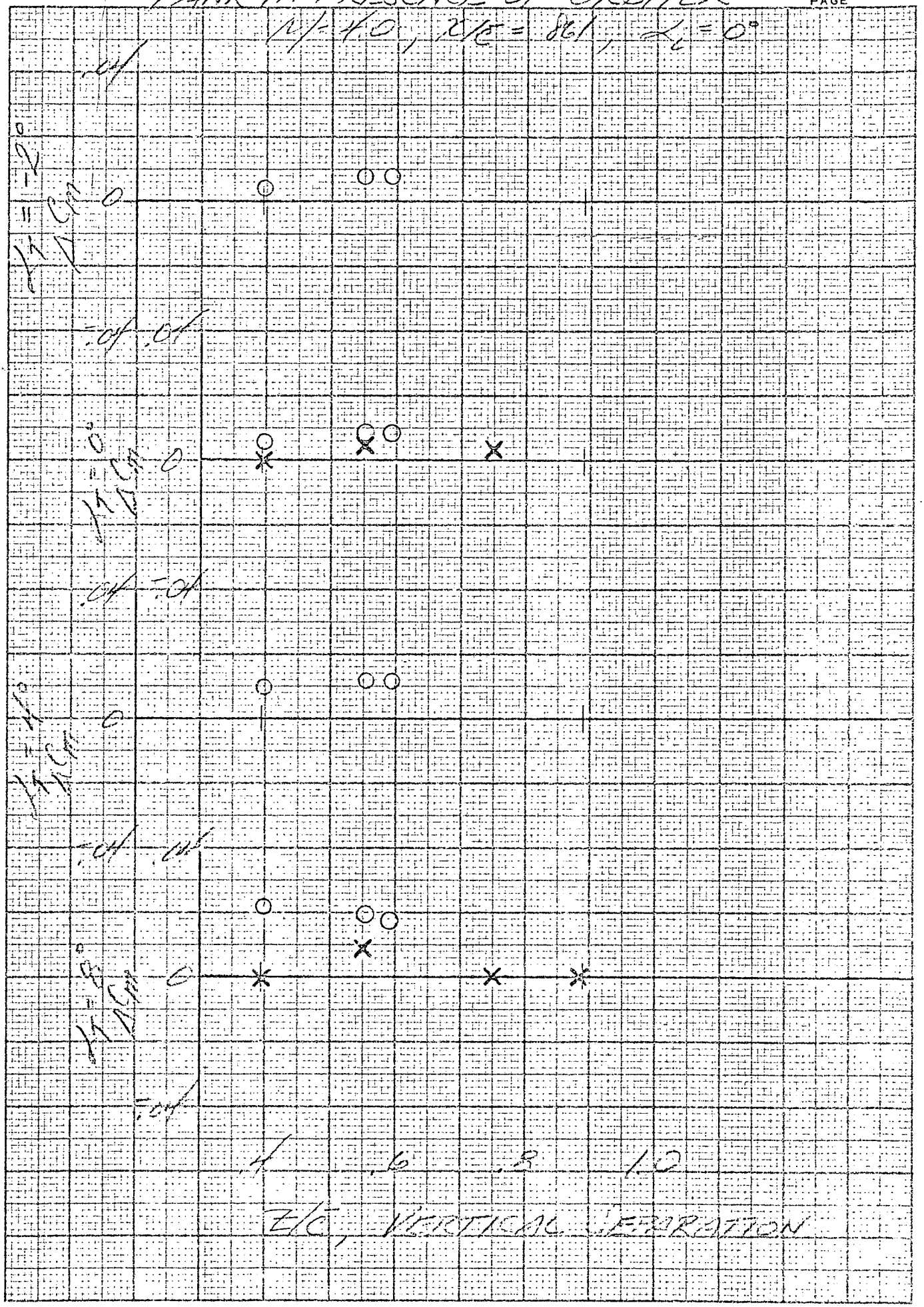

ORBITER IN PRESENCE OF TANK, C40A

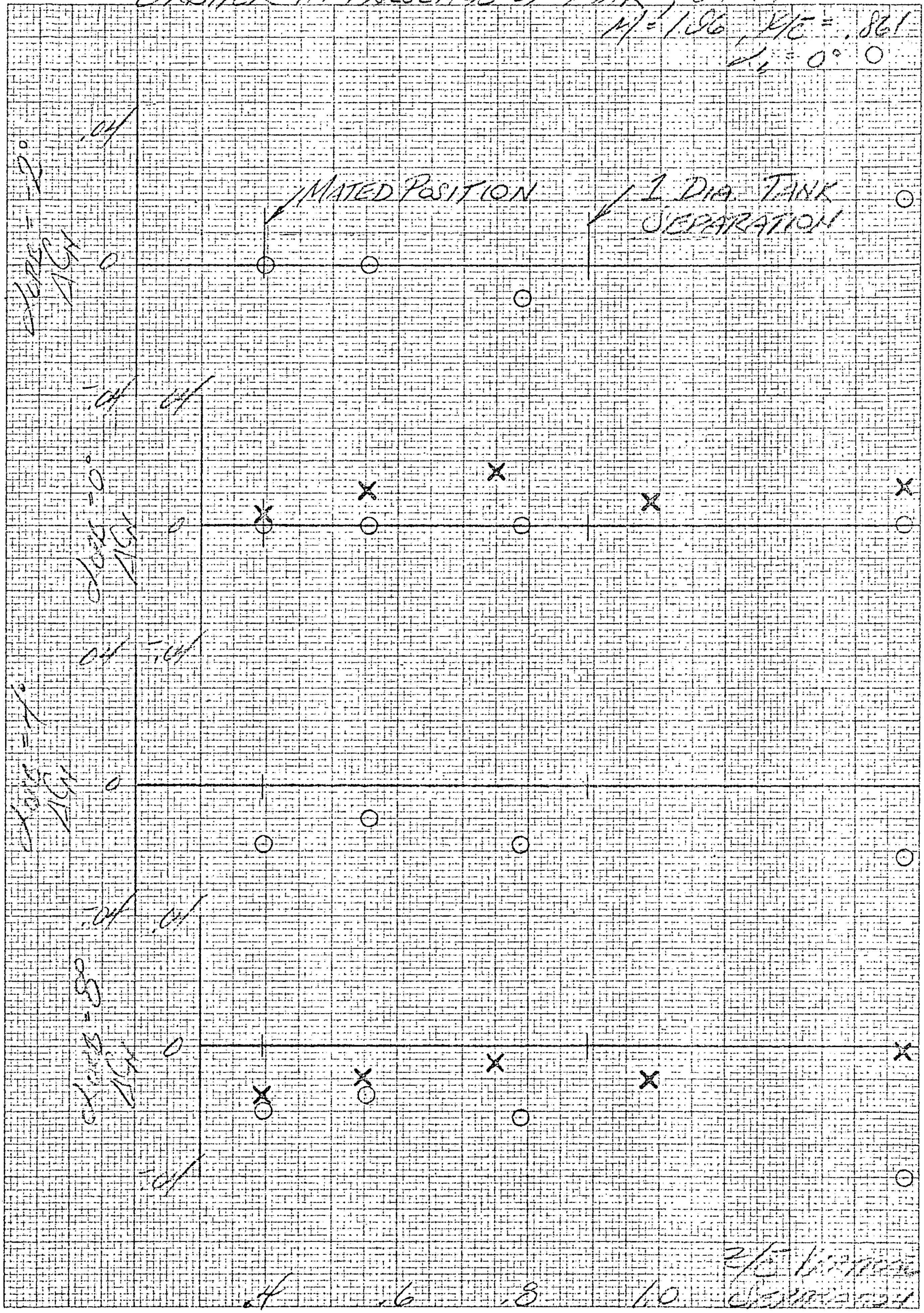

FIG. 10.5-1

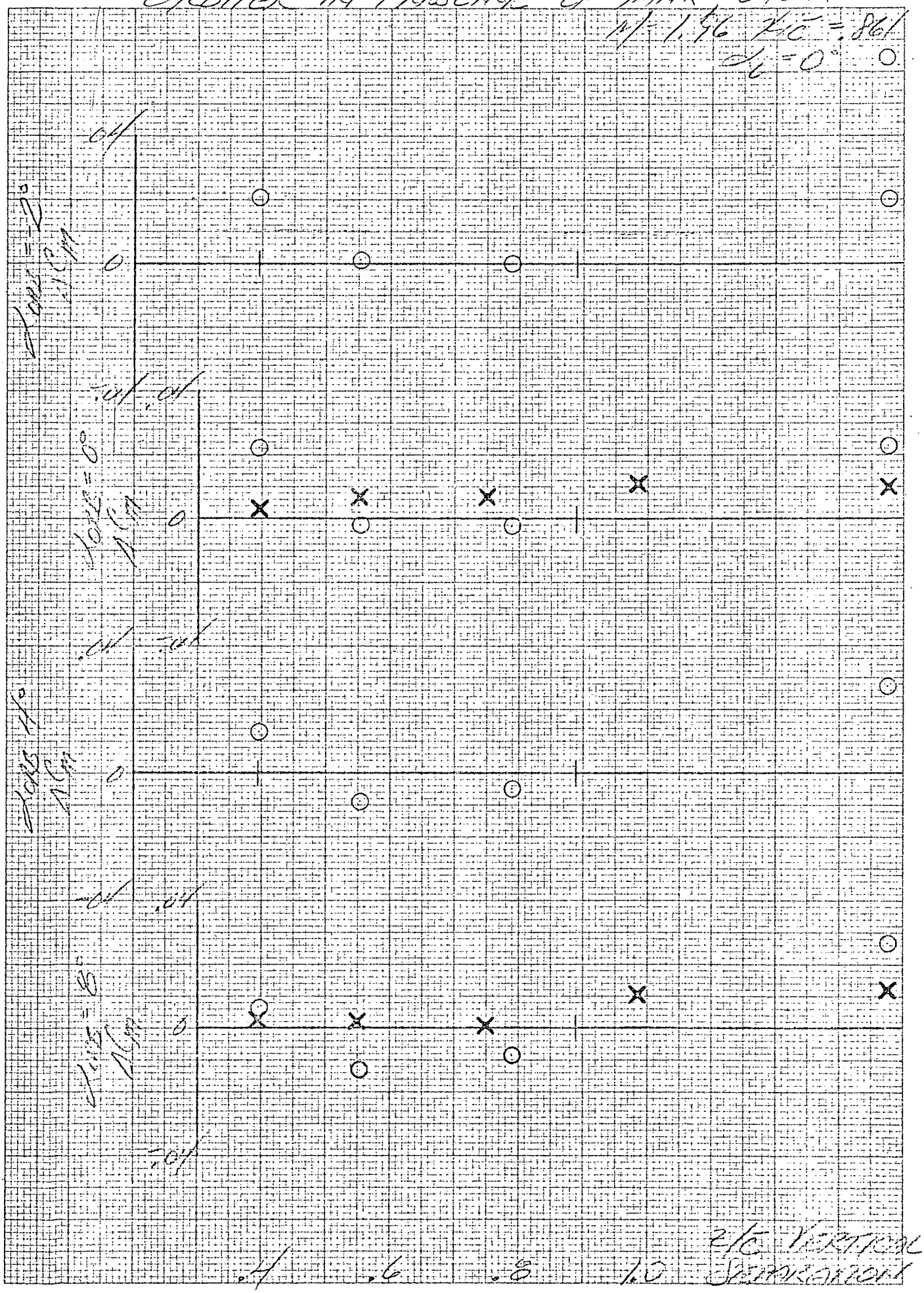

FIG. 10.5-2

ORBITER IN PRESENCE OF TANK

$M = 4.0$, $x/C = .86$, $\alpha = 0°$

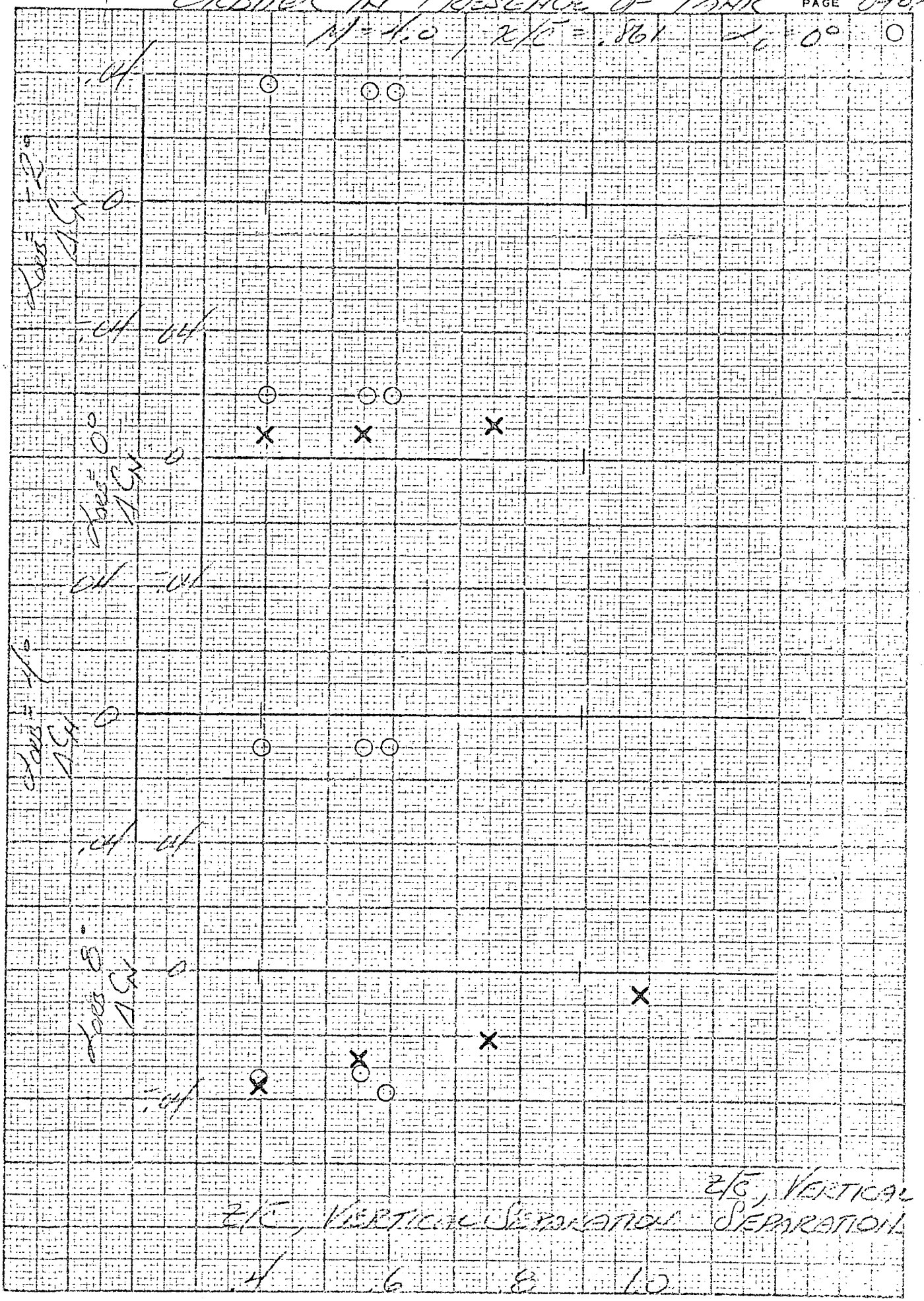

FIG. 10.5-5

ORBITER IN PRESENCE OF TANK C40-A

M=4.0, X/C=.861, ψ=0°

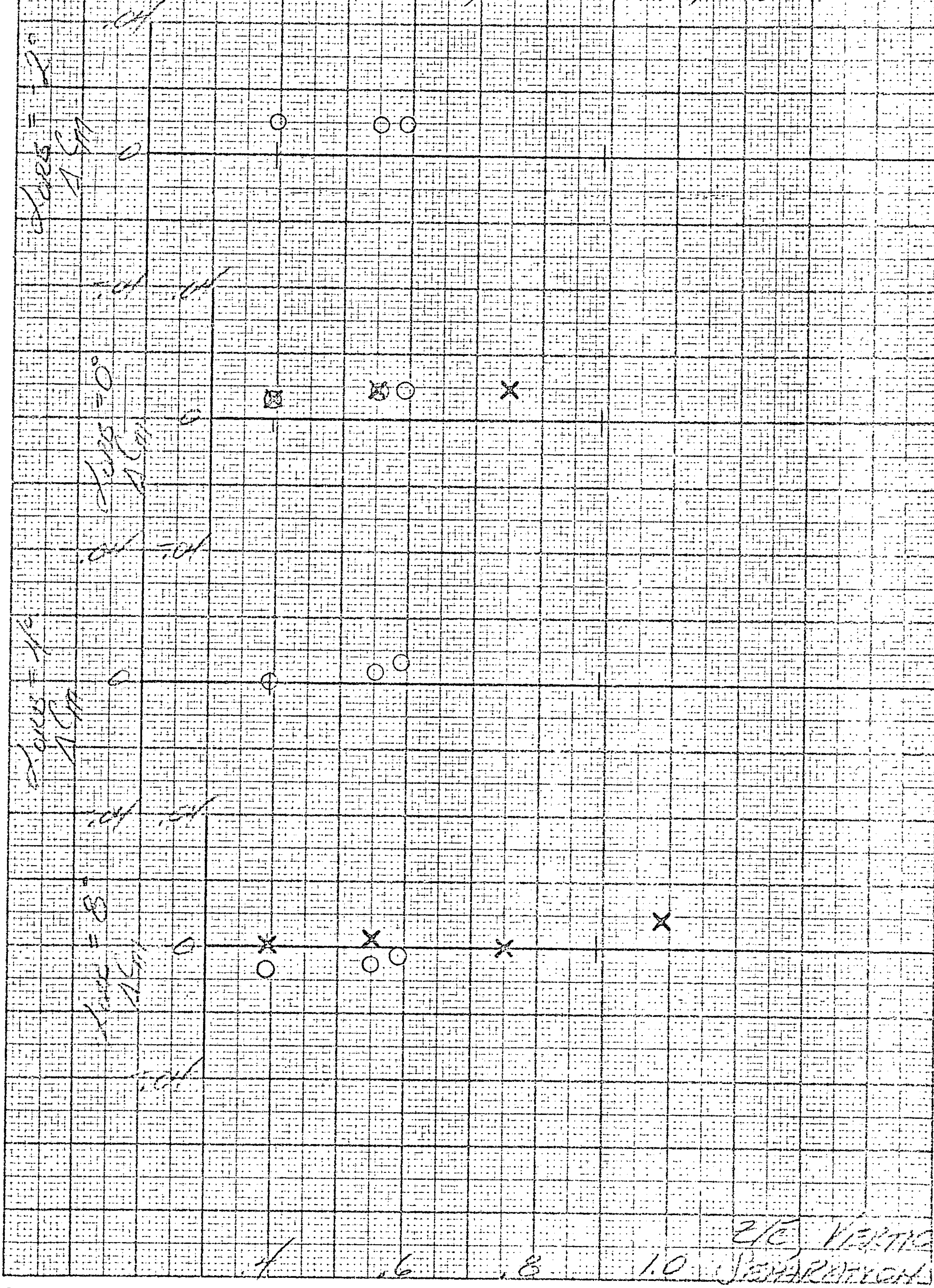

FIG. 10.5-4

TANK IN PRESENCE OF ORBITER OI0A

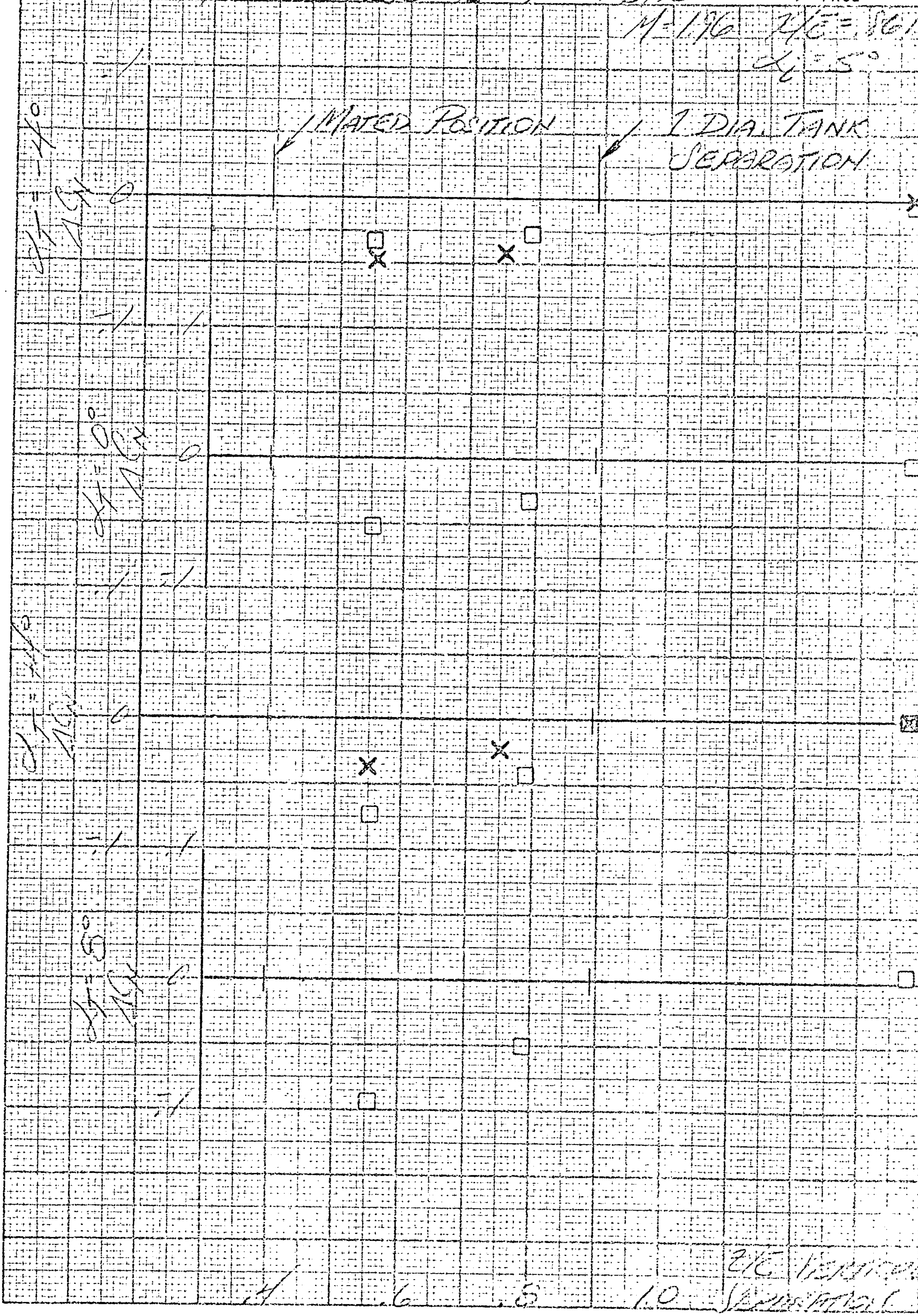

FIG. 10.6-1

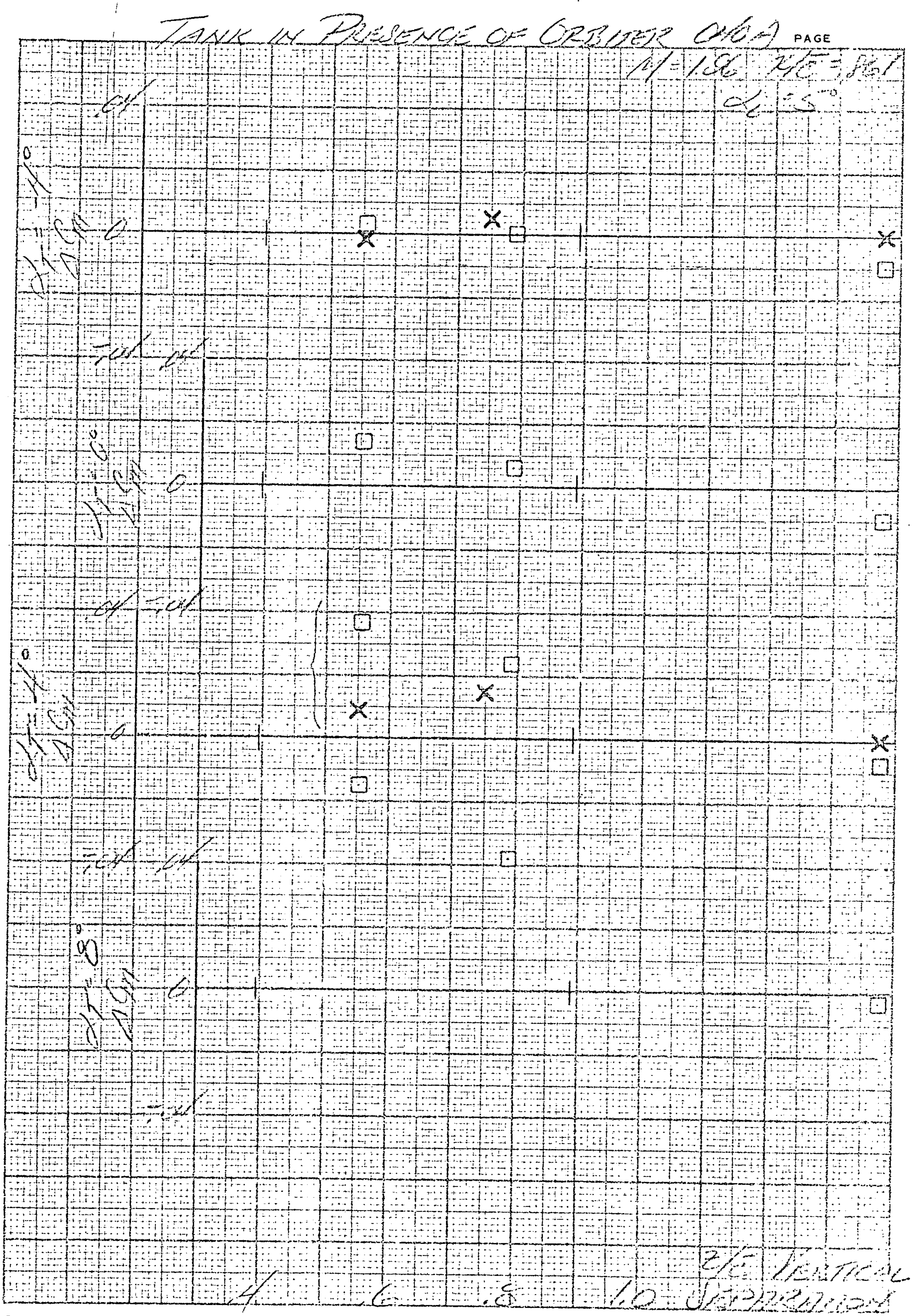

TANK IN PRESENCE OF ORBITER 040A
M=1.96 ψE=.861
δ=5°
0
0
0
0
.4
.6
.8
1.0
Z/E VERTICAL SEPARATION

PAGE

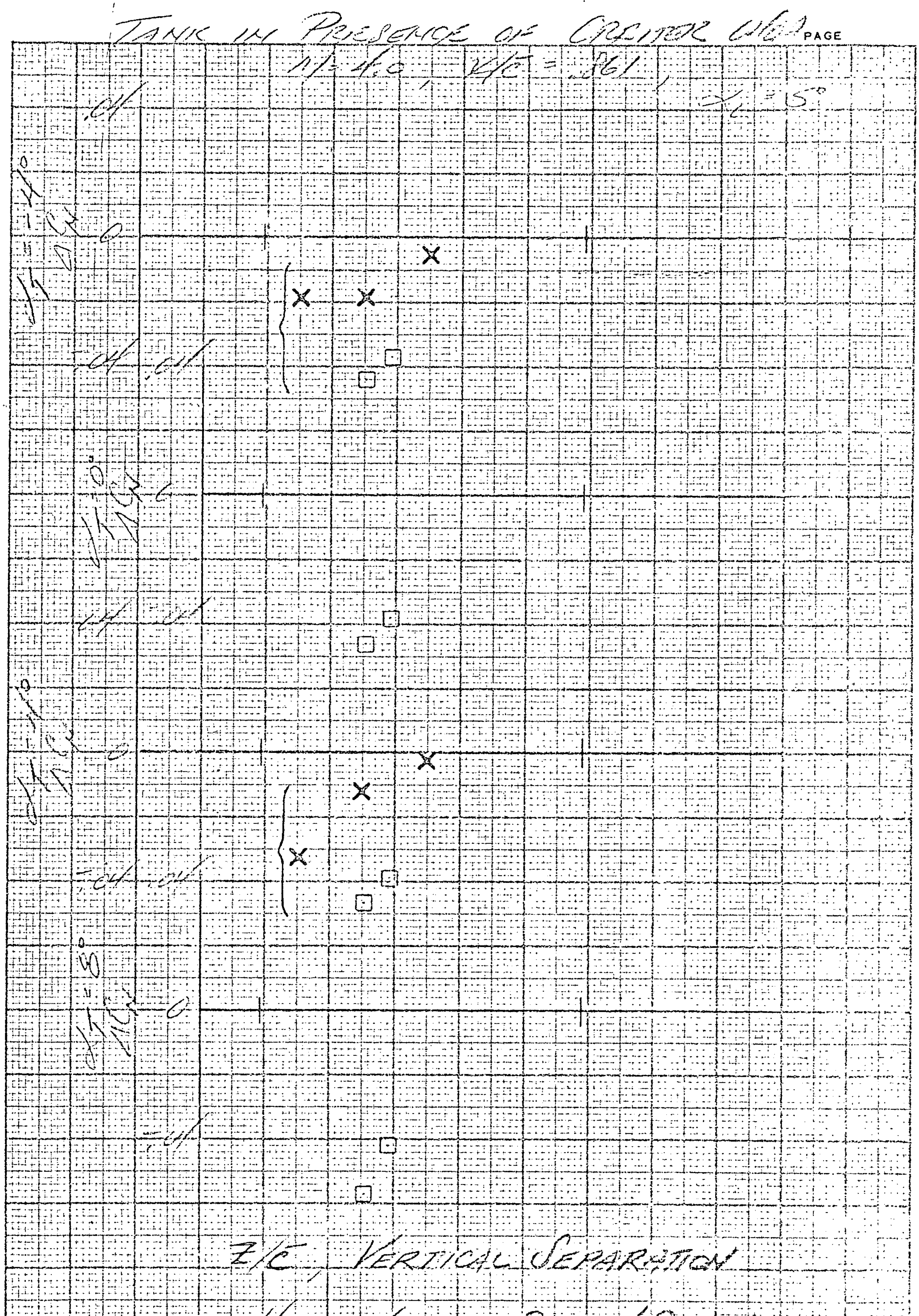
TANK IN PRESENCE OF CRESTER W&B
M = 4.0, Y/C = .361, λ = 15°
Z/C, VERTICAL SEPARATION
.4 .6 .8 1.0

TANK IN PRESENCE OF CIRCULAR - CYLINDER PAGE

M=4.0 RE = 1.2E7

$\alpha_c = 5°$

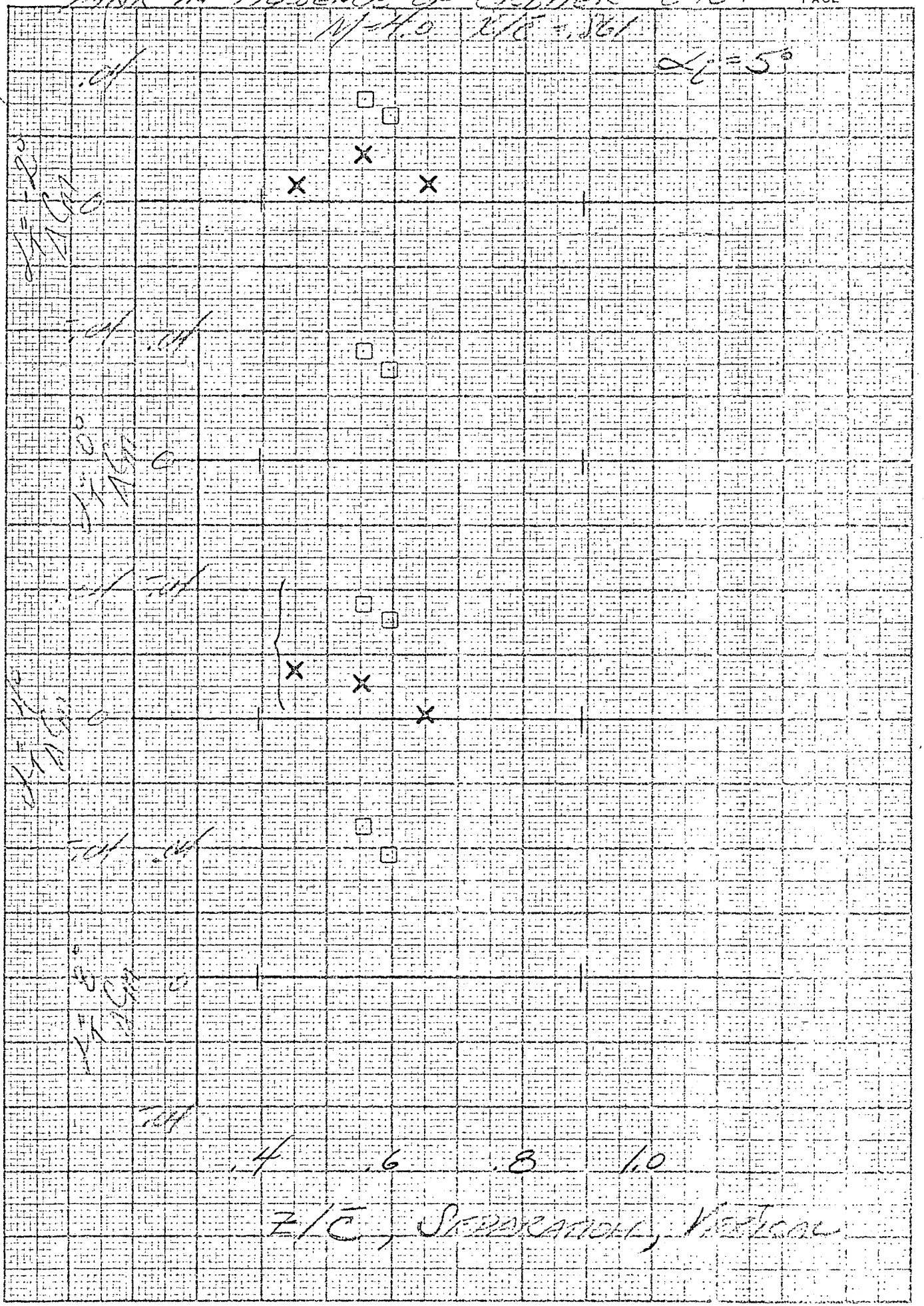

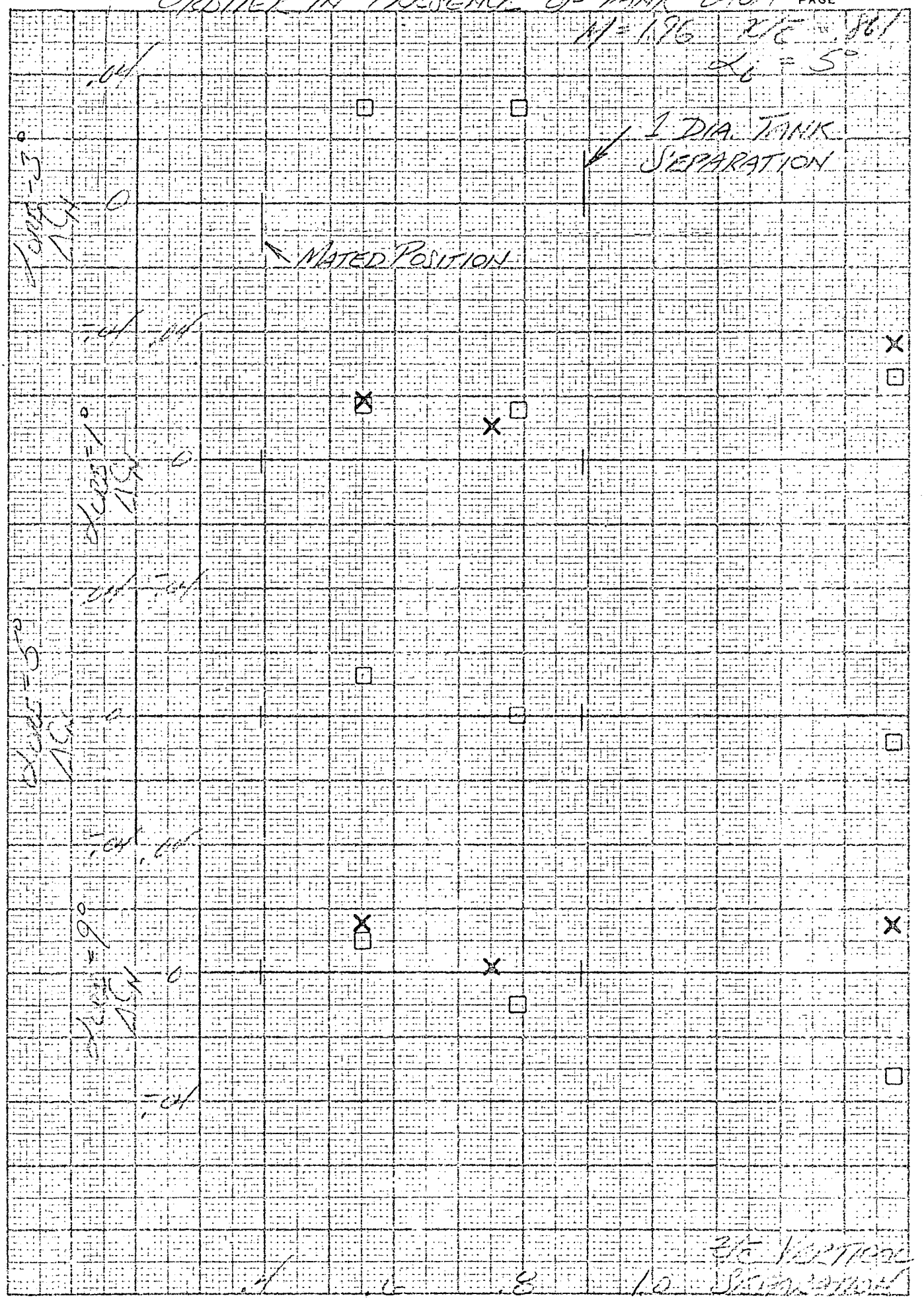
ORBITER IN PRESENCE OF TANK C404
M = 1.96 RE = 361
α = 5°
1 DIA. TANK SEPARATION
MATED POSITION

ORBITER IN PRESENCE OF TANK ONLY

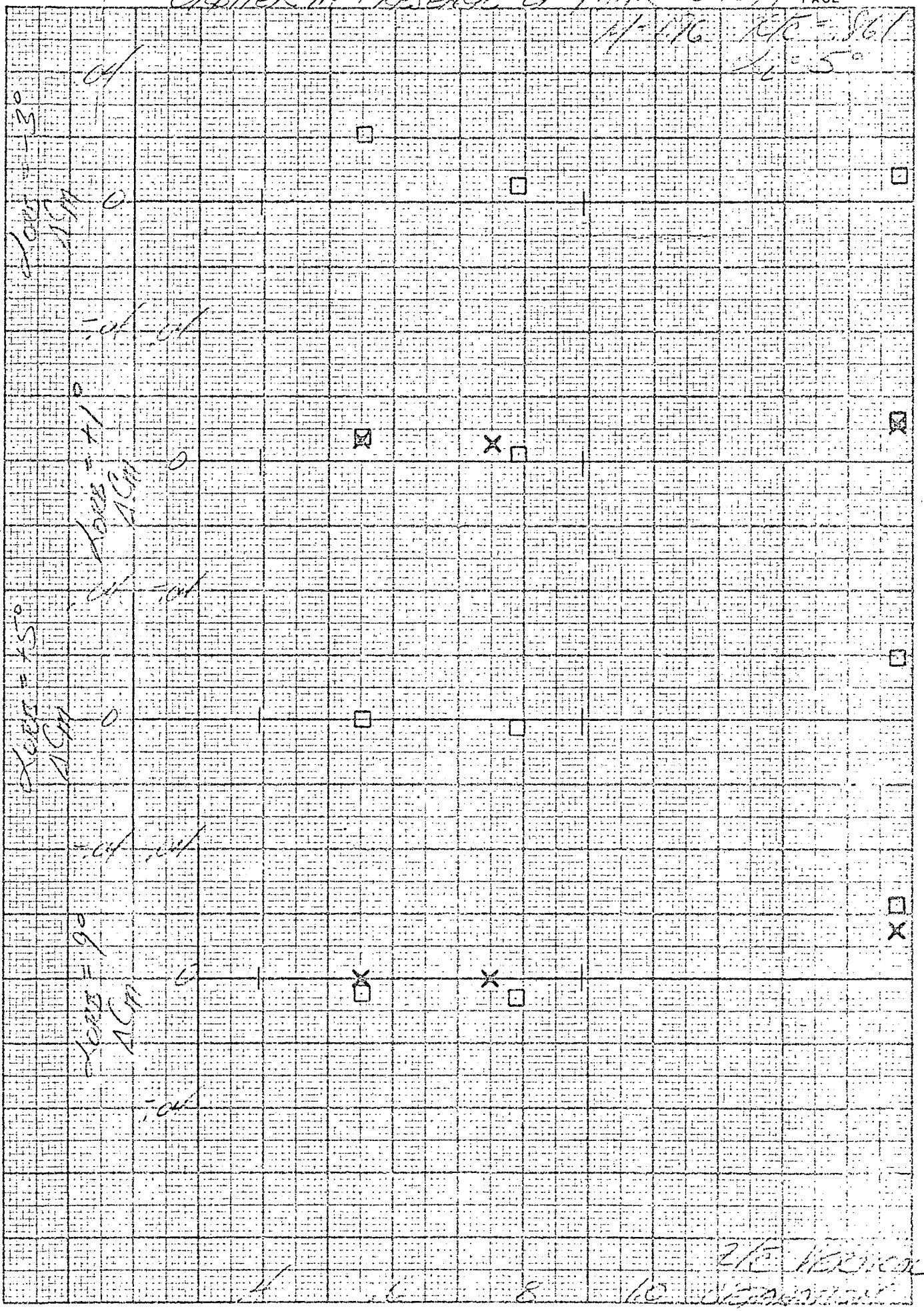

ORBITER IN PRESENCE OF TANK, 040-A

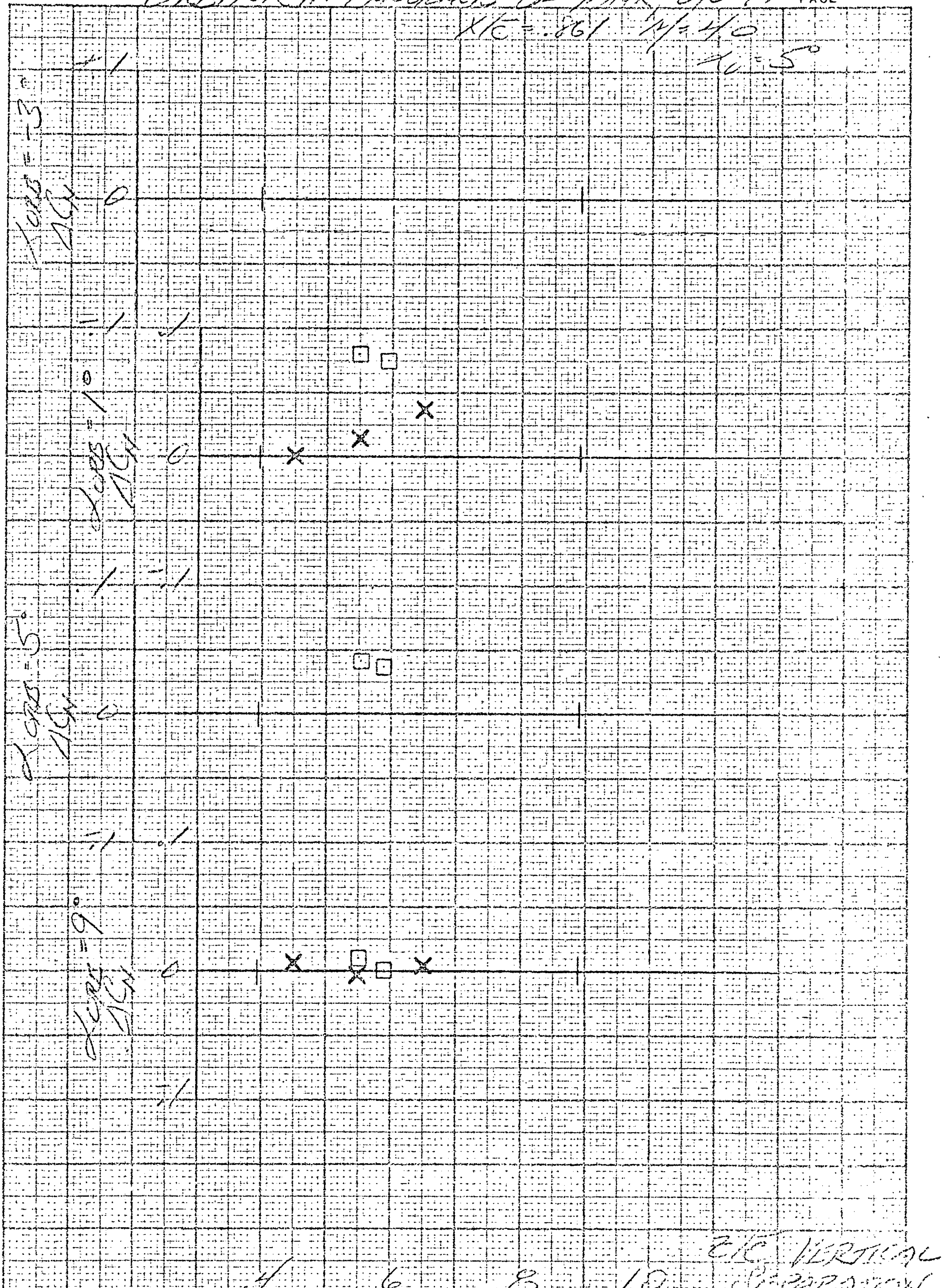

REPORT FIG 10.7-3
DATE
CODE 26512

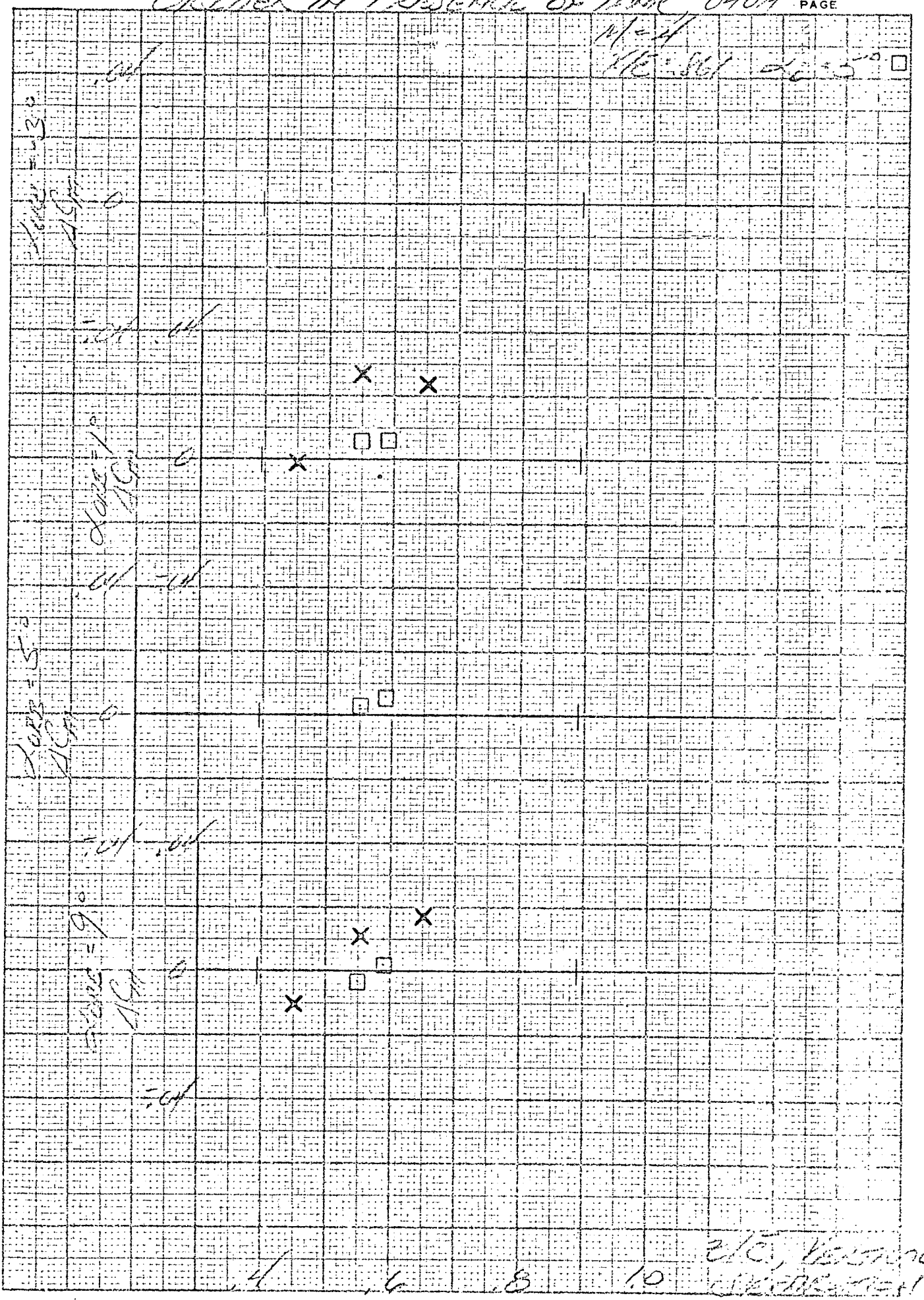

TANK IN PRESENCE OF ORBITER C/D-2

$M_f = 1.96$, $X_{CG} = -.123$ $\alpha = 0°$

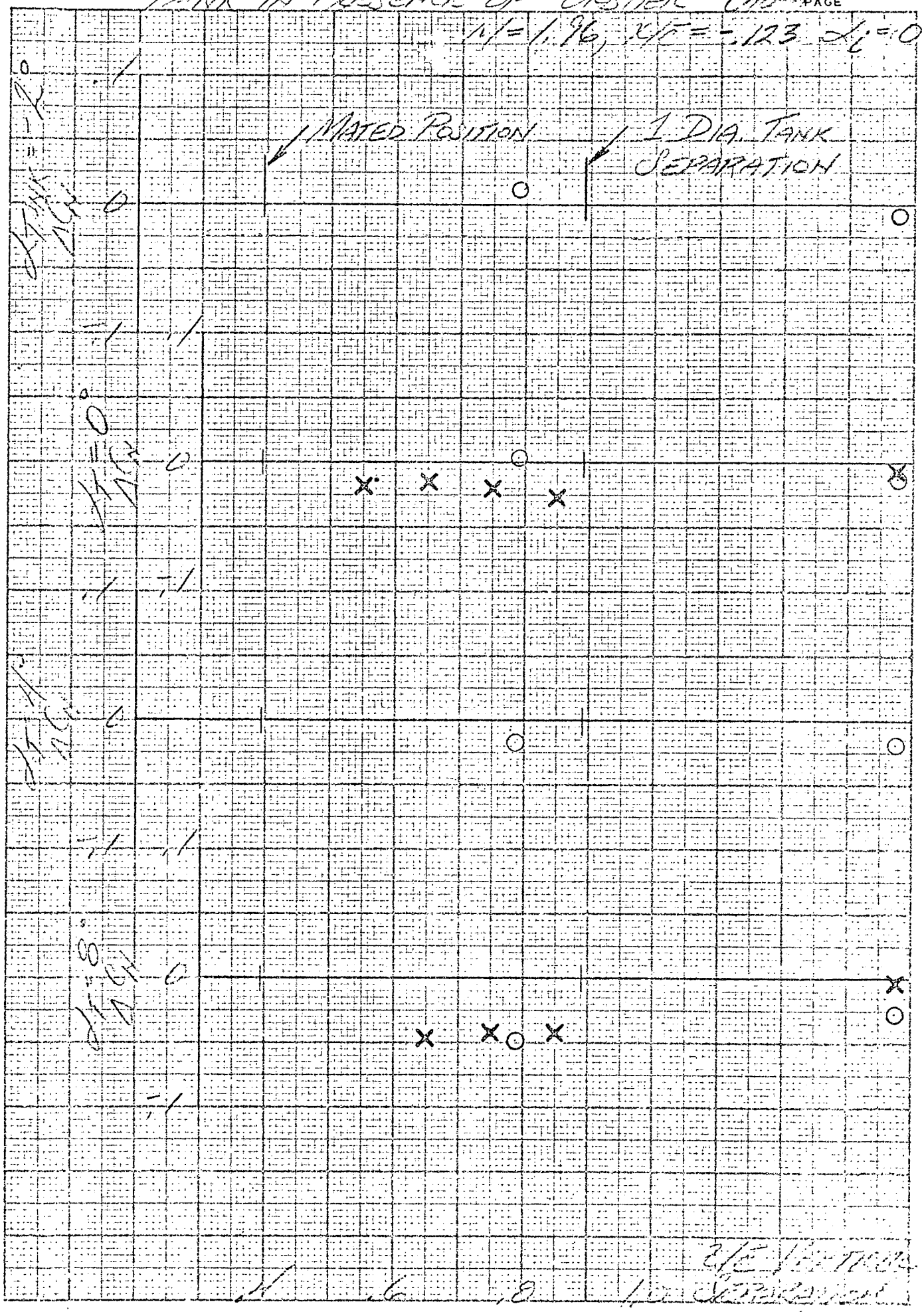

TANK IN PRESENCE OF ORBITER ONLY

$M_\infty = 1.96$, $\bar{x}_{cp} = -.123$

$\alpha_t = 0°$

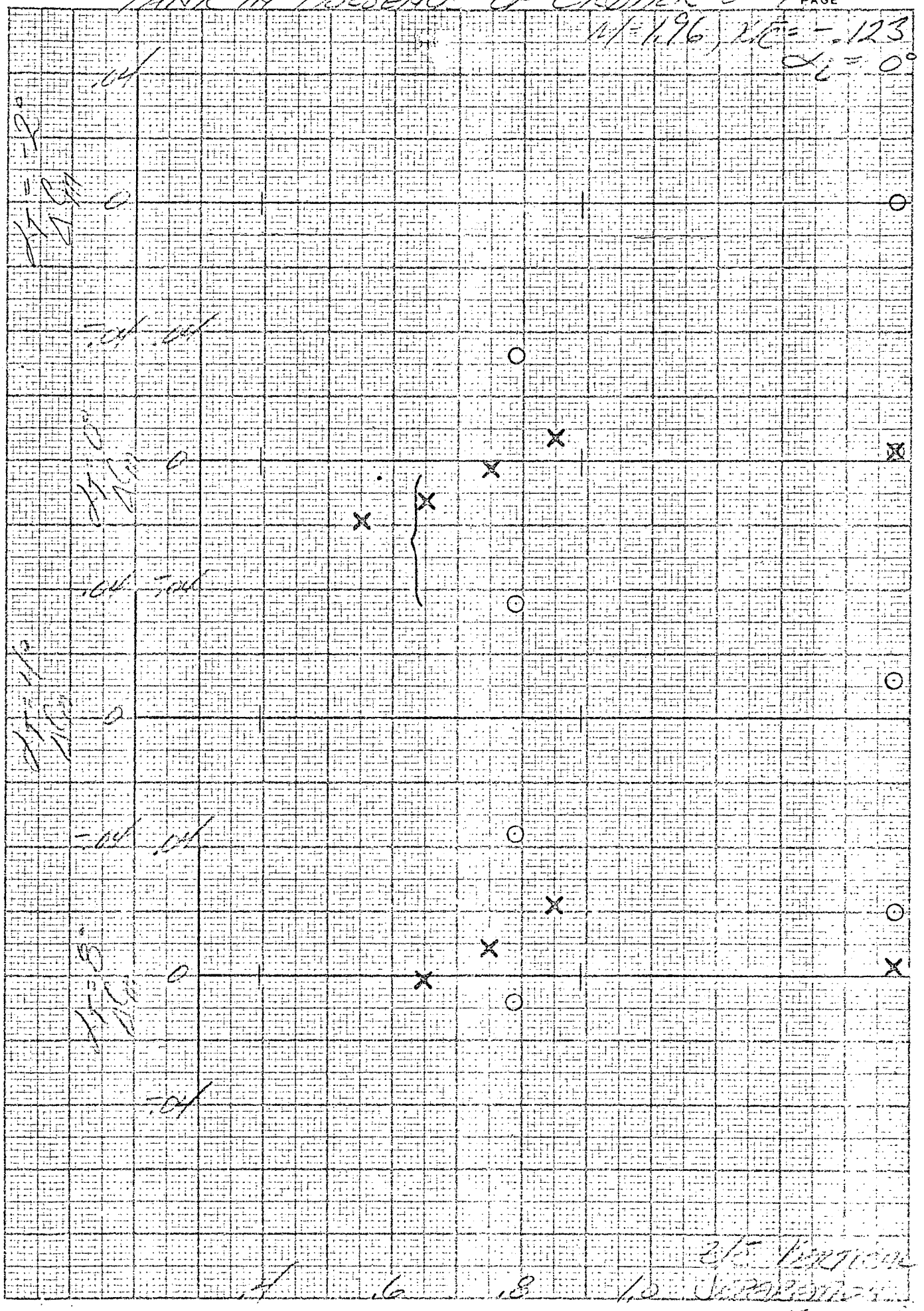

ORBITER IN PRESENCE OF TANK C40A

PAGE

M=1.96 ΔB=-.123

α = 0°

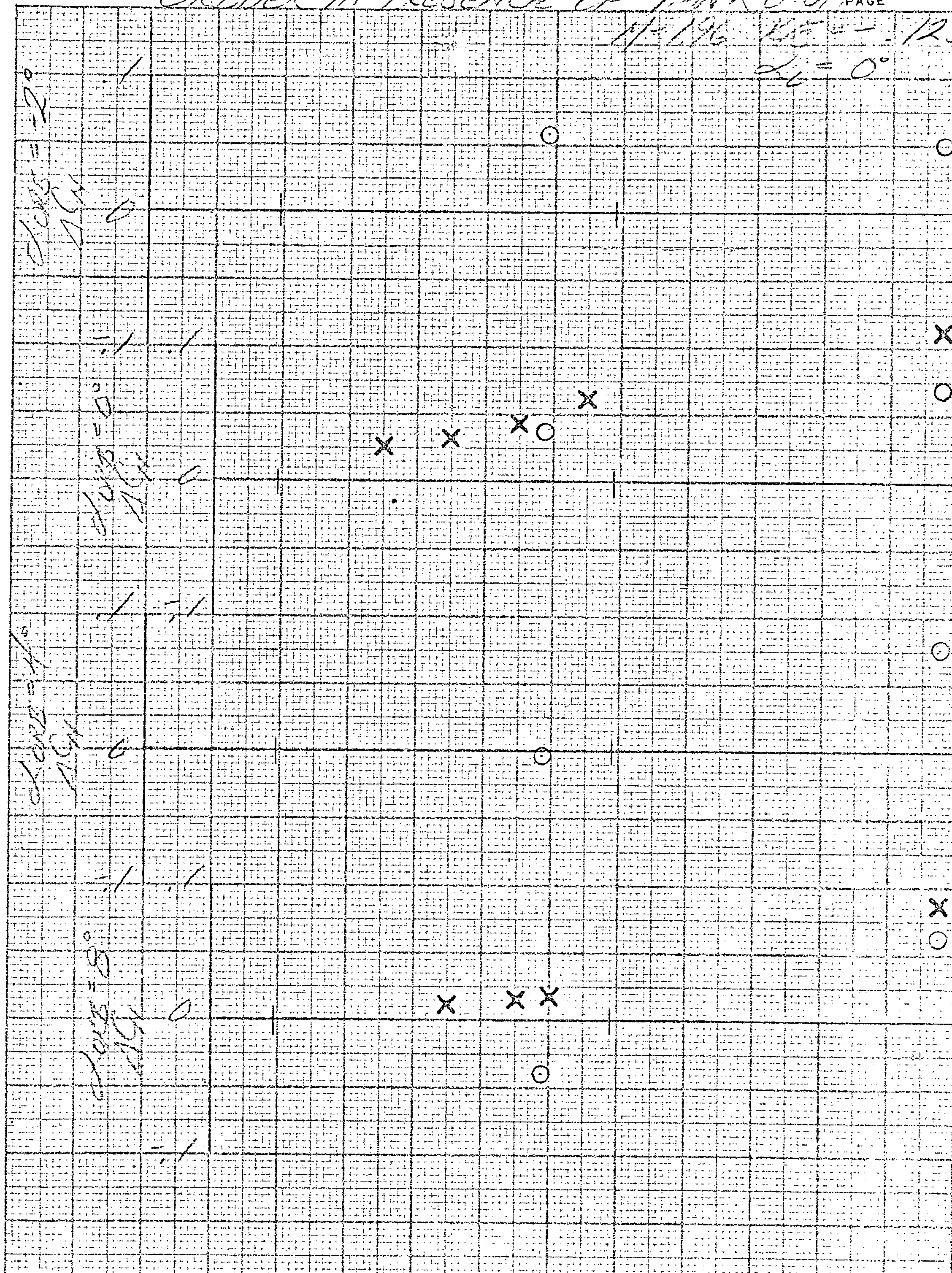

ORBITER IN PRESENCE OF TANK 640A

M=1.96, ΔZ=-.123

α=0°

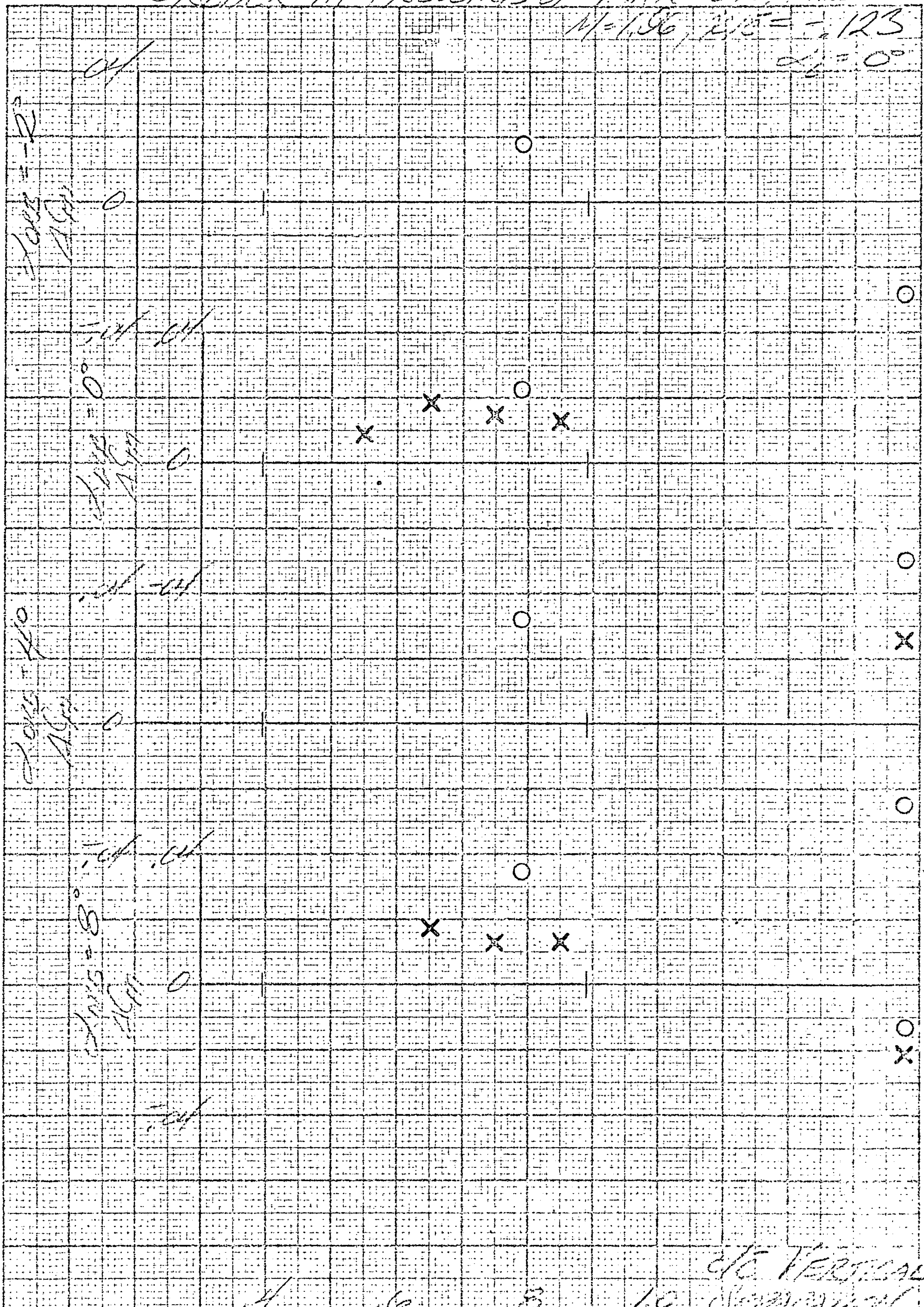

ΔC VERTICAL SEPARATION

Fig 10.8-1